ARMY RESEARCH LABORATORY

RESTRAN: Residual Strength Analysis of Impact Damaged Composite Laminates Volume I: Theoretical Manual

by Erik Saether

ARL-TR-2549 July 2001

The findings in this report are not to be construed as an official Department of the Army position unless so designated by other authorized documents.

Citation of manufacturer's or trade names does not constitute an official endorsement or approval of the use thereof.

Destroy this report when it is no longer needed. Do not return it to the originator.

Army Research Laboratory
Aberdeen Proving Ground, MD 21005-5069

ARL-TR-2549 July 2001

RESTRAN: Residual Strength Analysis of Impact Damaged Composite Laminates Volume I: Theoretical Manual

Erik Saether
Weapons and Materials Research Directorate, ARL

Abstract

The use of composite material systems in structural design has yielded significant improvements in material efficiency by minimizing weight while meeting static and dynamic strength requirements. The complexity of composite materials, however, has presented a spectrum of additional design considerations in the areas of fabrication, strength tailoring, failure mechanisms, and damage tolerance. Laminated composites exhibit a variety of damage and failure modes which include matrix cracking, fiber breakage, delamination propagation, and instability. Of prime concern is the predication of residual strength in composite structures subjected to damage-causing impact threats in the intended service environment. The present effort aims to account for many of the salient damage mechanisms utilizing a numerical, finite element-based approach. Such an approach permits a broad range of failure modes to be accounted for while allowing the modeling of complex geometries, support conditions, and applied loading. This report details the theoretical and algorithmic basis of a developed computer program denoted RESTRAN (REsidual STRength ANalysis), incorporating both material and structural failure modes in the prediction of residual strength in composite structures containing internal damage.

Table of Contents

INTENTIONALLY LEFT BLANK.

List of Figures

List of Tables

INTENTIONALLY LEFT BLANK.

1 Introduction

Modern structural design is making increasing use of advanced composite material systems to improve material efficiency by minimizing structural weight while meeting static and dynamic design strength criteria. While maximizing structural efficiency, these materials exhibit complex elastic and failure response under loading such as anisotropy and multimode failure mechanisms. Of particular interest is the susceptibility of these material systems to impact damage. In aerospace, submersible, and armored military vehicle design, the accurate prediction of residual strength due to impact damage is important for assessing survivability and damage tolerance to projected damage causing impact threats in the intended service environment. With an increasing need to reduce production costs associated with experimental testing, numerical simulation is being emphasized to assess evolving design concepts. A robust analytical approach is thus required to ensure a viable structure by accurately assessing the effect of assumed internal damage on residual strength.

The study of impact involves the complex dynamics between colliding bodies which potentially entails high energy transfer rates, stress wave phenomena, large deformations, material phase/property change, large strains, fragmentation, fracture, and a multitude of additional failure mechanisms many of which are material specific. Common analytical approaches define high- and low-velocity regimes to characterize the impact event and in which to apply various simplifying assumptions. In low energy impact, damage can be distributed significantly away from the contact zone due to longer contact duration in which large fractions of the impact energy can be transferred into elastic deflections within the target. In high energy regimes, through-penetration, explosive spalling, and diffuse fragmentation can characterize the material damage. If the ensuing material damage has compromised structural integrity, under subsequent loading, damage modes will propagate until total structural failure is precipitated. In laminated, fiber-reinforced composites, the heterogeneous, layered characteristics of the material system exhibit a highly complex combination of microscopic and macroscopic damage modes. These damage modes are pronounced in low velocity impact events and interact in a complex manner under subsequent loading. Damage modes include material failure through matrix cracking, fiber breakage, debonding along fiber-matrix interfaces and ply groups, and structural failure modes associated with sublaminate buckling due to delaminations. Depending on the geometric complexity of the problem being studied, various approaches have been used to model the problem. Mathematical models have utilized exact formulations based on elasticity theory, engineering approximations such as beam, plate and shell assemblages, and numerical approaches such as finite element analysis [1–16]. For a complete analysis, both the local and global response of the component to applied loading is required. This response includes the basic displacement and internal stress distribution from which local material failure modes and sublaminate instabilities may be predicted and the residual strength determined.

Of the myriad of analytical and numerical approaches that have hitherto been used to predict residual strength in composites, these analyses have generally been restricted to selected damage modes and idealized geometric configurations. Although these efforts have been important in elucidating an understanding of failure phenomenon in composites, they have not

permitted a direct application to the analysis of actual structural designs due to inherent simplifications. The current effort has been directed towards incorporating advanced analytical representations of composite damage/failure phenomena in a general analysis tool which can be applied to actual structural geometries and realistic damage states.

The finite element method provides a completely generic numerical approach to potentially incorporate all salient material behavior and failure modes while allowing arbitrary geometries, applied loads, and support conditions to be modeled in the analysis [17]. Prior efforts directed towards predicting residual strength using a finite element-based approach have fallen short of the development of a comprehensive analysis tool [18–25]. Limitations include restriction to two-dimensional problems, limited selection of failure criteria, and inability to assess both material and structural failure modes in a combined progressive analysis.

This report details a numerical finite element-based approach for predicting residual strength in general three-dimensional structures containing internal damage. The contribution of this effort to the prediction of residual strength is the development of a viable solution algorithm accounting for the coupled effects of nonlinear material response and both material and instability failure mechanisms which has not been presented in the literature. While emphasizing the analysis of progressive failure in laminated composites, the support of a layered media permits additional material systems to be modeled, such as sandwich-type constructions, piecewise linear approximations to homogeneous materials with varying properties along a thickness direction, and isotropic materials modeled as a single layer. This methodology has been incorporated into a computer program designated RESTRAN (REsidual STRength ANalysis) for determining the ultimate strength of composite structures with arbitrary geometric configurations and general loading and support conditions. The flow of execution is based on determining a sequence of scale factors to the initial applied loads to cause a series of incremental failures leading to ultimate collapse of the structure. The sequence of scale factors is not, in general, a monotonically increasing function; thus, the highest load multiplier attained during the course of the analysis is used to provide a measure of the residual strength. User-defined subroutine interfaces have been incorporated to allow alternative theoretical approaches to be applied in the assessment of residual strength, which thereby generalizes RESTRAN as a versatile research tool.

The following sections detail the finite element basis, failure modes, damage laws, analysis algorithms, and capabilities of the RESTRAN computer program.

2 Finite Element Formulation

RESTRAN has been developed as a specialized code to model sequential multimode failure in three-dimensional composites. The development of an extensive library of solid elements was excluded in favor of a single eight-node hexahedral element to model most expected geometries of interest. Higher-order hexahedrals were also avoided in the present effort because of the expected use to discretize the through-thickness resolution down to small ply groups or even local regions at the ply level such that a local linear displacement field was

deemed sufficient. The element formulation utilizes the hybrid stress technique in which both stresses and displacements are assumed as independent quantities to calculate elastic stiffness coefficients. Incompatible displacement modes are introduced to complete quadratic terms associated with bending and condensed into the element formulation to enhance element performance. This element is commonly referred to as the Pian-Tong Hexahedral [26]. To model geometric nonlinear response, differential stiffnesses are computed based on higher-order strain components and purely displacement-based shape functions. Within a finite element framework, structural failure through sublaminate buckling is accounted through a specialized eigenanalysis of instability modes and algorithmic processing of multiple delaminations in which contact constraints are enforced. The exceptional accuracy of stress recovery provided by the hybrid formulation yields highly accurate differential stiffness coefficients which lead to rapid convergence of buckling loads. Material degradation due to progressive ply failures is determined using selected failure criteria and specialized ply damage laws which are simulated through degradations made to element stiffness coefficients.

Basic geometric conventions, elastic and differential stiffness formulations, and nonlinear material and buckling solution algorithms are presented in the following subsections.

2.1 Coordinate Systems and Nomenclature

The finite element formulation in RESTRAN incorporates several conventions pertaining to coordinate system, laminate description, and tensor notation.

2.1.1 Global and Local Coordinates

The global Cartesian (x,y,z) coordinate system is used for describing the geometry and finite element discretization of the structural model. At a particular element, without the specification of a user-defined local coordinate system, a local (x',y'z') element coordinate system is assumed, which is offset and congruent to the global system in which to define laminate orientation. This coordinate system is depicted in Figure 1.

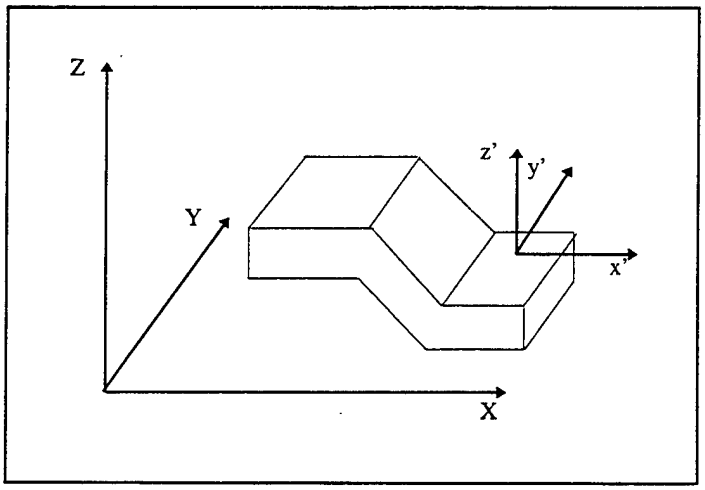

Figure 1. Global and local coordinate systems.

The description of the laminate layup assumes that ply layers are parallel to the local x'y'-plane and that the stacking sequence is a function of the local z'-coordinate, as shown in Figure 2(a). The principal ply directions (1,2,3) are defined by the offset angle from the x'–axis and are referred to as the longitudinal, transverse, and normal coordinates, respectively. These quantities are depicted in Figures 2(b) and 2(c).

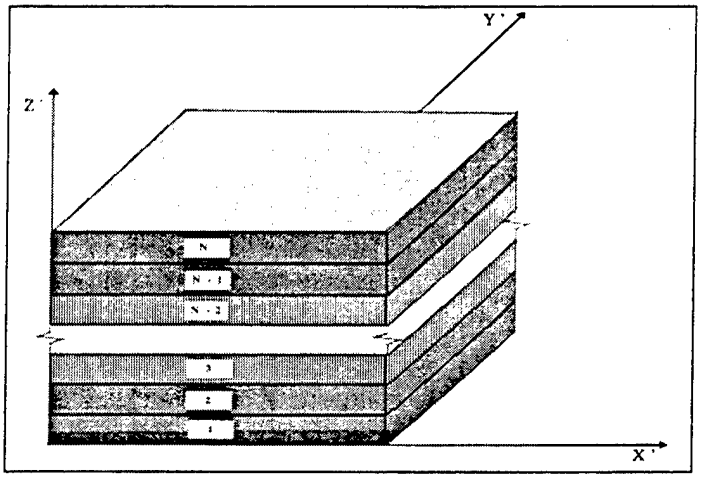

Figure 2(a). Laminate layup description.

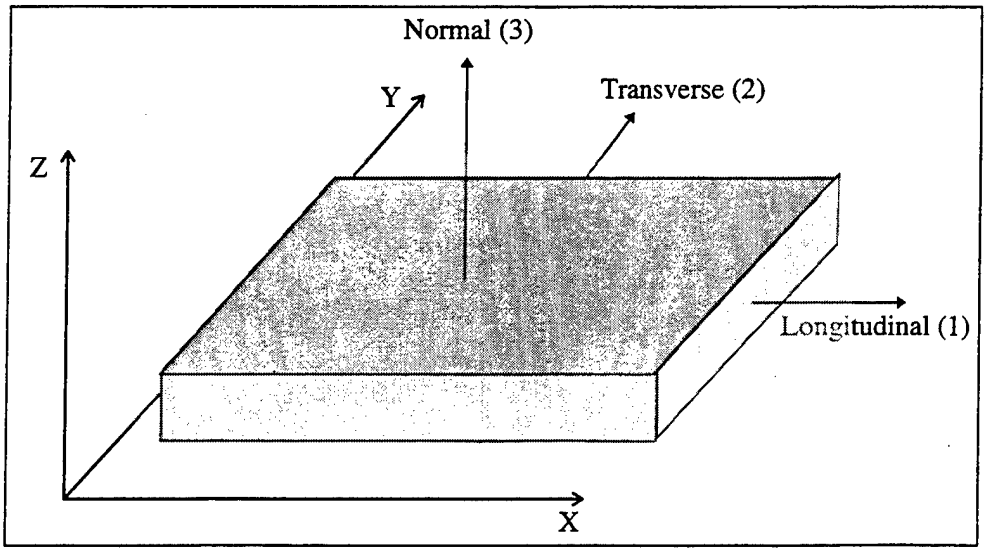

Figure 2(b). Principal ply directions.

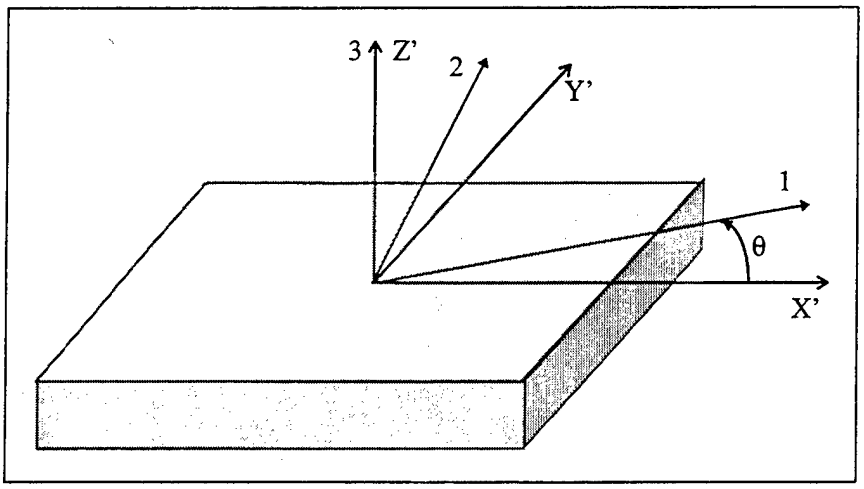

Figure 2(c). Ply orientation angle convention.

Components of the stress and strain tensors are labeled with respect to the global (x,y,z) or local (x',y',z') coordinates, as shown in Figure 3. When transformed to principal axes, the principal (1,2,3) coordinate designations are designated as longitudinal, transverse, and normal directions, respectively. Stress and strain vectors are ordered as

$$\begin{aligned} \{\boldsymbol{\sigma}\} &= [\sigma_{xx}, \sigma_{yy}, \sigma_{zz}, \sigma_{yz}, \sigma_{zx}, \sigma_{xy}]^T \\ \{\boldsymbol{\epsilon}\} &= [\epsilon_{xx}, , \epsilon_{yy}, \epsilon_{zz}, \epsilon_{yz}, \epsilon_{zx}, \epsilon_{xy}]^T \end{aligned} \tag{1}$$

which are related through the material constitutive law expressed in general as

$$\begin{Bmatrix} \sigma_{xx} \\ \sigma_{yy} \\ \sigma_{zz} \\ \sigma_{yz} \\ \sigma_{zx} \\ \sigma_{xy} \end{Bmatrix} = [\bar{\mathbf{C}}] \begin{Bmatrix} \epsilon_{xx} \\ \epsilon_{yy} \\ \epsilon_{zz} \\ \epsilon_{yz} \\ \epsilon_{zx} \\ \epsilon_{xy} \end{Bmatrix} \tag{2}$$

The $[\bar{\mathbf{C}}]$ matrix is assumed to be constituted by orthotropic lamina which possess the x-y plane as a plane of symmetry and are described by nine independent material moduli. With arbitrary orientation of the constituent layers, the assembled material stiffness matrix may assume a general monoclinic form given by

$$[\bar{\mathbf{C}}] = \begin{bmatrix} \bar{C}_{11} & \bar{C}_{12} & \bar{C}_{13} & 0 & 0 & \bar{C}_{16} \\ \bar{C}_{21} & \bar{C}_{22} & \bar{C}_{23} & 0 & 0 & \bar{C}_{26} \\ \bar{C}_{31} & \bar{C}_{32} & \bar{C}_{33} & 0 & 0 & \bar{C}_{36} \\ 0 & 0 & 0 & \bar{C}_{44} & \bar{C}_{45} & 0 \\ 0 & 0 & 0 & \bar{C}_{54} & \bar{C}_{55} & 0 \\ \bar{C}_{61} & \bar{C}_{62} & \bar{C}_{63} & 0 & 0 & \bar{C}_{66} \end{bmatrix} \tag{3}$$

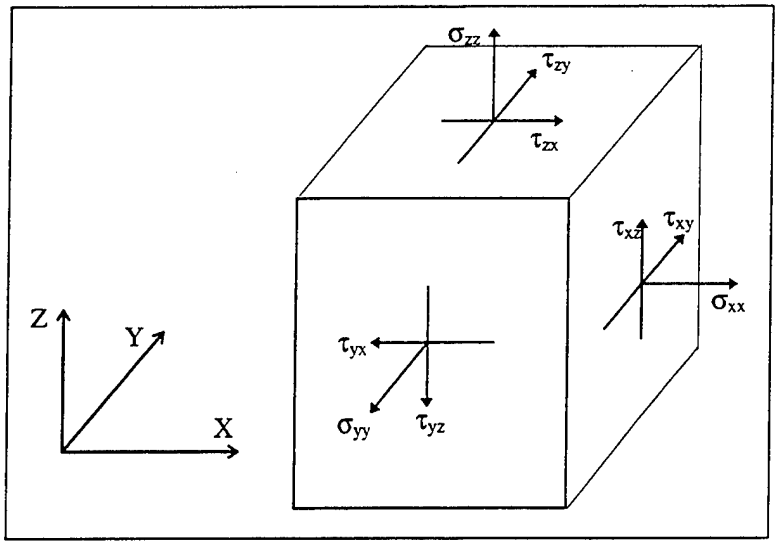

Figure 3. Stress and strain tensor notation.

2.1.2 Coordinate Transformations

A local material coordinate system $(\bar{x}, \bar{y}, \bar{z})$ may be specified for each element in RESTRAN to map element stresses, strains, and material properties, to account for any laminate orientation with respect to the local element (x',y',z') system. These Cartesian coordinate systems are depicted in Figure 4.

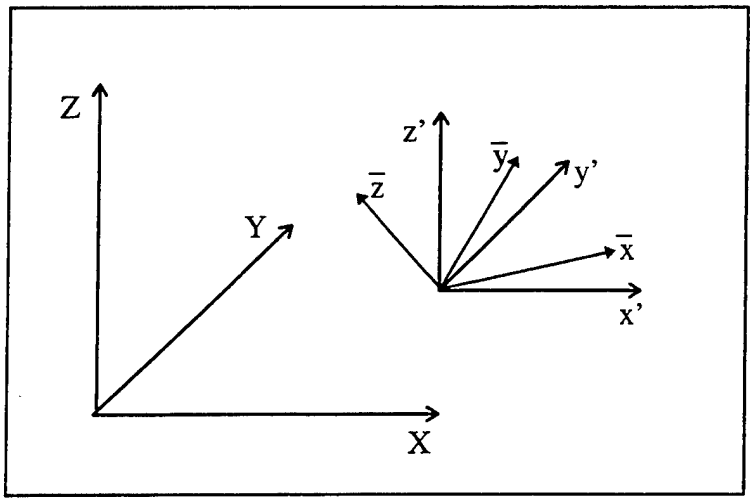

Figure 4. Local (x',y',z') and $(\bar{x}, \bar{y}, \bar{z})$ coordinate systems.

Transformation matrices are defined as

$$[\mathbf{T}_\epsilon] = \begin{bmatrix} \mathbf{T_q} & \mathbf{T_r} \\ \mathbf{T_s} & \mathbf{T_t} \end{bmatrix} \qquad [\mathbf{T}_\sigma] = \begin{bmatrix} \mathbf{T_q} & 2\mathbf{T_r} \\ \frac{1}{2}\mathbf{T_s} & \mathbf{T_t} \end{bmatrix} \tag{4}$$

where

$$[\mathbf{T_q}] = \begin{bmatrix} l_1^2 & m_1^2 & n_1^2 \\ l_2^2 & m_2^2 & n_2^2 \\ l_3^2 & m_3^2 & n_3^2 \end{bmatrix} \qquad [\mathbf{T_r}] = \begin{bmatrix} m_1^2 n_1^2 & n_1^2 l_1^2 & l_1^2 m_1^2 \\ m_2^2 n_2^2 & n_2^2 l_2^2 & l_2^2 m_2^2 \\ m_3^2 n_3^2 & n_3^2 l_3^2 & l_3^2 m_3^2 \end{bmatrix} \tag{5}$$

$$[\mathbf{T_s}] = \begin{bmatrix} 2l_2^2 l_3^2 & 2m_2^2 m_3^2 & 2n_2^2 n_3^2 \\ 2l_3^2 l_1^2 & 2m_3^2 m_1^2 & 2n_3^2 n_1^2 \\ 2l_1^2 l_2^2 & 2m_1^2 m_2^2 & 2n_1^2 n_2^2 \end{bmatrix} [\mathbf{T_t}] = \begin{bmatrix} m_2^2 n_3^2 + n_2^2 m_3^2 & n_2^2 l_3^2 + l_2^2 n_3^2 & l_2^2 m_3^2 + m_2^2 l_3^2 \\ m_3^2 n_1^2 + n_3^2 m_1^2 & n_3^2 l_1^2 + l_3^2 n_1^2 & l_3^2 m_1^2 + m_3^2 l_1^2 \\ m_1^2 n_2^2 + n_1^2 m_2^2 & n_1^2 l_2^2 + l_1^2 n_2^2 & l_1^2 m_2^2 + m_1^2 l_2^2 \end{bmatrix} \tag{6}$$

and where l, m, and n are the direction cosines between the two Cartesian systems defined as

$$\begin{Bmatrix} \bar{x} \\ \bar{y} \\ \bar{z} \end{Bmatrix} = \begin{bmatrix} l_1 & m_1 & n_1 \\ l_2 & m_2 & n_2 \\ l_3 & m_3 & n_3 \end{bmatrix} \begin{Bmatrix} x' \\ y' \\ z' \end{Bmatrix} \tag{7}$$

The transformation matrices have the property that

$$[\mathbf{T}_\epsilon]^{-1} = [\mathbf{T}_\sigma]^T \qquad [\mathbf{T}_\sigma]^{-1} = [\mathbf{T}_\epsilon]^T \tag{8}$$

which yield the relations for stress transformations

$$\{\bar{\boldsymbol{\sigma}}\} = [\mathbf{T}_\sigma]\{\boldsymbol{\sigma}'\} \qquad \{\boldsymbol{\sigma}'\} = [\mathbf{T}_\epsilon]^T\{\bar{\boldsymbol{\sigma}}\} \tag{9}$$

and relations for strain transformations

$$\{\bar{\boldsymbol{\epsilon}}\} = [\mathbf{T}_\epsilon]\{\boldsymbol{\epsilon}'\} \qquad \{\boldsymbol{\epsilon}'\} = [\mathbf{T}_\sigma]^T\{\bar{\boldsymbol{\epsilon}}\} \tag{10}$$

and finally, for material transformations as

$$[\bar{\mathbf{C}}] = [\mathbf{T}_\sigma][\mathbf{C}'][\mathbf{T}_\sigma{}^T] \qquad [\mathbf{C}] = [\mathbf{T}_\epsilon{}^T][\bar{\mathbf{C}}][\mathbf{T}_\epsilon] \tag{11}$$

2.2 Elastic Stiffness Formulation

The hybrid stress technique is utilized to form elastic stiffness coefficients. Details on the hybrid method may be found in References [26–30]. The structure of element matrices are defined by the Hellinger-Reissner functional given by

$$\Pi_R = \int_v [(-1/2)\boldsymbol{\sigma}^T\mathbf{S}\boldsymbol{\sigma} + \boldsymbol{\sigma}^T(\mathbf{L}\mathbf{u}_q) - (\mathbf{L}^T\boldsymbol{\sigma})^T\mathbf{u}_\lambda]dv \tag{12}$$

where $\boldsymbol{\sigma}$ is the assumed stress field, $\mathbf{S}$ is the material compliance matrix, $\mathbf{u}_q$ and $\mathbf{u}_\lambda$ are the assumed compatible and incompatible displacement fields, and $\mathbf{L}$ is the differential operator relating strains to displacements.

The assumed stresses are assumed as

$$\boldsymbol{\sigma} = \boldsymbol{P}\boldsymbol{\beta} \tag{13}$$

where $\mathbf{P}$ is a matrix of polynomial terms, and $\boldsymbol{\beta}$ is a vector of undetermined expansion coefficients. The displacement field is assumed over the element domain as

$$\mathbf{u} = \mathbf{u}_q + \mathbf{u}_\lambda \tag{14}$$

in which compatible and incompatible displacement components are given by

$$\mathbf{u}_q = \mathbf{N}\mathbf{q} \tag{15}$$

$$\mathbf{u}_\lambda = \mathbf{M}\lambda \tag{16}$$

where $\mathbf{N}$ and $\mathbf{M}$ are compatible and incompatible displacement shape functions, respectively, $\mathbf{q}$ are nodal displacements, and $\boldsymbol{\lambda}$ are Lagrange multipliers which enforce internal constraints. In the form of equation (12), performing the variation with respect to $\mathbf{u}_\lambda$, the incompatible displacements may be used to variationally enforce *a priori* the field equilibrium conditions through the last term in equation (12) which requires that

$$\delta \int_v (\mathbf{L}^T\boldsymbol{\sigma})^T \mathbf{u}_\lambda dv = 0 \tag{17}$$

or

$$\mathbf{L}^T\boldsymbol{\sigma} = 0 \tag{18}$$

Applying the constraints to the stress modes results in the reduced functional

$$\Pi_R = \int_v [(-1/2)\boldsymbol{\sigma}^T\mathbf{S}\boldsymbol{\sigma} + \boldsymbol{\sigma}^T(\mathbf{L}\mathbf{u}_q)]dv \tag{19}$$

Substituting equations (13), (15), and (16) into (12) yields

$$\Pi_R = \int_v [(-1/2)\boldsymbol{\beta}^T\mathbf{P}^T\mathbf{S}\mathbf{P}\boldsymbol{\beta} + \boldsymbol{\beta}^T\mathbf{P}^T(\mathbf{L}\mathbf{N})\mathbf{q}]dv \tag{20}$$

or

$$\Pi_R = (-1/2)\boldsymbol{\beta}^T\mathbf{H}\boldsymbol{\beta} + \boldsymbol{\beta}^T\mathbf{G}\mathbf{q} \tag{21}$$

where

$$\mathbf{H} = \int_v \mathbf{P}^T\mathbf{S}\mathbf{P}dv \tag{22}$$

$$\mathbf{G} = \int_v \mathbf{P}^T(\mathbf{L}\mathbf{N})dv = \int_v \mathbf{P}^T\mathbf{B}dv \tag{23}$$

Seeking a stationary value of the functional by taking the first variation with respect to $\boldsymbol{\beta}$ yields

$$\boldsymbol{\beta} = \mathbf{H}^{-1}\mathbf{G}\mathbf{q} \tag{24}$$

Substituting the resulting expression for $\boldsymbol{\beta}$ into equation (21), the variation with respect to $\mathbf{q}$ yields the element stiffness matrix as

$$\mathbf{K} = \mathbf{G}^T\mathbf{H}^{-1}\mathbf{G} \tag{25}$$

The element geometry and node numbering are depicted in Figure 5.

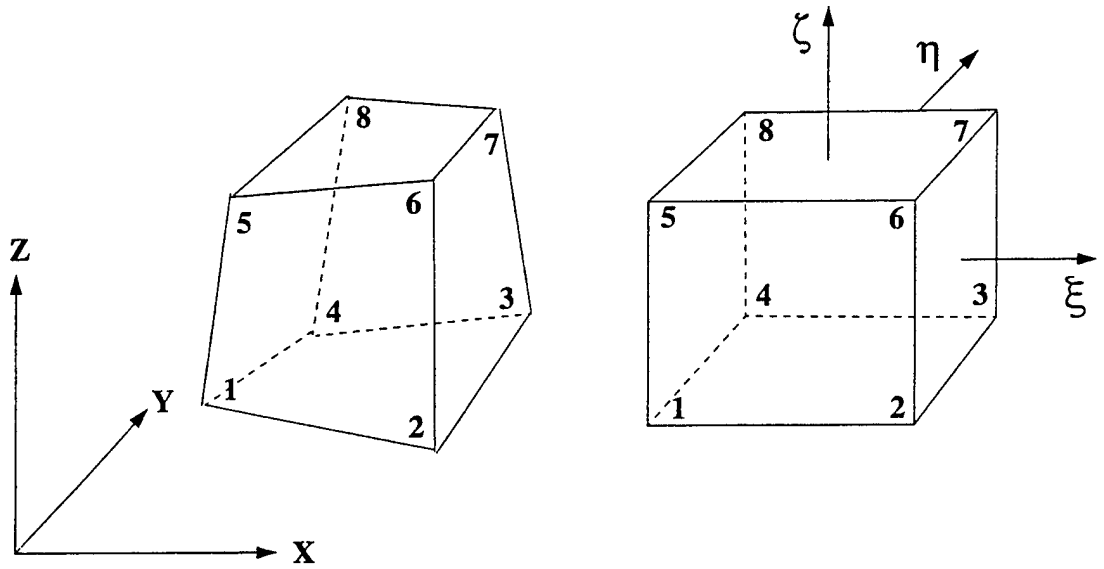

Figure 5. Hexahedral element configuration.

The displacement functions $\mathbf{u}_q$ are given by

$$\mathbf{u}_q = \left\{ \begin{array}{c} u_q \\ v_q \\ w_q \end{array} \right\} = \sum_{i=1}^{8} \frac{1}{8}(1+\xi_i\xi)(1+\eta_i\eta)(1+\zeta_i\zeta) \left\{ \begin{array}{c} u_i \\ v_i \\ w_i \end{array} \right\} \tag{26}$$

The isoparametric mapping between physical and natural coordinates is given by

$$\begin{array}{rcl} x & = & a_0 + a_1\xi + a_2\eta + a_3\zeta + a_4\xi\eta + a_5\xi\zeta + a_6\eta\zeta + a_7\xi\eta\zeta \\ y & = & b_0 + b_1\xi + b_2\eta + b_3\zeta + b_4\xi\eta + b_5\xi\zeta + b_6\eta\zeta + b_7\xi\eta\zeta \\ z & = & c_0 + c_1\xi + c_2\eta + c_3\zeta + c_4\xi\eta + c_5\xi\zeta + c_6\eta\zeta + c_7\xi\eta\zeta \end{array} \tag{27}$$

where

$$\left[\begin{array}{ccc} a_0 & b_0 & c_0 \\ a_1 & b_1 & c_1 \\ a_2 & b_2 & c_2 \\ a_3 & b_3 & c_3 \\ a_4 & b_4 & c_4 \\ a_5 & b_5 & c_5 \\ a_6 & b_6 & c_6 \\ a_7 & b_7 & c_7 \end{array} \right] = \frac{1}{8} \left[\begin{array}{cccccccc} 1 & 1 & 1 & 1 & 1 & 1 & 1 & 1 \\ -1 & 1 & 1 & -1 & -1 & 1 & 1 & -1 \\ -1 & -1 & 1 & 1 & -1 & -1 & 1 & 1 \\ -1 & -1 & -1 & -1 & 1 & 1 & 1 & 1 \\ 1 & -1 & 1 & -1 & 1 & -1 & 1 & -1 \\ 1 & -1 & -1 & 1 & -1 & 1 & 1 & -1 \\ 1 & 1 & -1 & -1 & -1 & -1 & 1 & 1 \\ -1 & 1 & -1 & 1 & 1 & -1 & 1 & -1 \end{array} \right] \left[\begin{array}{ccc} x_1 & y_1 & z_1 \\ x_2 & y_2 & z_2 \\ x_3 & y_3 & z_3 \\ x_4 & y_4 & z_4 \\ x_5 & y_5 & z_5 \\ x_6 & y_6 & z_6 \\ x_7 & y_7 & z_7 \\ x_8 & y_8 & z_8 \end{array} \right] \tag{28}$$

The stress field is initially assumed as complete quadratic expansions in natural or tensor coordinates given by

$$P = \begin{bmatrix} [P_0] & & & & & & \\ & [P_0] & & & & & \\ & & [P_0] & & & & \\ & & & [P_0] & & & \\ & & & & [P_0] & & \\ & & & & & [P_0] & \end{bmatrix} \tag{29}$$

where

$$[\mathbf{P}_0] = [1, \xi, \eta, \zeta, \xi\eta, \eta\zeta, \zeta\xi, \xi^2, \eta^2, \zeta^2] \tag{30}$$

As detailed in by Pian and Tong [26], incompatible displacement functions are assumed such that the polynomial order the total displacement field is cubic thereby yielding a resultant quadratic strain field of the same order as the assumed stresses. The assumed stress modes are then subjected to the constraint given by equation (18), yielding an element stress field with 18 independent stress modes given by

$$\begin{array}{rcl} \tau^{11} &=& \beta_1 + \beta_2\eta + \beta_3\zeta + \beta_4\eta\zeta \\ \tau^{22} &=& \beta_5 + \beta_6\xi + \beta_7\zeta + \beta_8\xi\zeta \\ \tau^{33} &=& \beta_9 + \beta_{10}\xi + \beta_{11}\eta + \beta_{12}\xi\eta \\ \tau^{23} &=& \beta_{13} + \beta_{14}\zeta \\ \tau^{31} &=& \beta_{15} + \beta_{16}\xi \\ \tau^{12} &=& \beta_{17} + \beta_{18}\eta \end{array} \tag{31}$$

To preserve the constant stress terms, the natural stresses are mapped to physical space through a contravariant transformation using Jacobians computed at the element centroid

$$\sigma^{kl} = (J_o)^k_i (J_o)^l_j \tau^{ij} \tag{32}$$

The stress field expressed in physical or Cartesian coordinates is given by

$$P = \begin{bmatrix} [P_1] & [P_2] & [P_3] \end{bmatrix} \tag{33}$$

where

$$[P_1] = \begin{bmatrix} 1.0 & 0.0 & 0.0 & 0.0 & 0.0 & 0.0 \\ 0.0 & 1.0 & 0.0 & 0.0 & 0.0 & 0.0 \\ 0.0 & 0.0 & 1.0 & 0.0 & 0.0 & 0.0 \\ 0.0 & 0.0 & 0.0 & 1.0 & 0.0 & 0.0 \\ 0.0 & 0.0 & 0.0 & 0.0 & 1.0 & 0.0 \\ 0.0 & 0.0 & 0.0 & 0.0 & 0.0 & 1.0 \end{bmatrix} \tag{34}$$

$$[P_2] = \begin{bmatrix} a_1^2\eta & a_1^2\zeta & a_2^2\xi & a_2^2\zeta & a_3^2\xi & a_3^2\eta \\ b_1^2\eta & b_1^2\zeta & b_2^2\xi & b_2^2\zeta & b_3^2\xi & b_3^2\eta \\ c_1^2\eta & c_1^2\zeta & c_2^2\xi & c_2^2\zeta & c_3^2\xi & c_3^2\eta \\ b_1c_1\eta & b_1c_1\zeta & b_2c_2\xi & b_2c_2\zeta & b_3c_3\xi & b_3c_3\eta \\ a_1c_1\eta & a_1c_1\zeta & a_2c_2\xi & a_2c_2\zeta & a_3c_3\xi & a_3c_3\eta \\ a_1b_1\eta & a_1b_1\zeta & a_2b_2\xi & a_2b_2\zeta & a_3b_3\xi & a_3b_3\eta \end{bmatrix} \tag{35}$$

$$[P_3] = \begin{bmatrix} 2a_1a_2\zeta & 2a_2a_3\xi & 2a_1a_3\eta & a_1^2\eta\zeta & a_2^2\xi\zeta & a_3^2\xi\eta \\ 2b_1b_2\zeta & 2b_2b_3\xi & 2b_1b_3\eta & b_1^2\eta\zeta & b_2^2\xi\zeta & b_3^2\xi\eta \\ 2c_1c_2\zeta & 2c_2c_3\xi & 2c_1c_3\eta & c_1^2\eta\zeta & c_2^2\xi\zeta & c_3^2\xi\eta \\ (b_2c_1+b_1c_2)\zeta & (b_2c_3+b_3c_2)\xi & (b_1c_3+b_3c_1)\eta & b_1c_1\eta\zeta & b_2c_2\zeta\xi & b_3c_3\xi\eta \\ (a_2c_1+a_1c_2)\zeta & (a_2c_3+a_3c_2)\xi & (a_1c_3+a_3c_1)\eta & a_1c_1\eta\zeta & a_2c_2\zeta\xi & a_3c_3\xi\eta \\ (a_2b_1+a_1b_2)\zeta & (a_2b_3+a_3b_2)\xi & (a_1b_3+a_3b_1)\eta & a_1b_1\eta\zeta & a_2b_2\zeta\xi & a_3b_3\xi\eta \end{bmatrix} \tag{36}$$

The eight-node hexahedral element formulation based on hybrid element theory is a robust element with excellent behavior in normal stretching and bending deformation modes.

2.3 Modeling Material Nonlinearity

The RESTRAN analysis program supports nonlinear elastic material properties and nonlinear inelastic behavior due to ply-level failures. The combined elastic and inelastic nonlinearities are accommodated in the solution algorithm by assuming that the nonlinear elastic response is independent of material failure and maintains the same differential stress/strain relationship at each point during unloading. As depicted in Figure 6, any reduction in moduli due to the occurrence of a partial failure mode is assumed to result in a stress/strain relation self-similar to the initial nonlinear elastic curve. These two forms of material nonlinearity are processed sequentially. The primary unknown in the overall RESTRAN solution algorithm is the scale factor applied to the initial set of external loads to cause the next failure event. For material failure, this factor is determined by a linear extrapolation using the selected failure criteria and is thus a function of the current stress-strain state. If buckling failure is included, scale factors are also computed to cause the next instability failure. Thus, convergence to the desired equilibrium state requires stationarity of the scaled applied load to cause next failure and force equilibrium between external and internal loads as a function of the nonlinear stress-strain relations. Therefore, the algorithmic implementation in RESTRAN first converges the nonlinear elastic state to obtain the vector of external loads to cause the next failure. This set of loads is then used to compute stresses for evaluation in selected failure criteria. A typical cascade of element material failures is subsequently accounted, and convergence is assumed when no additional ply failures occur due to internal stress redistribution at the current load level.

Assuming small strains, at some applied load level, $\mathbf{F}_k$, the stress/strain relationship may be expressed as

$$\boldsymbol{\sigma}^k = \mathbf{C}^k(\bar{\epsilon})\boldsymbol{\epsilon}^k \tag{37}$$

where $\mathbf{C}^k(\bar{\epsilon})$ is the strain dependent material stiffness matrix, and $\boldsymbol{\sigma}^k$ and $\boldsymbol{\epsilon}^k$ are the stress and strain vectors at the k^{th} load level. For greatest generality, the particular nonlinear stress-strain relation is input into RESTRAN via a user-defined subroutine as described in the user's manual [31].

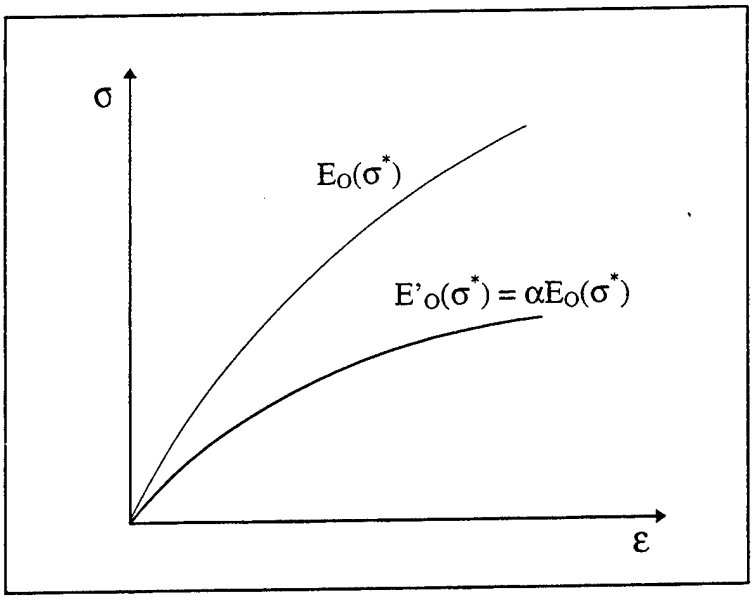

Figure 6. Partial failure in nonlinear elastic material.

To solve the nonlinear system of equations, an iterative scheme is employed to obtain the equilibrium state. Because convergence is sought to the load at which the next failure event will occur, the overall nonlinearity is due to contributions from the nonlinear stress/strain relations, the extrapolations of the selected material failure criteria which may be quadratic, and the calculation of eigenvalues associated with bifurcation buckling states. The potential volatility of the solution suggests a simple iterative approach using updated secant stiffnesses as opposed to more involved tangent matrix methods such as Newton-Rahpson iteration or matrix update schemes such as the BFGS technique. For the k^{th} analysis cycle, iterations are performed such that the sequence of loads, F_i, converge in the limit: F_1, F_2, F_3, $\rightarrow$, P^k. In the current implementation, at the i^{th} iteration, the calculated load multiplier, λ_i, is used to scale loads converged at the last k^{th} analysis cycle to obtain a new set of external loads as

$$\mathbf{F}_i = \lambda_i \mathbf{P}^k \tag{38}$$

The i^{th} approximation to the total displacements, $\mathbf{D_i}$, and stress dependent secant stiffness are used to compute the internal load, Q_i, as

$$\mathbf{Q}_i = \mathbf{K}_i \mathbf{D}_i \tag{39}$$

The residual load vector measuring the difference between external and internal loads, R_i, is obtained from

$$\mathbf{\Delta R}_i = \mathbf{F}_i - \mathbf{Q}_i \tag{40}$$

The increment in displacements is calculated using the residual as

$$\mathbf{\Delta D}_{i+1} = \mathbf{K}_i^{-1} \mathbf{\Delta R}_i \tag{41}$$

and the new estimate for total displacements satisfying equilibrium is given by

$$\mathbf{D}_{i+1} = \mathbf{D}_i + \Delta\mathbf{D}_{i+1} \tag{42}$$

In the course of determining a sequence of scale factors to precipitate the next failure, the secant moduli act to stabilize convergence for the case of changing external loads which may increase or decrease during iterations due to extapolations made from nonlinear failure criteria. This scheme is depicted in Figure 7.

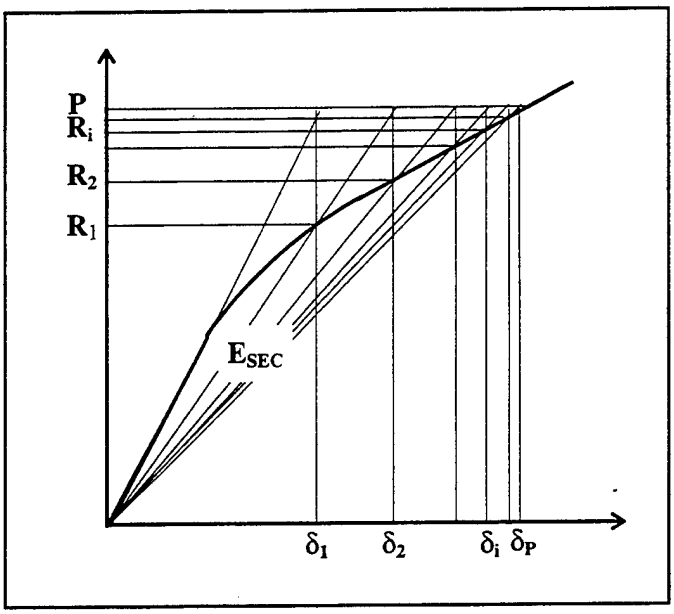

Figure 7. Iterative solution for nonlinear materials.

This nonlinear solution procedure is sufficient for weakly to moderately nonlinear systems. The extrapolated scale factors obtained from material failure criteria and the eigenvalues obtained from linear stability analysis function as line searches towards the desired minimum scale factor to cause the next failure event.

Iterations are continued until the vector norm of the residual load vector is less than a prescribed tolerance

$$|\Delta\mathbf{R}_i| \leq Tol \tag{43}$$

Because nonlinearities present in the system may shift the target applied load to cause the next failure, a modification of the current scale factor is made to damp out oscillations and speed convergence. At the i^{th} iteration, the scale factor, λ_i, is formed as a product accounting

for the previous estimate for the next failure λ_{i-1} and the scale factor obtained directly from the selected failure criteria, α_i. This relationship is expressed as

$$\lambda_i = \lambda_{i-1}\alpha_i \tag{44}$$

The estimate for α_i is modified using a biasing factor, β_i, to speed convergence. This modification is given by

$$\lambda_i = \begin{cases} \lambda_{i-1}[1 + (\frac{1}{2} + \beta)(\alpha_i - 1)] & for \quad \alpha_i > 1 \\ \lambda_{i-1}[\alpha_i + (\frac{1}{2} - \beta)(1 - \alpha_i)] & for \quad \alpha_i < 1 \end{cases} \tag{45}$$

where the biasing factor is formed as an accumulated sum based on all previous estimates for α_i as

$$\beta_i = \frac{1}{2} + \sum_{k=1}^{i} \frac{\alpha_k}{|\alpha_k|}(\frac{1}{10}) \tag{46}$$

and subjected to the restriction that $0.1 \leq \beta_i \leq 0.9$. When the nonlinear system of equations has converged to an equilibrim state corresponding to the applied load $\mathbf{P}^k$, ply failures or sublaminate instabilities are then processed.

2.4 Modeling Geometric Nonlinearity

Geometric instability in impact damaged laminated structures constitutes an important and common failure mode which results in local or global buckling failure. These modes become prevalent when the damage state contains significant regions of reduced stiffness due to material failure or extended planes of delaminations between ply groups. Buckling defines an unstable equilibrium state at which the structure cannot elastically resist an infinitesimal departure from the current configuration under the applied loads. This condition is characterized by the change in the total potential energy associated with an arbitrary displacement, δq, from equilibrium is an extremum or equivalently, that the total potential satisfies the Trefftz criterion [32] given by

$$\mathbf{\Pi} = \mathbf{U} + \mathbf{V} \tag{47}$$

and

$$\frac{\delta^2 \mathbf{\Pi}}{\delta \phi^2} = 0 \tag{48}$$

in which $\mathbf{\Pi}$ is the total potential, $\mathbf{U}$ is the strain energy, $\mathbf{V}$ is the potential energy, and ϕ is the generalized displacement. In the linear theory of buckling, a solution is sought at the point where the locus of equilibrium states bifurcate, as depicted in Figure 8.

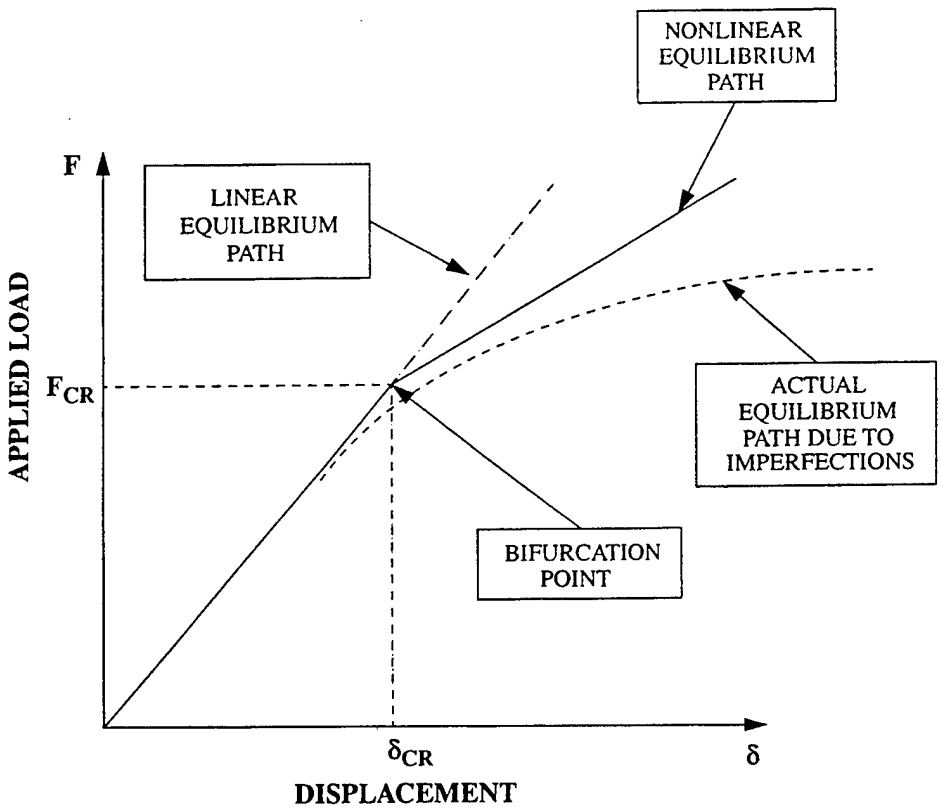

Figure 8. Bifurcation of equilibrium states.

In order to approximate the nonlinear geometric buckling behavior, higher-order strain terms are used to compute the differential or geometric stiffness matrix $\mathbf{K}_\sigma$. The geometric stiffness matrix is formulated using the assumed displacement fields in (26) and is given by

$$[\mathbf{K}_\sigma] = \int_v [\mathbf{B}_{NL}]^T [\mathbf{\Gamma}][\mathbf{B}_{NL}] dv \tag{49}$$

where

$$[\mathbf{\Gamma}] = \begin{bmatrix} [\mathbf{S}] & \mathbf{0} & \mathbf{0} \\ \mathbf{0} & [\mathbf{S}] & \mathbf{0} \\ \mathbf{0} & \mathbf{0} & [\mathbf{S}] \end{bmatrix} \tag{50}$$

and

$$[\mathbf{S}] = \begin{bmatrix} \sigma_{xx0} & \tau_{xy0} & \tau_{zx0} \\ \tau_{xy0} & \sigma_{yy0} & \tau_{yz0} \\ \tau_{xz0} & \tau_{yz0} & \sigma_{zz0} \end{bmatrix} \tag{51}$$

The $\mathbf{B}_{NL}$ matrix is given by

$$[\mathbf{B}_{NL}] = \begin{bmatrix} [\mathbf{G}] & \mathbf{0} & \mathbf{0} \\ \mathbf{0} & [\mathbf{G}] & \mathbf{0} \\ \mathbf{0} & \mathbf{0} & [\mathbf{G}] \end{bmatrix} \tag{52}$$

where

$$[\mathbf{G}] = \begin{bmatrix} \mathbf{N}_{1,x} & \mathbf{0} & \mathbf{0} & \mathbf{N}_{2,x} & \dots & \mathbf{N}_{8,x} \\ \mathbf{N}_{1,y} & \mathbf{0} & \mathbf{0} & \mathbf{N}_{2,y} & \dots & \mathbf{N}_{8,y} \\ \mathbf{N}_{1,z} & \mathbf{0} & \mathbf{0} & \mathbf{N}_{2,z} & \dots & \mathbf{N}_{8,z} \end{bmatrix} \tag{53}$$

The resulting nonlinear equilibrium relationship is given by

$$(\mathbf{K} + \mathbf{K}_\sigma)\mathbf{X} = \mathbf{R} \tag{54}$$

Determining the load level at which bifurcation occurs requires the solution to the following generalized eigenvalue problem

$$(\mathbf{K} - \lambda \mathbf{K}_\sigma)\mathbf{X} = \mathbf{0} \tag{55}$$

The critical buckling load is then given by

$$\mathbf{R}_{crit} = \lambda \mathbf{R} \tag{56}$$

where λ corresponds to the lowest positive eigenvalue of the global system.

For large systems wherein a small set of eigenvalues are sought, algorithms have been incorporated into RESTRAN based on subspace iteration [33-40]. The basic subspace iteration utilizes an initial set of iteration vectors, $\mathbf{X}_k$, which are selected to span the space defined by the desired eigenvectors, $\mathbf{\Phi}$, with the corresponding eigenvalues, $\mathbf{\Delta}$. Iterations are then performed to converge the eigenvectors and eigenvalues in the limit

$$\mathbf{\Lambda}_k \longrightarrow \mathbf{\Delta} \;\; and \;\; \mathbf{X}_k \longrightarrow \mathbf{\Phi} \;\; as \;\; k \longrightarrow \infty \tag{57}$$

The subspace mapping is defined by

$$\mathbf{K}\bar{\mathbf{X}}_{k+1} = \mathbf{K}_\sigma \mathbf{X}_k \tag{58}$$

The mapping or iteration vectors are selected in accordance with procedures outlined by Bathe [33]. The selection is specified such that the first column in $\mathbf{X}$ is taken as the diagonal in $\mathbf{K}_\alpha$, while remaining columns are assigned a unit value in the row position corresponding to $min(k_{ii}/k_{\alpha ii})$. The global elastic and differential stiffness matrices are then mapped into the subspace as

$$\bar{\mathbf{K}}_{k+1} = \bar{\mathbf{X}}_{k+1}^T \mathbf{K} \bar{\mathbf{X}}_{k+1} \tag{59}$$

$$\bar{\mathbf{K}}_{\sigma_{k+1}} = \bar{\mathbf{X}}_{k+1}^T \mathbf{K}_\sigma \bar{\mathbf{X}}_{k+1} \tag{60}$$

resulting in the reduced eigenvalue problem given by

$$\mathbf{K}_{k+1}\mathbf{Q}_{k+1} = \mathbf{K}_{\sigma_{k+1}}\mathbf{Q}_{k+1}\mathbf{\Lambda}_{k+1} \tag{61}$$

where Λ is a diagonal matrix of the system eigenvalues. Because the initial iteration vectors are usually approximate, an improvement to the system eigenvectors is given by

$$\mathbf{X}_{k+1} = \bar{\mathbf{X}}_{k+1}\mathbf{Q}_{k+1} \tag{62}$$

and an iteration of the subspace is continued until the desired set of eigenvalues at the $(k+1)^{st}$ iteration reach a stationary value defined by a tolerance as

$$\frac{|\lambda_i^{k+1} - \lambda_i^k|}{|\lambda_i^{k+1}|} \leq tol \quad , \quad i = 1, 2, 3, ..., n \tag{63}$$

During iterations, a check is made to ensure that the smallest eigenvalues are being obtained by using the Sturm sequence property of the characteristic polynomials of eigensystems. If a shift μ is introduced slightly greater than the current estimate of λ_n, the factorization

$$\mathbf{K}_s = \mathbf{K} - \mu\mathbf{K}_\sigma = \mathbf{L}\mathbf{D}\mathbf{L}^T \tag{64}$$

yields a diagonal matrix $\mathbf{D}$, in which the number of negative diagonals is equal to the number of eigenvalues smaller than μ.

An additional eigenvalue extraction technique has been implemented in RESTRAN, which is based on the Arnoldi method and is a powerful extension of subspace iteration [34,35]. After reducing the generalized eigenvalue problem definition to a standard format through a Cholesky reduction of $\mathbf{K} = \mathbf{L^T L}$, pre- and post-multiplying $\mathbf{K}_\sigma$ such that

$$A = L^{-1}K_\sigma L \tag{65}$$

yields a symmetric $\mathbf{A}$ matrix. Arnoldi's method for finding a few eigenvalues of $\mathbf{A}$ proceeds as follows: given an initial vector $\mathbf{x_1}$ with unit norm, at each step m construct an orthonormal basis $\mathbf{X_m} = [\mathbf{x_1}, \mathbf{x_2}, ..., \mathbf{x_m}]$ for the Kyrlov subspace $\mathbf{K_m}$ spanned by $[\mathbf{x_1}, \mathbf{Ax_1}, ..., \mathbf{A^{m-1}x_1}]$ by computing $\mathbf{w} = \mathbf{Ax_{m1}}$ and orthonormalizing $\mathbf{w}$ with respect to $\mathbf{x_1}, \mathbf{x_2}, ..., \mathbf{x_{m-1}}$ to obtain $\mathbf{x_m}$. The matrix $\mathbf{H} = \mathbf{X^T A X}$ is upper Hessenberg, and its eigenvalues provide approximations to m eigenvalues of $\mathbf{A}$. The main steps in the basic Arnoldi algorithm for finding λ_i may be summarized as follows:

1. *Initialization*: Choose the number of steps m and an initial vector $\mathbf{x_1}$ with unit norm.

2.*Arnoldi steps* for j = 1, 2, ... , m:

(a) $\mathbf{w_j} = \mathbf{Ax_j}$
(b) $\mathbf{h_{ij}} = \mathbf{x_i^T w_j}, \quad \mathbf{i = 1, 2, ..., j}.$
(c) $\mathbf{s_j} = \mathbf{w_j} - \sum_{\mathbf{j=1}}^{\mathbf{j}} \mathbf{x_i h_{ij}}$
(d) $\mathbf{h_{j+1,j}} = ||\mathbf{s_j}||_2, \quad \mathbf{x_{j+1}} = \mathbf{s_j / h_{j+1,j}}.$

Set $\mathbf{X} = [\mathbf{x_1}, \mathbf{x_2}, ..., \mathbf{x_m}]$

3. *Eignevalue computation*: Reduce the upper Hessenberg matrix $\mathbf{H} = \{\mathbf{h_{ij}}\}$ to real Schur

form $\mathbf{T} = \mathbf{Z}^T\mathbf{H}\mathbf{Z}$, where $\mathbf{T}$ is a block triangular matrix with the eigenvalues, λ_i, ordered in descending order of their absolute values along the diagonal. Set $\mathbf{X} = \mathbf{X}\mathbf{Z}$.

4. *Convergence test*: If the first column $\mathbf{x_i}$ of $\mathbf{X}$ satisfies the convergence criteria for the residual

$$\mathbf{res_i} = \frac{||(\mathbf{AX} - \mathbf{XT})_i||_2}{||\mathbf{A}||_2} \tag{66}$$

then accept λ_1; otherwise, return to step 2 and repeat.

In a complex structure, the various load paths will yield positive and negative eigenvalues corresponding to load multipliers to cause a buckling failure. For the automated interpretation of instability failure, if all eigenvalues are negative or complex, no reversal of input loads is considered; it is assumed that either the initial set of applied loads preclude a buckling response or that element failures have progressed to a terminal failure state. In the event of severe numerical difficulty in obtaining eigenvalues due to widespread material degradation, the stability analysis is bypassed, and any further failure events prior to prediction of catastrophic collapse are accounted through material failure modes.

3 Laminated Material Representation

RESTRAN is formulated to represent layered materials such as laminated composites. In such a representation, the material is assumed to consist of an assemblage of orthotropic laminae or plies. The discretization of the model into finite elements associates the element properties with a single ply or with a number of plies forming a local sublaminate group.

3.1 Effective Material Moduli

An effective approximation to the the mechanical properties of an assembled sublaminate is obtained by averaging ply properties. For thin, plate-like structures under long-wavelength loading, classical lamination theory (CLT) has been adequate for obtaining overall mechanical response [41,42]. For thick laminates, however, more accurate formulations for effective three-dimensional properties have been developed [43-45] of which the formulation of Sun and Liao [45] has been incorporated into RESTRAN.

The sublaminate constitutive relationship is assumed as

$$\begin{Bmatrix} \sigma_{xx} \\ \sigma_{yy} \\ \sigma_{zz} \\ \sigma_{yz} \\ \sigma_{zx} \\ \sigma_{xy} \end{Bmatrix} = [\bar{\mathbf{C}}] \begin{Bmatrix} \epsilon_{xx} \\ \epsilon_{yy} \\ \epsilon_{zz} \\ \epsilon_{yz} \\ \epsilon_{zx} \\ \epsilon_{xy} \end{Bmatrix} \tag{67}$$

where the $[\bar{\mathbf{C}}]$ matrix is assumed to be constituted by lamina which may be generally orthotropic and described by nine independent material moduli. In general, the assembled material stiffness matrix may possess only symmetry about z = 0 and assume an anisotropic monoclinic form given by

$$[\bar{\mathbf{C}}] = \begin{bmatrix} \bar{C}_{11} & \bar{C}_{12} & \bar{C}_{13} & 0 & 0 & \bar{C}_{16} \\ \bar{C}_{21} & \bar{C}_{22} & \bar{C}_{23} & 0 & 0 & \bar{C}_{26} \\ \bar{C}_{31} & \bar{C}_{32} & \bar{C}_{33} & 0 & 0 & \bar{C}_{36} \\ 0 & 0 & 0 & \bar{C}_{44} & \bar{C}_{45} & 0 \\ 0 & 0 & 0 & \bar{C}_{54} & \bar{C}_{55} & 0 \\ \bar{C}_{61} & \bar{C}_{62} & \bar{C}_{63} & 0 & 0 & \bar{C}_{66} \end{bmatrix} \tag{68}$$

The effective three-dimensional components $\bar{C}_{ij}$ are given by

$$\bar{C}_{11} = \sum_{k=1}^{N} \nu_k \bar{Q}_{11}^k + \sum_{k=2}^{N} (\bar{Q}_{13}^k - \lambda_{13}) \nu_k (\bar{Q}_{13}^1 - \bar{Q}_{13}^k) / \bar{Q}_{33}^k \tag{69}$$

$$\bar{C}_{12} = \sum_{k=1}^{N} \nu_k \bar{Q}_{12}^k + \sum_{k=2}^{N} (\bar{Q}_{13}^k - \lambda_{13}) \nu_k (\bar{Q}_{23}^1 - \bar{Q}_{23}^k) / \bar{Q}_{33}^k \tag{70}$$

$$\bar{C}_{13} = \sum_{k=1}^{N} \nu_k \bar{Q}_{13}^k + \sum_{k=2}^{N} (\bar{Q}_{33}^k - \lambda_{33}) \nu_k (\bar{Q}_{13}^1 - \bar{Q}_{13}^k) / \bar{Q}_{33}^k \tag{71}$$

$$\bar{C}_{16} = \sum_{k=1}^{N} \nu_k \bar{Q}_{16}^k + \sum_{k=2}^{N} (\bar{Q}_{13}^k - \lambda_{13}) \nu_k (\bar{Q}_{36}^1 - \bar{Q}_{36}^k) / \bar{Q}_{33}^k \tag{72}$$

$$\bar{C}_{22} = \sum_{k=1}^{N} \nu_k \bar{Q}_{22}^k + \sum_{k=2}^{N} (\bar{Q}_{23}^k - \lambda_{23}) \nu_k (\bar{Q}_{26}^1 - \bar{Q}_{26}^k) / \bar{Q}_{33}^k \tag{73}$$

$$\bar{C}_{23} = \sum_{k=1}^{N} \nu_k \bar{Q}_{23}^k + \sum_{k=2}^{N} (\bar{Q}_{33}^k - \lambda_{33}) \nu_k (\bar{Q}_{23}^1 - \bar{Q}_{23}^k) / \bar{Q}_{33}^k \tag{74}$$

$$\bar{C}_{26} = \sum_{k=1}^{N} \nu_k \bar{Q}_{26}^k + \sum_{k=2}^{N} (\bar{Q}_{23}^k - \lambda_{23}) \nu_k (\bar{Q}_{36}^1 - \bar{Q}_{36}^k) / \bar{Q}_{33}^k \tag{75}$$

$$\bar{C}_{33} = \left(\sum_{k=1}^{N} \frac{\nu_k}{\bar{Q}_{16}^k} \right)^{-1} \tag{76}$$

$$\bar{C}_{36} = \sum_{k=1}^{N} \nu_k \bar{Q}_{36}^k + \sum_{k=2}^{N} (\bar{Q}_{33}^k - \lambda_{33}) \nu_k (\bar{Q}_{36}^1 - \bar{Q}_{36}^k) / \bar{Q}_{33}^k \tag{77}$$

$$\bar{C}_{44} = \left(\sum_{k=1}^{N} \nu_k \bar{Q}_{44}^k \right) / \Delta \tag{78}$$

$$\bar{C}_{45} = \left(\sum_{k=1}^{N} \nu_k \bar{Q}_{45}^k \right) / \Delta \tag{79}$$

$$\bar{C}_{55} = \left(\sum_{k=1}^{N} \nu_k \bar{Q}^k_{55}\right)/\Delta \tag{80}$$

where

$$\lambda_{13} = \bar{C}_{13} \quad \lambda_{23} = \bar{C}_{23} \quad \lambda_{33} = \bar{C}_{33} \quad \lambda_{36} = \bar{C}_{36} \tag{81}$$

$$\Delta = \left(\sum_{k=1}^{N} \frac{\nu_k \bar{Q}^K_{44}}{\Delta_k}\right)\left(\sum_{k=1}^{N} \frac{\nu_k \bar{Q}^K_{55}}{\Delta_k}\right) - \left(\sum_{k=1}^{N} \frac{\nu_k \bar{Q}^K_{44}}{\Delta_k}\right)^2 \tag{82}$$

$$\Delta_k = \bar{Q}^k_{44}\bar{Q}^k_{55} - \bar{Q}^k_{45} \qquad \nu_k = h_k/H \tag{83}$$

The transformed stiffnesses for the k^{th} ply are given by

$$\begin{aligned}
\bar{Q}^k_{11} &= Q^k_{11}cos^4\theta^k + Q^k_{22}sin^4\theta^k + 2Q^k_{12}sin^2\theta^k cos^2\theta^k + 4Q^k_{66}cos^2\theta^k sin^2\theta^k \\
\bar{Q}^k_{22} &= Q^k_{11}sin^4\theta^k + Q^k_{22}cos^4\theta^k + 2(Q^k_{12} + 2Q^k_{66})sin^2\theta^k cos^2\theta^k \\
\bar{Q}^k_{33} &= Q^k_{33} \\
\bar{Q}^k_{44} &= Q^k_{44}cos^2\theta^k + Q^k_{55}sin^2\theta^k \\
\bar{Q}^k_{55} &= Q^k_{55}cos^2\theta^k + Q^k_{44}sin^2\theta^k \\
\bar{Q}^k_{66} &= Q^k_{66} + (Q^k_{11} + Q^k_{22} - 2Q^k_{12} - 4Q^k_{66})sin^2\theta^k cos^2\theta^k \\
\bar{Q}^k_{12} &= Q^k_{12} + (Q^k_{11} + Q^k_{22} - 2Q^k_{12} - 4Q^k_{66})sin^2\theta^k cos^2\theta^k \\
\bar{Q}^k_{13} &= Q^k_{13}cos^2\theta^k + Q^k_{23}sin^2\theta^k \\
\bar{Q}^k_{23} &= Q^k_{13}sin^2\theta^k + Q^k_{23}cos^2\theta^k \\
\bar{Q}^k_{16} &= (Q^k_{11}cos^2\theta^k - Q^k_{22}sin^2\theta^k - cos2\theta^k(Q^k_{12} + 2Q^k_{66}))cos\theta^k sin\theta^k \\
\bar{Q}^k_{26} &= (Q^k_{11}sin^2\theta^k - Q^k_{22}cos^2\theta^k + cos2\theta^k(Q^k_{12} + 2Q^k_{66}))sin\theta^k cos\theta^k \\
\bar{Q}^k_{36} &= (Q^k_{13} - Q^k_{23})sin\theta^k cos\theta^k \\
\bar{Q}^k_{45} &= (Q^k_{55} - Q^k_{44})sin\theta^k cos\theta^k
\end{aligned} \tag{84}$$

in which

$$\begin{aligned}
Q^k_{11} &= E^k_1(1 - \nu^k_{23}\nu^k_{32})/(E^k_2 E^k_3 \Omega^k) \\
Q^k_{12} &= E^k_2(\nu^k_{12} + \nu^k_{32}\nu^k_{13})/(E^k_1 E^k_3 \Omega^k) \\
Q^k_{13} &= E^k_3(\nu^k_{13} + \nu^k_{12}\nu^k_{23})/(E^k_1 E^k_2 \Omega^k) \\
Q^k_{22} &= E^k_2(1 - \nu^k_{13}\nu^k_{31})/(E^k_1 E^k_3 \Omega^k) \\
Q^k_{23} &= E^k_3(\nu^k_{23} + \nu^k_{21}\nu^k_{13})/(E^k_1 E^k_2 \Omega^k) \\
Q^k_{33} &= E^k_3(1 - \nu^k_{12}\nu^k_{21})/(E^k_1 E^k_2 \Omega^k) \\
Q^k_{44} &= G^k_{23} \\
Q^k_{55} &= G^k_{31} \\
Q^k_{66} &= G^k_{12}
\end{aligned} \tag{85}$$

and

$$\nu^k_{21} = \nu^k_{12}(E^k_2/E^k_1)$$

$$\begin{aligned} \nu_{32}^k &= \nu_{23}^k(E_3^k/E_2^k) \\ \nu_{31}^k &= \nu_{13}^k(E_3^k/E_1^k) \\ \Omega^k &= (1-\nu_{12}^k\nu_{21}^k-\nu_{23}^k\nu_{32}^k-\nu_{13}^k\nu_{31}^k-2\nu_{21}^k\nu_{32}^k\nu_{13}^k) \end{aligned} \tag{86}$$

E_{ij}, G_{ij}, ν_{ij} and θ are the Young's normal and shear moduli, Poisson ratios and fiber orientation angle, respectively.

In the case of a composite material system with a balanced $[\pm\Theta]$ layup, the effective material properties reduce to those obtained using classical three-dimensional lamination theory in which the material stiffnesses coefficients, $\mathbf{C}_{ij}$, are obtained simply as

$$\mathbf{C}_{ij} = \frac{1}{H}\sum_{k=1}^{N} h_k \bar{\mathbf{Q}}_{ij}^k \tag{87}$$

where H is the local sublaminate thickness, h_k are the individual ply thicknesses and N is the total number of plies in the sublaminate.

The assumption of a layered medium permits the modeling of a large class of material systems: laminated composites, sandwich-type constructions, piecewise linear approximations to homogeneous materials with varying properties, and isotropic materials represented as a single ply.

3.2 Ply-Level Stress and Strain Recovery

The effective material constitutive relationship developed by Sun and Liao [45] is based on the assumption of long wavelength loading and that the thickness of the sublaminate is small compared to the total laminate thickness. This leads to the consequence that in the recovery of average or effective stresses and strains at the element level using

$$\{\bar{\boldsymbol{\epsilon}}\} = [\mathbf{B}]\{\mathbf{u}\} \qquad\qquad \{\bar{\boldsymbol{\sigma}}\}[\bar{\mathbf{C}}] = \{\bar{\boldsymbol{\epsilon}}\} \tag{88}$$

where $[\mathbf{B}]$ is the strain-displacement matrix and $\{\mathbf{u}\}$ is the displacement vector, the inplane strains and transverse normal stresses are assumed constant. This condition may be stated as

$$\begin{aligned} \bar{\epsilon}_{xx} &= \epsilon_{xx}^k, \quad \bar{\epsilon}_{yy} = \epsilon_{yy}^k, \quad \bar{\epsilon}_{xy} = \epsilon_{xy}^k \\ \bar{\sigma}_{zz} &= \sigma_{zz}^k, \quad \bar{\sigma}_{yz} = \sigma_{yz}^k, \quad \bar{\sigma}_{zx} = \sigma_{zx}^k \end{aligned} \tag{89}$$

Using the constitutive relation for the k^{th} ply given by

$$\{\boldsymbol{\sigma}^k\} = [\mathbf{C}^k]\{\boldsymbol{\epsilon}^k\} \tag{90}$$

the following equation for the out-of-plane stresses results in

$$\begin{Bmatrix} \sigma_{zz} \\ \sigma_{yz} \\ \sigma_{xz} \end{Bmatrix}_k = \begin{Bmatrix} \bar{\sigma}_{zz} \\ \bar{\sigma}_{yz} \\ \bar{\sigma}_{xz} \end{Bmatrix} = \begin{bmatrix} C_{31} & C_{32} & C_{36} \\ C_{41} & C_{42} & C_{46} \\ C_{51} & C_{52} & C_{56} \end{bmatrix}_k \begin{Bmatrix} \bar{\epsilon}_{xx} \\ \bar{\epsilon}_{yy} \\ \bar{\epsilon}_{xy} \end{Bmatrix}_k + \begin{bmatrix} C_{33} & C_{34} & C_{35} \\ C_{43} & C_{44} & C_{45} \\ C_{53} & C_{54} & C_{55} \end{bmatrix}_k \begin{Bmatrix} \bar{\epsilon}_{zz} \\ \bar{\epsilon}_{yz} \\ \bar{\epsilon}_{zx} \end{Bmatrix}_k \tag{91}$$

and the unknown out-of-plane strain components may then be calculated from

$$\left\{ \begin{array}{c} \epsilon_{zz} \\ \epsilon_{yz} \\ \epsilon_{zx} \end{array} \right\}_k = \left[\begin{array}{ccc} C_{33} & C_{34} & C_{35} \\ C_{43} & C_{44} & C_{45} \\ C_{53} & C_{54} & C_{55} \end{array} \right]_k^{-1} \left\{ \left\{ \begin{array}{c} \sigma_{zz} \\ \sigma_{yz} \\ \sigma_{xz} \end{array} \right\}_k - \left[\begin{array}{ccc} C_{31} & C_{32} & C_{36} \\ C_{41} & C_{42} & C_{46} \\ C_{51} & C_{52} & C_{56} \end{array} \right]_k \left\{ \begin{array}{c} \bar{\epsilon}_{zz} \\ \bar{\epsilon}_{yz} \\ \bar{\epsilon}_{zx} \end{array} \right\}_k \right\} \tag{92}$$

With the complete strain vector for the k^{th} ply layer determined, the remaining stress components are obtained using equation (90).

3.3 Nonlinear Elastic Moduli

As shown in Figure 9, nonlinear elastic materials are those which exhibit a nonlinear stress/ strain response under applied loads. Many nonlinear materials exhibit an elastic response below the fracture or yield limit in which deflections follow the same load-displacment curve without permanent deformation under unloading. The material moduli for these materials may therefore be expressed as continuous functions of the stress or strain state as

$$\mathbf{C_{ij}} = \mathbf{C_{ij}}(\sigma^*, \epsilon^*) \tag{93}$$

where σ^* and ϵ^* represent individual stress or strain components or combined measures that represent unit potential energy or strain energy density.

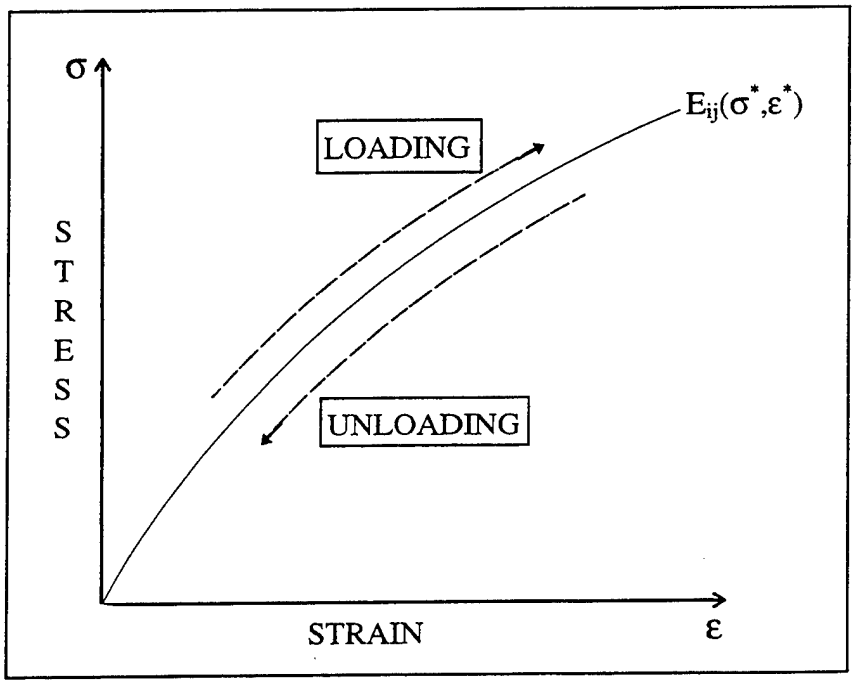

Figure 9. Nonlinear elastic stress-strain relation.

For greatest generality in defining nonlinear properties, nonlinear stress/strain relations are input as secant moduli from a required user-defined subroutine. This subroutine may be written in FORTRAN or C, and then compiled to link with the main RESTRAN executable. Through a standardized arqument interface, RESTRAN provides stresses and strains interpolated to each ply and at element integration or Guass points. The user-defined routine must calculate reduction factors, ψ_i, which are used to obtain current measures of the secant material moduli depicted in Figure 10. The secant moduli are computed as

$$\begin{aligned} \bar{E}_1^k &= \psi_1 E_1^k \\ \bar{E}_2^k &= \psi_2 E_2^k \\ \bar{E}_3^k &= \psi_3 E_3^k \\ \bar{G}_{23}^k &= \psi_4 G_{23}^k \\ \bar{G}_{31}^k &= \psi_5 G_{31}^k \\ \bar{G}_{12}^k &= \psi_6 G_{12}^k \end{aligned} \tag{94}$$

A full description of this subroutine is contained in the RESTRAN User's Manual [31].

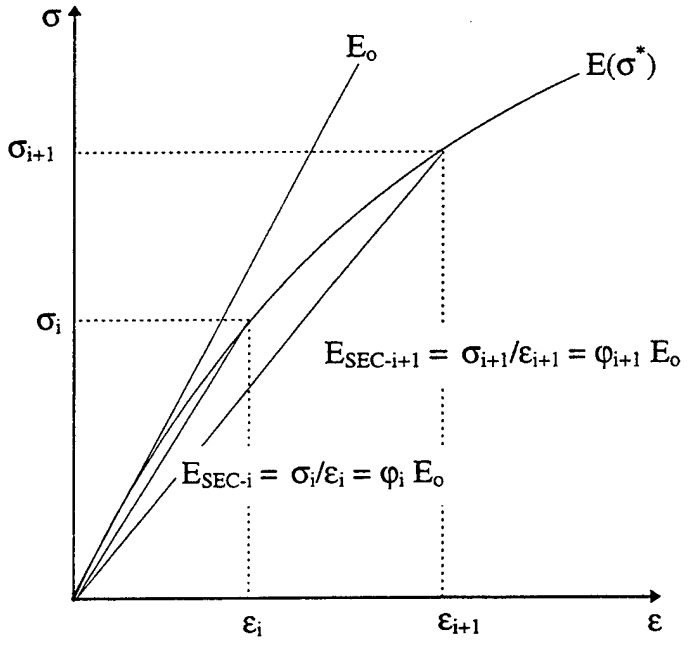

Figure 10. Secant moduli depiction.

4 Material Failure Modes

Composite materials exhibit a wide range of failure modes including microscopic fiber breakage, shear–out failure, kink band formation, and microbuckling, matrix tensile cracking and compressive failure, and macroscopic multilayered delamination growth. The RESTRAN analysis code models various material failure modes at the element ply level using selected failure criteria and associated damage laws. The current implementation of material failure prediction is restricted to criteria defined at a point. Nonlocal failure criteria based on averaged stress or strain values necessarily require the definition of characteristic integration paths which would extend over many element domains and is difficult to automate in a progressive failure analysis without introducing some degree of problem specificity. In addition, failure modes associated with delamination extension are currently not accounted for.

In order to maximize versatility by allowing specialized tailoring of the analysis, RESTRAN incorporates user-defined subroutine interfaces to allow any material failure criterion and damage law to be applied. The format for these subroutines are discussed in detail in the RESTRAN User's Manual [31].

4.1 Material Failure Criteria

A primary consideration in the analysis of residual strength in composite structures is the accurate prediction of ply failure due to a specific state of stress. In composite materials, the micromechanical complexity of the ply material makes the analysis of local failure difficult. Under applied external loading, the local stresses contribute to a large number of identifiable failure interactions and damage modes, any one of which can become a critical 'weak–link' in the prediction of ply failure. A large number of criteria have been derived to relate internal stresses and experimental measures of material strength to the onset of failure [46-58]. All criteria may be classed as degenerate cases of the general tensor polynomial failure criterion which has been developed with the general form given by

$$FI = F_i\sigma_i + F_{ij}\sigma_i\sigma_j + F_{ijk}\sigma_i\sigma_j\sigma_k + ... \tag{95}$$

where σ_i are stress tensor components in principal material directions, F_i, F_{ij}, F_{ijk} are components of the strength tensors, and FI is the failure index which predicts failure when $FI \geq 1$. For practical applications, the terms in equation (95) higher than quadratic are usually set to zero due to the diminishing returns of including higher-order polynomial terms in predicting failure together with the increased cost of experimentally determining these higher–order strength components.

Developed failure criteria exhibit a wide range of predictive capability. The simplest utilize individual stress or strain component relations in which each component is assumed to act independently while other criteria account for coupling and interactions in the stress/strain

state. In addition, many criteria simply predict an unidentified failure state, while others differentiate between competing failure modes. For use in failure criteria, principal tensor components are computed for each layer in laminated composites along longitudinal, transverse, and normal ply coordinates. For laminates exhibiting monoclinic, orthotropic, or transversely isotropic material properties, global stresses in the local (x',y',z') coordinate system are first mapped into the local material $(\bar{x}, \bar{y}, \bar{z})$ coordinate system if the laminate is arbitrarily oriented in space. Next, principal ply stresses in the lamina (1,2,3) coordinate system are obtained using direction cosines which are determined soley by the fiber orientation angle. This transformation is given by

$$\begin{Bmatrix} \sigma_1 \\ \sigma_2 \\ \sigma_3 \\ \sigma_{23} \\ \sigma_{31} \\ \sigma_{12} \end{Bmatrix} = \begin{bmatrix} l_1^2 & m_1^2 & 0 & 0 & 0 & 2l_1m_1 \\ l_2^2 & m_2^2 & 0 & 0 & 0 & 2l_2m_2 \\ 0 & 0 & 1 & 0 & 0 & 0 \\ 0 & 0 & 0 & m_2 & l_2 & 0 \\ 0 & 0 & 0 & m_1 & l_1 & 0 \\ l_1l_2 & m_1m_2 & 0 & 0 & 0 & l_1m_2 + l_2m_1 \end{bmatrix} \begin{Bmatrix} \sigma_{xx} \\ \sigma_{yy} \\ \sigma_{zz} \\ \sigma_{yz} \\ \sigma_{zx} \\ \sigma_{xy} \end{Bmatrix} \tag{96}$$

Principal strains are obtained similarily as

$$\begin{Bmatrix} \epsilon_1 \\ \epsilon_2 \\ \epsilon_3 \\ \epsilon_{23} \\ \epsilon_{31} \\ \epsilon_{12} \end{Bmatrix} = \begin{bmatrix} l_1^2 & m_1^2 & 0 & 0 & 0 & l_1m_1 \\ l_2^2 & m_2^2 & 0 & 0 & 0 & l_2m_2 \\ 0 & 0 & 1 & 0 & 0 & 0 \\ 0 & 0 & 0 & m_2 & l_2 & 0 \\ 0 & 0 & 0 & m_1 & l_1 & 0 \\ 2l_1l_2 & 2m_1m_2 & 0 & 0 & 0 & l_1m_2 + l_2m_1 \end{bmatrix} \begin{Bmatrix} \epsilon_{xx} \\ \epsilon_{yy} \\ \epsilon_{zz} \\ \epsilon_{yz} \\ \epsilon_{zx} \\ \epsilon_{xy} \end{Bmatrix} \tag{97}$$

The direction cosines are given by

$$\begin{array}{lllllll} l_1 & = & cos\beta & & m_1 & = & sin\beta \\ l_2 & = & -sin\beta & & m_2 & = & cos\beta \end{array} \tag{98}$$

where β is the fiber orientation angle.

For homogeneous isotropic materials, the principal stresses are determining by projecting the six components of stress onto a plane where the shear stress components vanish. This leads to the relation

$$\begin{bmatrix} (\sigma - \sigma_x) & -\tau_{xy} & -\tau_{xz} \\ -\tau_{xy} & (\sigma - \sigma_y) & -\tau_{yz} \\ -\tau_{xz} & -\tau_{yz} & (\sigma - \sigma_z) \end{bmatrix} \begin{Bmatrix} l \\ m \\ n \end{Bmatrix} = \begin{Bmatrix} 0 \\ 0 \\ 0 \end{Bmatrix} \tag{99}$$

from which principal stresses and principal planes may be determined. An additional geometric constraint relates the direction cosines l,m,n as

$$l^2 + m^2 + n^2 = 1 \tag{100}$$

For a nontrivial solution, the determinant of the system given in equation (99) must vanish, which leads to a cubic equation for the principal stresses given by

$$\sigma^3 + \lambda_2\sigma^2 + \lambda_1\sigma + \lambda_0 = 0 \tag{101}$$

where

$$\begin{aligned} \lambda_2 &= \sigma_{xx} + \sigma_{yy} + \sigma_{zz} \\ \lambda_1 &= \sigma_{xx}\sigma_{yy} + \sigma_{yy}\sigma_{zz} + \sigma_{zz}\sigma_{xx} - {\tau_{xy}}^2 - {\tau_{xz}}^2 - {\tau_{yz}}^2 \\ \lambda_0 &= \sigma_{xx}\sigma_{yy}\sigma_{zz} + 2\tau_{xy}\tau_{xz}\tau_{yz} - \sigma_{xx}{\tau_{yz}}^2 - \sigma_{yy}{\tau_{xz}}^2 - \sigma_{zz}{\tau_{xy}}^2 \end{aligned} \tag{102}$$

To obtain the solution, the following quantities are defined

$$q = \frac{1}{3}\lambda_1 - \frac{1}{9}{\lambda_2}^2 \tag{103}$$

$$r = \frac{1}{6}(\lambda_1\lambda_2 - 3\lambda_0) - \frac{1}{27}{\lambda_2}^3$$

$$\begin{aligned} s_1 &= [r + (q^3 + r^2)^{\frac{1}{2}}]^{\frac{1}{2}} \\ s_2 &= [r - (q^3 + r^2)^{\frac{1}{2}}]^{\frac{1}{2}} \end{aligned} \tag{104}$$

in which, for stress and strain tensor transformations, the quantity $q^3 + r^2 \geq 0$ thus guaranteeing that all roots are real. The principal normal stresses are then given by

$$\begin{aligned} \sigma_1 &= (s_1 + s_2) - \frac{a_2}{3} \\ \sigma_2 &= -\frac{1}{2}(s_1 + s_2) - \frac{a_2}{3} + \frac{i\sqrt{3}}{2}(s_1 - s_2) \\ \sigma_3 &= -\frac{1}{2}(s_1 + s_2) - \frac{a_2}{3} - \frac{i\sqrt{3}}{2}(s_1 - s_2) \end{aligned} \tag{105}$$

Principal shear stresses may be expressed in terms of the principal normal stresses as

$$\begin{aligned} \sigma_4 &= |\sigma_2 - \sigma_3| \\ \sigma_5 &= |\sigma_1 - \sigma_3| \\ \sigma_6 &= |\sigma_1 - \sigma_2| \end{aligned} \tag{106}$$

A variety of failure criteria have been incorporated into the RESTRAN analysis code to predict ply failures under external applied loads and are described in the following subsections. These criteria have been used to form the central material failure analysis capability in other state-of-the-art analysis codes [59]. Strains are recovered at the Gauss points and interpolated to each ply at the centroid from which layer stresses are obtained. It is at these locations that the available failure criteria are applied. For greatest generality, a user-defined subroutine may be used to incorporate any specific failure criterion. Both interpolated and Gauss point stresses and strains are passed into the routine. This subroutine is described in the RESTRAN User's Manual [31].

4.1.1 Maximum Stress Criterion

Of the various anisotropic failure criteria, the maximum stress criterion combines early investigations into failure mechanisms due to Rankine and Tresca. The failure strength, σ_f, may be based on fracture strength, yield strength, proportional limit, endurance limit, maximum working stress or some other scalar parameter, depending on the expected failure mode or design criterion. The failure modes predicted by this criterion are each dependent on only one stress component and are summarized in Table 1. In general, for ductile materials, the maximum normal stress criterion yields poor failure predictions, while the maximum shearing stress predictions produce good results. For brittle materials, the maximum stress criterion generally produces good predictions of failure strength. In applying this criterion, ultimate ply failure is predicted when any one of the following conditions are satisfied

$$\begin{array}{lllllllll} \sigma_1 & \geq & X_t; & \sigma_1 & \leq & X_c; & |\sigma_4| & \geq & R \\ \sigma_2 & \geq & Y_t; & \sigma_2 & \leq & Y_c; & |\sigma_5| & \geq & S \\ \sigma_3 & \geq & Z_t; & \sigma_3 & \leq & Z_c; & |\sigma_6| & \geq & T \end{array} \tag{107}$$

where σ_1, σ_2, and σ_3 are the principal normal stress components and σ_4, σ_5, and σ_6 are the principal shear stress components. The strength measures are given by X_t, X_c, Y_t, Y_c, Z_t, and Z_c, which are the normal tensile and compressive strengths in the principal 1, 2 and 3 directions, respectively, and R, S, and T are the shear strengths defined in the 23, 13, and 12 planes, respectively. Expressed in tensor polynomial form, the maximum stress criterion may be written as

$$(\sigma_1 - X_t)(\sigma_1 + X_c)(\sigma_2 - Y_t)(\sigma_2 + Y_c)(\sigma_3 - Z_t)(\sigma_3 + Z_c)(|\sigma_4| - R)(|\sigma_5| - S)(|\sigma_6| - T) = 0 \tag{108}$$

Table 1. Maximum stress criterion failure modes.

Condition	Failure Mode
$\sigma_1 \geq X_t$ and $\sigma_1 > 0$	Fiber failure in tension
$\sigma_1 \leq X_c$ and $\sigma_1 < 0$	Fiber failure in compression
$\sigma_2 \geq Y_t$ and $\sigma_2 > 0$	Matrix failure in tension
$\sigma_2 \leq Y_c$ and $\sigma_2 < 0$	Matrix failure in compression
$\sigma_3 \geq Z_t$ and $\sigma_3 > 0$	Matrix failure in tension
$\sigma_3 \leq Z_c$ and $\sigma_3 < 0$	Matrix failure in compression
$\lvert\sigma_4\rvert \geq 1$	Interlaminar shear failure
$\lvert\sigma_5\rvert \geq 1$	Interlaminar shear failure
$\lvert\sigma_6\rvert \geq 1$	Inplane shear failure

4.1.2 Maximum Strain Criterion

The maximum strain criterion is of identical form as the above with stresses replaced by corresponding strains and strength measures replaced by associated ultimate strain measures. This criterion is founded on early developments made by St. Venant. As with the maximum

stress criterion, a number of failure modes may be identified as listed in Table 2. Ultimate ply failure is predicted when any one of the following conditions are satisfied

$$\begin{array}{lllllllll} \epsilon_1 & \geq & X_t; & \epsilon_1 & \leq & X_c; & |\epsilon_4| & \geq & R \\ \epsilon_2 & \geq & Y_t; & \epsilon_2 & \leq & Y_c; & |\epsilon_5| & \geq & S \\ \epsilon_3 & \geq & Z_t; & \epsilon_3 & \leq & Z_c; & |\epsilon_6| & \geq & T \end{array} \tag{109}$$

where ϵ_1, ϵ_2, and ϵ_3 are the principal normal strain components and ϵ_4, ϵ_5, and ϵ_6 are the principal shear strain components. The ultimate strain measures are given by X_t, X_c, Y_t, Y_c, Z_t, and Z_c which are the normal tensile and compressive strains in the principal 1, 2, and 3 directions, respectively, and R, S, and T are the shear strains in the 23, 13, and 12 planes, respectively.

Table 2. Maximum strain criterion failure modes.

Condition	Failure Mode
$\epsilon_1 \geq X_t$ and $\epsilon_1 > 0$	Fiber failure in tension
$\epsilon_1 \leq X_c$ and $\epsilon_1 < 0$	Fiber failure in compression
$\epsilon_2 \geq Y_t$ and $\epsilon_2 > 0$	Matrix failure in tension
$\epsilon_2 \leq Y_c$ and $\epsilon_2 < 0$	Matrix failure in compression
$\epsilon_3 \geq Z_t$ and $\epsilon_3 > 0$	Matrix failure in tension
$\epsilon_3 \leq Z_c$ and $\epsilon_3 < 0$	Matrix failure in compression
$\lvert\epsilon_4\rvert \geq 1$	Interlaminar shear failure
$\lvert\epsilon_5\rvert \geq 1$	Interlaminar shear failure
$\lvert\epsilon_6\rvert \geq 1$	Inplane shear failure

4.1.3 Beltrami Criterion

The Beltrami failure criterion assumes material isotropy and is based on comparing the total strain energy per unit volume of a multiaxial stress state with the strain energy produced by a uniaxial test at failure. This criterion is given by

$$\sigma_c = [{\sigma_1}^2 + {\sigma_2}^2 + {\sigma_3}^2 - 2\nu(\sigma_1\sigma_2 + \sigma_2\sigma_3 + \sigma_3\sigma_1)]^{\frac{1}{2}} \tag{110}$$

and failure is predicted when the combined stress measure equals or exceeds the critical stress, σ_y, to cause failure in a uniaxial test.

$$\sigma_c \geq \sigma_y \tag{111}$$

4.1.4 Von Mises Criterion

The Von Mises failure criterion assumes material isotropy and is based on a decomposition of the strain energy density into volumetric or dilatational energy and distortional energy. This combined stress measure assumes that failure in a multiaxial stress state is due solely to the distortional energy of the system. The resulting failure criterion may be expressed

using principal stresses as

$$\sigma_c = \frac{\sqrt{2}}{2}[(\sigma_1 - \sigma_2)^2 + (\sigma_2 - \sigma_3)^2 + (\sigma_3 - \sigma_1)^2]^{\frac{1}{2}} \tag{112}$$

wherein failure is predicted when the combined stress measure exceeds the ultimate yield strength of the material or

$$\sigma_c \geq \sigma_y \tag{113}$$

4.1.5 Hoffman Criterion

The three-dimensional Hoffman criterion [52,57] is given by

$$\begin{aligned} FI \;=\; & F_1\sigma_1 + F_2\sigma_2 + F_3\sigma_3 + F_{11}\sigma_1^2 + F_{12}\sigma_1\sigma_2 + F_{13}\sigma_1\sigma_3 + F_{22}\sigma_2^2 + \\ & F_{23}\sigma_2\sigma_3 + F_{33}\sigma_3^2 + F_{44}\sigma_4^2 + F_{55}\sigma_5^2 + F_{66}\sigma_6^2 \end{aligned} \tag{114}$$

where

$$\begin{aligned} F_1 &= \frac{1}{X_t} - \frac{1}{X_c};\quad F_2 = \frac{1}{Y_t} - \frac{1}{Y_c};\quad F_3 = \frac{1}{Z_t} - \frac{1}{Z_c} \\ F_{11} &= \frac{1}{X_t X_c};\qquad F_{22} = \frac{1}{Y_t Y_c};\qquad F_{33} = \frac{1}{Z_t Z_c} \\ F_{44} &= \frac{1}{R^2};\qquad F_{55} = \frac{1}{S^2};\qquad F_{66} = \frac{1}{T^2} \\ F_{12} &= -\frac{1}{2}\left(\frac{1}{X_t X_c} + \frac{1}{Y_t Y_c} - \frac{1}{Z_t Z_c}\right) \\ F_{13} &= -\frac{1}{2}\left(\frac{1}{X_t X_c} + \frac{1}{Z_t Z_c} - \frac{1}{Y_t Y_c}\right) \\ F_{23} &= -\frac{1}{2}\left(\frac{1}{Z_t Z_c} + \frac{1}{Y_t Y_c} - \frac{1}{X_t X_c}\right) \end{aligned} \tag{115}$$

For two-dimensional plane problems, assuming $\sigma_3 = \sigma_{13} = \sigma_{23} = 0$ and due to symmetry about the 2,3 axis, $Y = Z$, the Hoffman criterion reduces to

$$FI = \left(\frac{1}{X_t} - \frac{1}{X_c}\right)\sigma_1 + \left(\frac{1}{Y_t} - \frac{1}{Y_c}\right)\sigma_2 + \frac{{\sigma_1}^2}{X_t X_c} + \frac{{\sigma_2}^2}{Y_t Y_c} + \frac{\sigma_{12}^2}{T^2} - \frac{\sigma_1\sigma_2}{X_t X_c} \tag{116}$$

4.1.6 Hill Criterion

The three-dimensional Hill criterion [50] is based on exclusively quadratic terms given by

$$FI = F_{11}\sigma_1^2 + F_{12}\sigma_1\sigma_2 + F_{13}\sigma_1\sigma_3 + F_{22}\sigma_2^2 + F_{23}\sigma_2\sigma_3 + F_{33}\sigma_3^2 + F_{44}\sigma_4^2 + F_{55}\sigma_5^2 + F_{66}\sigma_6^2 \tag{117}$$

where

$$F_{11} = \frac{1}{X^2};\qquad F_{22} = \frac{1}{Y^2};\qquad F_{33} = \frac{1}{Z^2}$$

$$F_{44} = \frac{1}{R^2}; \quad F_{55} = \frac{1}{S^2}; \quad F_{66} = \frac{1}{T^2}$$
$$F_{12} = -\frac{1}{2}(\frac{1}{X^2} + \frac{1}{Y^2} - \frac{1}{Z^2}) \tag{118}$$
$$F_{13} = -\frac{1}{2}(\frac{1}{X^2} + \frac{1}{Z^2} - \frac{1}{Y^2})$$
$$F_{23} = -\frac{1}{2}(\frac{1}{Z^2} + \frac{1}{Y^2} - \frac{1}{X^2})$$

in which the value for the normal strengths X, Y, and Z are taken as compressive or tensile, depending on the sign of the corresponding normal stresses. For two-dimensional plane problems, assuming $\sigma_3 = \sigma_{13} = \sigma_{23} = 0$ and due to symmetry about the 2,3 axis, $Y = Z$, the Hoffman criterion reduces to

$$FI = F_{11}\sigma_1^2 + F_{12}\sigma_1\sigma_2 + F_{22}\sigma_2^2 + F_{66}\sigma_6^2 \tag{119}$$

4.1.7 Tsai-Wu Criterion

The three-dimensional Tsai-Wu criterion [53] is given by

$$\begin{aligned} FI \;=\; & F_1\sigma_1 + F_2\sigma_2 + F_3\sigma_3 + F_{11}\sigma_1^2 + F_{12}\sigma_1\sigma_2 + F_{13}\sigma_1\sigma_3 + F_{22}\sigma_2^2 + \\ & F_{23}\sigma_2\sigma_3 + F_{33}\sigma_3^2 + F_{44}\sigma_4^2 + F_{55}\sigma_5^2 + F_{66}\sigma_6^2 \end{aligned} \tag{120}$$

where

$$F_1 = \frac{1}{X_t} - \frac{1}{X_c}; \quad F_2 = \frac{1}{Y_t} - \frac{1}{Y_c}; \quad F_3 = \frac{1}{Z_t} - \frac{1}{Z_c}$$
$$F_{11} = \frac{1}{X_t X_c}; \quad F_{22} = \frac{1}{Y_t Y_c}; \quad F_{33} = \frac{1}{Z_t Z_c}$$
$$F_{44} = \frac{1}{R^2}; \quad F_{55} = \frac{1}{S^2}; \quad F_{66} = \frac{1}{T^2}$$
$$F_{12} = -\frac{1}{2}/(\sqrt{X_t X_c Y_t Y_c}) \tag{121}$$
$$F_{13} = -\frac{1}{2}/(\sqrt{X_t X_c Z_t Z_c})$$
$$F_{23} = -\frac{1}{2}/(\sqrt{Y_t Y_c Z_t Z_c})$$

For two-dimensional plane problems, assuming a slightly different form for the interaction term F_{12}, the Tsai-Wu criterion reduces to

$$FI = (\frac{1}{X_t} - \frac{1}{X_c})\sigma_1 + (\frac{1}{Y_t} - \frac{1}{Y_c})\sigma_2 + \frac{{\sigma_1}^2}{X_t X_c} + \frac{{\sigma_2}^2}{Y_t Y_c} + \frac{{\sigma_{12}}^2}{T^2} - \frac{\sigma_1\sigma_2}{X_t Y_t + X_c Y_c} \tag{122}$$

4.1.8 Christensen Criterion

The Christensen failure criterion differentiates failure into three possible modes [48]. These are fiber tension, fiber compression, and matrix failure. Fiber failure in tension is predicted when

$$\left|\frac{X_t}{\sigma_1 - \nu_{12}\sigma_2 - \nu_{13}\sigma_3}\right| \leq 1 \quad for \quad (\sigma_1 - \nu_{12}\sigma_2 - \nu_{13}\sigma_3) \geq 0 \tag{123}$$

Fiber failure in compression is predicted when

$$\left|\frac{X_c}{\sigma_1 - \nu_{12}\sigma_2 - \nu_{13}\sigma_3}\right| \leq 1 \quad for \quad (\sigma_1 - \nu_{12}\sigma_2 - \nu_{13}\sigma_3) \leq 0 \tag{124}$$

Matrix failure is predicted when the following condition is satisfied

$$\begin{aligned} &A_1\sigma_1 + A_2(\sigma_2 + \sigma_3) + A_3{\sigma_1}^2 + A_4({\sigma_2}^2 + {\sigma_3}^2) + \\ &A_5\sigma_1(\sigma_2 + \sigma_3) + A_6\sigma_2\sigma_3 + A_7{\sigma_4}^2 + A_8({\sigma_5}^2 + {\sigma_6}^2) \quad \geq \quad 1 \end{aligned} \tag{125}$$

where the constants $A_1 \rightarrow A_8$ are given by

$$\begin{aligned} A_1 &= \alpha(1 - 2\nu_{12})/(\beta^2 E_1) \\ A_2 &= \alpha(1 - \nu_{21} - \nu_{23})/(\beta^2 E_2) \\ A_3 &= 2(1 + \nu_{12})^2/(3\beta^2 {E_1}^2) \\ A_4 &= 2[(1 + \nu_{21} + {\nu_{21}}^2) + \nu_{23}(1 - \nu_{21}) + {\nu_{23}}^2]/(3\beta^2 {E_2}^2) \\ A_5 &= 2[(2\nu_{21} + \nu_{23})(1 + \nu_{12})]/(3\beta^2 E_1 E_2) \\ A_6 &= 2[(-1 + 2\nu_{21} + 2{\nu_{21}}^2) - 2\nu_{23}(2 + \nu_{21}) - {\nu_{23}}^2]/(3\beta^2 {E_2}^2) \\ A_7 &= 1/(2\beta^2 {G_{23}}^2) \\ A_8 &= 1/(2\beta^2 {G_{12}}^2) \end{aligned} \tag{126}$$

and where the constants α and β are determined experimentally for the particular material system being used.

4.1.9 Feng Criterion

The Feng failure criterion is based on strain invariants and predicts fiber breakage and matrix cracking failure modes [47]. Matrix failure is predicted when

$$A_1 J_1 + A_2 {J_1}^2 + A_3 J_2 \geq 1 \tag{127}$$

and fiber failure is predicted when

$$A_4 J_5 + A_5 {J_5}^2 + A_6 J_4 \geq 1 \tag{128}$$

In the above equations, $A_1 \rightarrow A_6$ are experimentally determined constants, and J_i are strain invariants given by

$$\begin{aligned} J_1 &= \epsilon_1 + \epsilon_2 + \epsilon_3 \\ J_2 &= \frac{1}{6}[(\epsilon_1 - \epsilon_2)^2 + (\epsilon_3 - \epsilon_2)^2 + (\epsilon_1 - \epsilon_3)^2 + {\epsilon_4}^2 + {\epsilon_5}^2 + {\epsilon_6}^2] \\ J_4 &= {\epsilon_4}^2 + {\epsilon_5}^2 \\ J_5 &= \epsilon_1 \end{aligned} \tag{129}$$

4.1.10 Modified Hashin Criterion

The modified Hashin failure criterion [49] differentiates between fiber and matrix failure modes. Fiber failure is predicted on the basis of whether the fiber or longitudinal stresses exceed the maximum fiber directional strength. Thus, fiber failure in tension is predicted when

$$\frac{\sigma_1}{X_t} \geq 1 \quad for \quad \sigma_1 \geq 0 \tag{130}$$

and fiber failure in compression is predicted when

$$\frac{\sigma_1}{X_c} \geq 1 \quad for \quad \sigma_1 < 0 \tag{131}$$

Matrix failure is predicted using maximum normal and transverse stress components in the 2-3 plane defined by

$$\begin{aligned} \sigma_{nn} &= (\frac{\sigma_2 + \sigma_3}{2}) + (\frac{\sigma_2 - \sigma_3}{2})cos(2\beta) + \sigma_{23} sin(2\beta) \\ \sigma_{nt} &= -(\frac{\sigma_2 - \sigma_3}{2})sin(2\beta) + \sigma_{23} cos(2\beta) \\ \sigma_{nl} &= \sigma_{13} sin(\beta) + \sigma_{12} cos(\beta) \end{aligned} \tag{132}$$

in which β defines the principal direction. Matrix failure in tension is given by

$$\frac{{\sigma_{nn}}^2}{X_t} + \frac{{\sigma_{nt}}^2}{Y_c} + \frac{{\sigma_{nl}}^2}{T} \geq 1 \quad for \quad \sigma_{nn} \geq 0 \tag{133}$$

and matrix failure in compression is given by

$$\frac{{\sigma_{nt}}^2}{Y_c} + \frac{{\sigma_{nl}}^2}{T} \geq 1 \quad for \quad \sigma_{nn} < 0 \tag{134}$$

4.2 Progressive Material Failure Prediction

Estimating the required load to cause the next material failure is performed by calculating scale factors for each ply in each element to precipitate material failure using selected failure criteria and assuming a linear load–deflection response. These scale factors, α, are defined as the linear multiplier to the current stresses to reach the critical value given by

$$\sigma^{cr} = \alpha\sigma \tag{135}$$

such that the failure index, FI, is equal to unity or

$$FI = f(\sigma_{ij}) = 1 \tag{136}$$

In the general tensorial criteria described previously, this leads to determining roots to an n^{th} order polynomial of the form

$$S_n\alpha^n + S_{n-1}\alpha^{n-1} + ... + S_0 = 0 \tag{137}$$

The suite of failure criteria available in RESTRAN are limited to linear and quadratic expressions involving stresses and material strengths such that the highest order failure criterion requires only the roots to a second-order equation of the form

$$S_2\alpha^2 + S_1\alpha + S_0 = 0 \tag{138}$$

to be determined to yield the minimum positive multiplier, α. This factor is calculated for each ply in each element and is stored in an external file. The lowest factor to cause the next material failure is selected as

$$\bar{\alpha} = min(\alpha_{ij}^1, \alpha_{ij}^2, ..., \alpha_{ij}^k) \tag{139}$$

where i is the element number, j is the element ply number, and k is the failure mode. To speed convergence, a factor s is applied to the determined load multiplier to provide a scaling slightly above the minimum predicted. This factor may be input to override the default value of 1.01. These factors multiply the vector of input loads yielding the next set of applied loads as

$$\mathbf{F} = s\bar{\alpha}\mathbf{P} \tag{140}$$

In the case when nonlinear material properties are specified, the linear or quadratic extrapolation used to determine $\bar{\alpha}$ will introduce an additional nonlinear effect and cause the estimate for the next failure load to vary during the iterative solution of the nonlinear equilibrium equations.

4.3 Material Damage Models

Once ply failure is predicted, various damage laws have been incorporated into RESTRAN to account for material degradation. The simplest damage law reduces all lamina properties to zero regardless of damage mode. Thus, for the i^{th} ply, a null constitutive relation is assumed as

$$[\mathbf{C}]_i = [\mathbf{0}] \tag{141}$$

This assumption is regarded as extreme, and more specialized property reductions models have been advanced for the representation of ply damage in the attempt to refine failure predictions.

Extending the model developed by Reddy and Pandey [56] to three-dimensional for compressive or tensile matrix failure, the in-plane transverse modulus, E_2, G_{23}, and Poisson's ratios μ_{ij} in the damaged ply is set to zero while all other elastic constants are unchanged. This results in the ply stiffness matrix for the i^{th} ply given by

$$[\mathbf{C}]_i = \begin{bmatrix} E_1 & 0.0 & 0.0 & 0.0 & 0.0 & 0.0 \\ 0.0 & 0.0 & 0.0 & 0.0 & 0.0 & 0.0 \\ 0.0 & 0.0 & E_3 & 0.0 & 0.0 & 0.0 \\ 0.0 & 0.0 & 0.0 & 0.0 & 0.0 & 0.0 \\ 0.0 & 0.0 & 0.0 & 0.0 & G_{13} & 0.0 \\ 0.0 & 0.0 & 0.0 & 0.0 & 0.0 & G_{12} \end{bmatrix} \tag{142}$$

Similarily, for fiber failure, E_1, G_{12}, G_{13}, and $\mu_{ij}, = 0$, yielding

$$[\mathbf{C}]_i = \begin{bmatrix} 0.0 & 0.0 & 0.0 & 0.0 & 0.0 & 0.0 \\ 0.0 & E_2 & 0.0 & 0.0 & 0.0 & 0.0 \\ 0.0 & 0.0 & E_3 & 0.0 & 0.0 & 0.0 \\ 0.0 & 0.0 & 0.0 & G_{23} & 0.0 & 0.0 \\ 0.0 & 0.0 & 0.0 & 0.0 & 0.0 & 0.0 \\ 0.0 & 0.0 & 0.0 & 0.0 & 0.0 & 0.0 \end{bmatrix} \tag{143}$$

A more specialized damage law is presented by Chang and Chang [18]. This law is based on an interactive degradation model using the Tsai-Wu failure criterion expressed as

$$FI = F_i\sigma_i + F_{ij}\sigma_i\sigma_j \tag{144}$$

where FI is the failure index. Specific failure modes are determined by calculating the failure index using selected stress components. The implementation in RESTRAN generalizes this approach to any selected quadratic failure criterion. A stiffness reduction coefficient, α, is utilized to degrade material properties. This coefficient is experimentally determined and is assumed as a material property constant for the composite material system being used. Fiber breakage is assumed if $max\{FI(\sigma_i)\}$ is due to σ_1. The damage law for this mode is given by

$$\begin{aligned} \bar{E}_1 &= \alpha E_1 \\ \bar{G}_{13} &= \alpha G_{13} \\ \bar{G}_{12} &= \alpha G_{12} \\ \bar{\nu}_{13} &= \alpha \nu_{13} \\ \bar{\nu}_{12} &= \alpha \nu_{12} \end{aligned} \tag{145}$$

with all other moduli left unaltered. Matrix cracking is assumed if $max\{FI(\sigma_i)\}$ is due to σ_2 or σ_6; the corresponding damage law for this mode is given by

$$\begin{aligned} \bar{E}_2 &= \alpha E_2 \\ \bar{G}_{23} &= \alpha G_{23} \\ \bar{G}_{12} &= \alpha G_{12} \\ \bar{\nu}_{21} &= \alpha \nu_{21} \\ \bar{\nu}_{23} &= \alpha \nu_{23} \end{aligned} \tag{146}$$

Delamination failure is assumed if $max\{FI(\sigma_i)\}$ is due to σ_3, σ_4, or σ_5, and the corresponding damage law for this mode is given by

$$\begin{aligned} \bar{E}_3 &= \alpha E_3 \\ \bar{G}_{23} &= \alpha G_{23} \\ \bar{G}_{13} &= \alpha G_{13} \\ \bar{\nu}_{31} &= \alpha \nu_{31} \\ \bar{\nu}_{32} &= \alpha \nu_{32} \end{aligned} \tag{147}$$

For partial failure, the material constitutive matrix will generally be rank deficient, which will lead to an n^{th}-order singularity during inversion. This is processed through an element-level condensation of the indefinite moduli prior to the inversion. The reduced constitutive matrix is subsequently expansed to the original material matrix dimension and is then used in forming element stiffness coefficients. The resulting element stiffness matrix will possess zero–energy modes in addition to those associated with rigid body modes. After assembly of elements into a global system, any degrees of freedom associated with zero stiffness are statically condensed out of the system prior to analysis.

The failure and damage models built into RESTRAN reflect both those in common use and those that are the result of current research into modeling failure mechanisms in composites. However, RESTRAN incorporates a standardized subroutine interface described in the user's manual [31] which allows any additional material failure/damage model to be applied through the creation of a user-defined subroutine linked into the RESTRAN code.

5 Structural Failure Modes

Structural members exhibit a variety of buckling responses to applied loads. Long, slender members such as beams or columns tend to displace in a simple fundamental mode with a single wavelength deflection pattern. Plate-like components demonstrate various numbers of longitudinal and transverse wavelength deflection patterns which depend on geometry and material aspect ratios. Thick composite laminates with delaminations show global, local, and mixed instability modes as depicted in Figure 11. In complex geometries, instability modes can preclude any clear categorization. The algorithmic treatment of delamination buckling in RESTRAN allows the specification of any number of delaminations to contribute to local

and mixed instability modes. Each delamination may be defined with arbitrary configuration and location at ply interface planes. The growth of delaminations prior to buckling is currently not calculated in RESTRAN. This exclusion is based in part on the necessary limitation of the current developmental effort, together with the observed behavior of actual delminated composites undergoing buckling. Due to imperfections, misalignments, and loss of load symmetry, predictions of delamination growth prior to or concurrent with buckling using an idealized mathematical model tend to give way to growth occurring subsequent to buckling and being a phenomenon in the post-buckled regime [11].

For a computationally viable analysis, buckling failure is predicted through a linear eigenanalyis to obtain critical load multipliers to cause local sublaminate and overall instability. As will be discussed in the following sections, issues arise in modeling contact constraint effects and in representing post-buckled material behavior. To fully simulate these phenomena, an iterative nonlinear large displacement solution procedure is required which would present an impractical computational cost in processing multiple delaminations. Thus, various simplifications have been incorporated to provide a tractable analysis.

The interpretation of buckling modes has been automated for delaminations defined along ply interface planes. For more complicated states of delamination damage, RESTRAN incorporates user-defined subroutine interfaces to allow problem-specific interpretation of buckling failure modes for complicated delamination profiles in three-dimensional geometries.

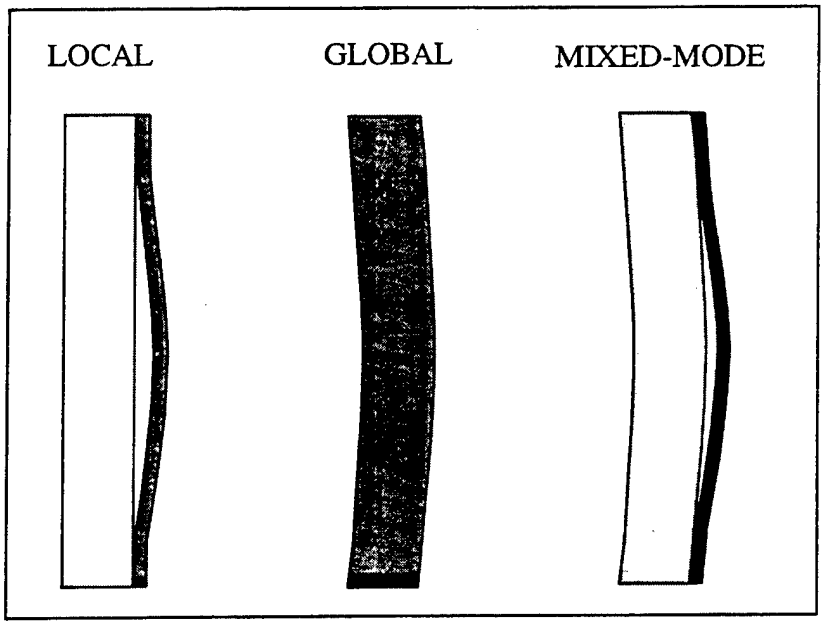

Figure 11. Global, local, and mixed buckling modes in thick laminates.

5.1 Multiple Delaminations

The analysis of multiple delaminations in composites has not been widely investigated [60]. In RESTRAN, delamination damage is idealized as an array of planes of discontinuity; this is schematically depicted in Figure 12. In low-velocity impacts of plate-like geometries, the location of internal delaminations is highly dependent on the relative orientation of ply pairs through the layup. Other effects such as bending and stress wave interactions tend to concentrate the creation of fracture surface or delamination planes towards the opposite face of the panel [61–66]. In high velocity, through-penetration type impact events, delaminations may be uniformly distributed through the laminate thickness concentric about a removed hollow core.

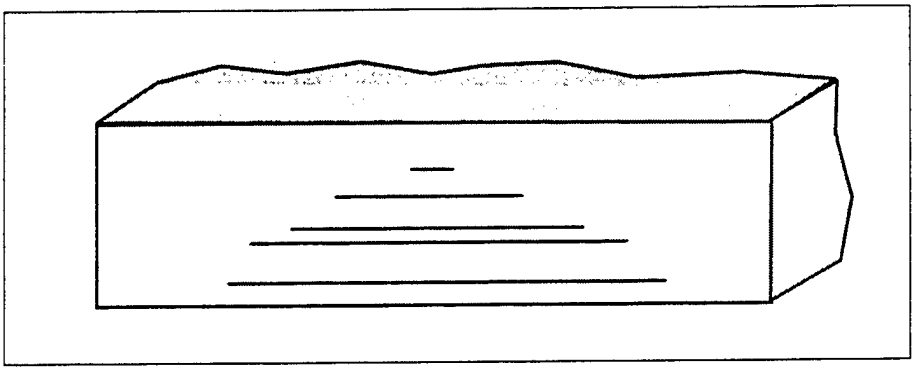

Figure 12. Laminate with multiple embedded delaminations.

The stability analysis of multiply-delaminated laminates is complicated by the number of potential instability modes. If delaminations are simply modeled as planes of element discontinuity and a linear buckling analysis is performed with out enforcing contact constraints, predicted buckling modes may include both physical modes and nonphysical modes in which the instability failure of interior sublayers deform into surrounding laminate material. This behavior is depicted in Figure 13.

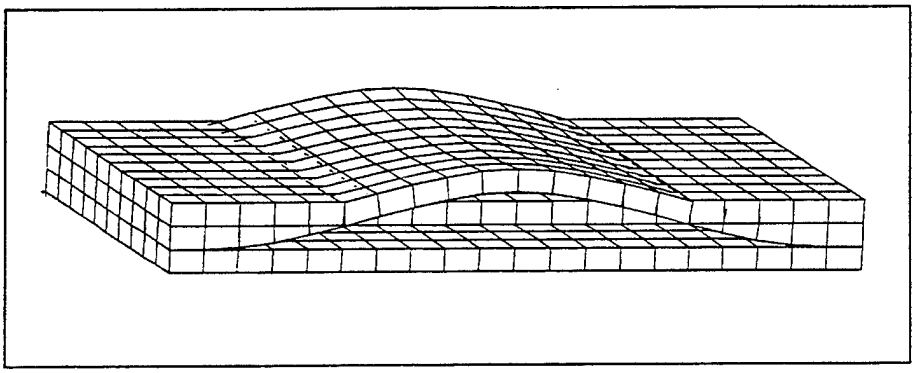

Figure 13. Example of a nonphysical sublaminate buckling mode.

With the possible presence of numerous delaminations with arbitrary location and configuration, several assumptions have been used in the development of a general analysis capability in RESTRAN to make the analysis of multiple delaminations tractable. The first assumption is that each sublaminate buckling instability can be considered individually. Experimental results have shown that with the presence of multiple delaminations, instability behavior is typically dependent on the most critical delamination, while the other delaminations remain closed [11]. This procedure assumes that during instability of a particular delamination, all other delamination planes have infinite frictional contact and are, as a consequence, condensed out of the model. This is depicted in Figure 14. This process is repeated sequentially for all delaminations in the model, and the delamination with the lowest critical load is assumed to exhibit the next failure due to buckling. The task reduces to automating the analysis of single buckling mode shapes and ultimately determining which particular sublaminate layer is most critical to instability and determining which elements are involved in the buckled sublaminate. This procedure eliminates the difficulty of automatically screening out nonphysical buckling modes and replaces simultaneous buckling of multiple delaminations with a sequence of individual local instability failures. The sequential processing of individual local delamination failures will provide overall estimates for the maximum applied load to cause local failure via sublaminate buckling. In a study of local buckling in laminated composites, the presence of additional, symmetrically located delaminations have only a slight effect on the predicted buckling load over those predicted with other delaminations removed from the model [12]. A schematic of sequential buckling failure is depicted in Figure 15.

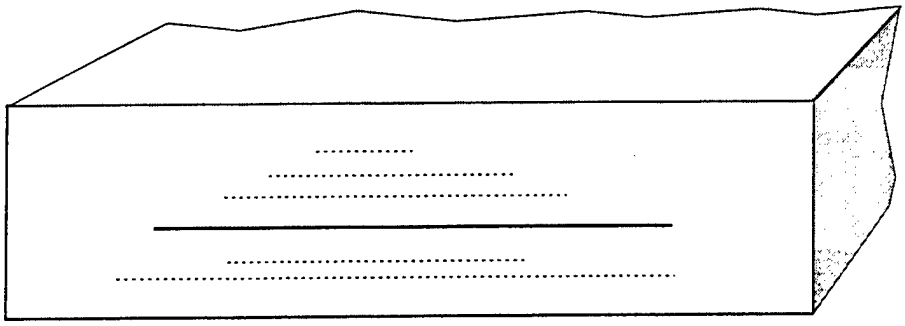

Figure 14. Condensation of multiple delaminations.

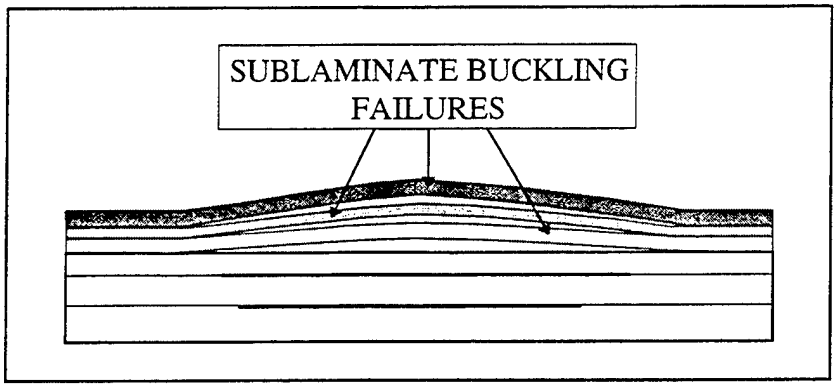

Figure 15. Sequential buckling failure.

Although sequentially processing individual delaminations removes the possibility of predicting embedded sublaminates to undergo buckling deformation and deforming through other layers, as depicted in Figure 13, contact constraints must be imposed on isolated delaminations to correct for local interpenetration of the buckling mode, as shown in Figure 16. RESTRAN incorporates an effective iterative procedure for satisfying contact or compatability constraints on the buckling mode shape. This feature is explained in detail in the following subsection.

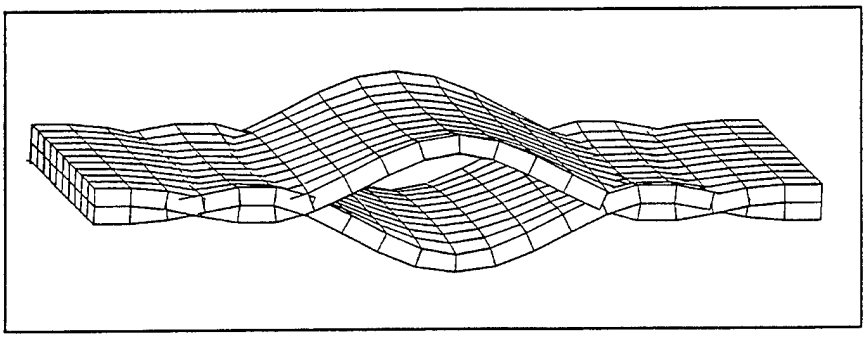

Figure 16. Local compatability violation in layer buckling.

5.2 Algorithmic Assessment of Local Buckling Failure

Delaminations are assumed to exist on distinct planes which may be of arbitrary shape and extent. Each delamination is defined by a declared set of nodes through which the fracture surface extends. For each node set, RESTRAN automatically generates a set of coincident nodes and redefines the element connectivity to provide a kinematic freedom of motion between the upper and lower surfaces. Each element is accessed, and the nodes forming the element faces F_2, F_3, and F_6 (as defined in Figure 17) are scanned for inclusion in the delamination node set. Once determined, the elements are scanned, and those containing nodes on

the opposing F_4, F_1, or F_6 faces, which are a subset of the nodes defining the delamination, are assigned the coincident nodes. The resulting placement of coincident nodes is depicted in Figure 18.

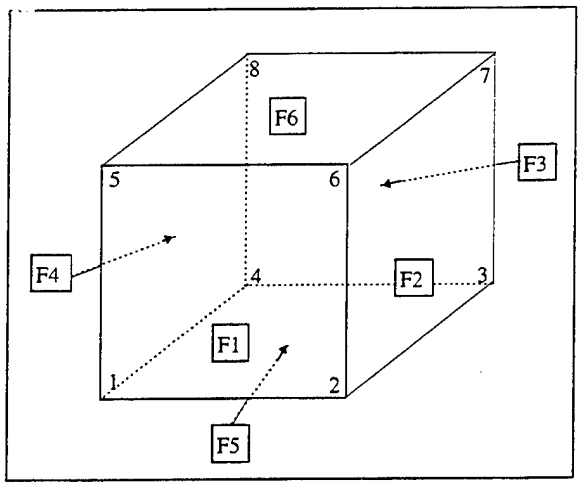

Figure 17. Designation of element faces.

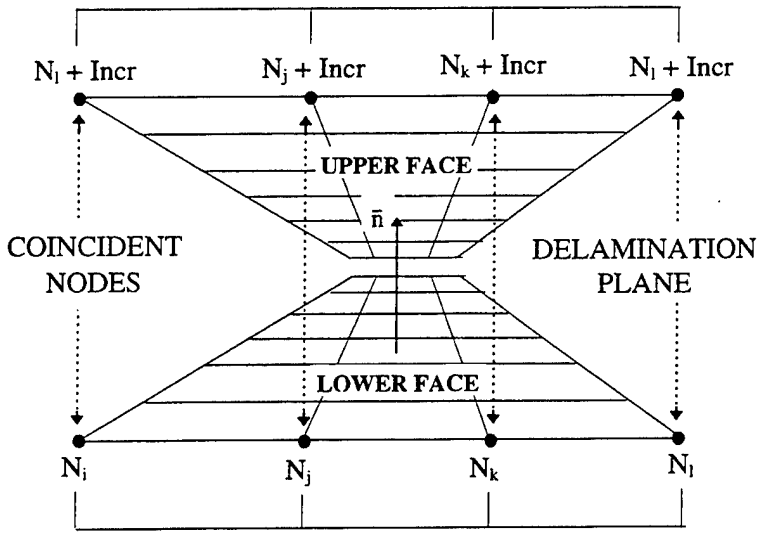

Figure 18. Generation of coincident nodes.

The global elastic and differential stiffness matrices are then formed containing all generated coincident node planes simulating the required delaminations. A sequential processing of each delamination is performed, and a condensation is performed to temporarily remove all but the current delamination. An eigenanalysis of the condensed global system is then invoked. Each fundamental mode shape is subjected to an automated interpretation. The first

test determines the type of buckling mode. Simple global buckling is identified if no delaminations have been input or after all delaminations have been failed. A mixed global-local buckling mode is detected if the maximum normalized modal displacement occurs outside the domain of the delamination plane. This mode is predicted when the ratio between the maximum modal deflection in the delamination plane and the maximum overall deflection is less than an input tolerance or

$$\delta_{local}^{max}/\delta_{global}^{max} \leq Tol \tag{148}$$

If these modes are not exhibited, the default mode is local sublaminate buckling. These buckling modes are depicted in Figure 11.

Global or mixed global-local buckling modes are assumed to cause catastrophic failure if the corresponding critical load is less than the predicted load to cause material failure at the current progressive failure cycle.

For local sublaminate buckling modes, an iterative procedure can be invoked to satisfy contact constraints. The automated analysis of the buckling mode is based entirely on the mode shape which is arbitrary in magnitude and sign. An estimate for the amplitude of the buckling mode within a linear solution scheme can be made by assuming the area of the delaminated section remains constant and that the membrane stress in the buckled laminate is the same as the buckling stress [6]. For assessing contact, however, the actual magnitude is not needed, and the pattern of the normalized eigenmode is used to determine modal displacements and modal stresses and strains. Iterations begin by first checking whether the buckling mode is demonstrating a physical opening mode or nonphysical closing mode, as shown in Figure 19.

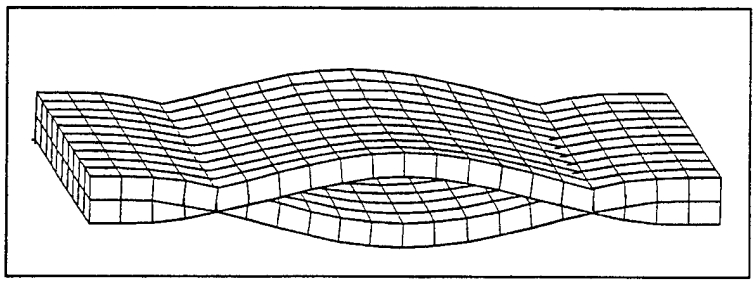

CLOSING MODE

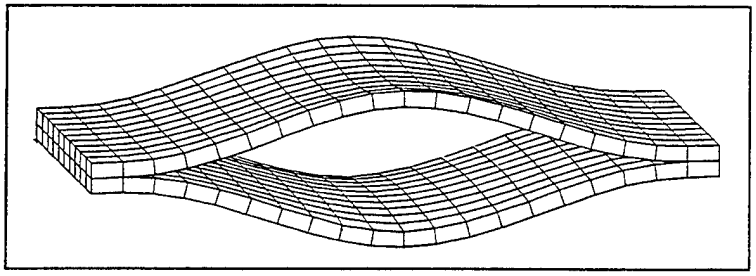

OPENING MODE

Figure 19. Opening and closing buckling modes.

If a closing mode is detected, the arbitrary signs of the modal displacements are flipped. A test is performed to assess the degree of interpenetration of the buckling layer into the upper or lower substrate. The inital processing of interpenetrating delaminations is to remove the coincident nodes where contact conditions are violated. This has, as a first approximation, the effect of fitting an opening half wavelength to the delamination plane. A minimum energy surface may, however, extend beyond this border, and further computations are performed to refine the inital estimate of constrained layer buckling. This is performed by repeating the eigenanalysis with the augmented connectivity and utilizing the recovered mode shape which, although arbitrary in magnitude and sign, provides the necessary qualitative information. After testing for interpenetrating nodes and accumulating these in an exclusion set, prior nodes included in this set are tested for possible release due to predicted normal tensile strains at the node location. This estimate is based on tensile stresses associated with nodes, or equivalently, nodal displacements above and below the delamination plane moving apart, thereby generating tensile strains normal to the plane which act to open that portion of the delamination. These nodes are restored in the delamination node set and the linear analysis rerun. The nodes used for estimating modal strains about a particular coincident node are shown in Figure 20.

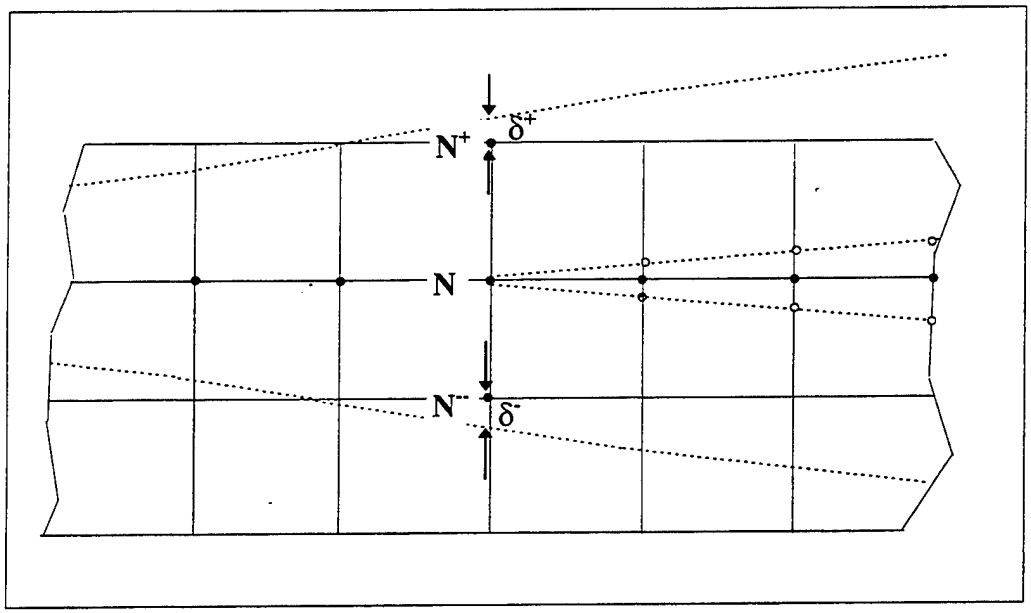

Figure 20. Nodes used to calculate normal modal strain.

The coordinates x_i and modal deflections δ_i are then used to calculate a measure of normal strain as a stretch factor given by

$$\epsilon_n = \frac{S_1 - S_o}{S_o} = \frac{[\sum_{i=1}^{3}(x_i^+ + \delta_i^+ - x_i^- - \delta_i^-)^2]^{1/2} - [\sum_{i=1}^{3}(x_i^+ - x_i^-)^2]^{1/2}}{[\sum_{i=1}^{3}(x_i^+ - x_i^-)^2]^{1/2}} \tag{149}$$

If the criteria $\epsilon_n > Tol$ is satisfied, the coincident node previously removed through condensation is reintroduced. Other approaches, such as using iterative conjugate gradient

methods, have been applied to satisfy buckling layer contact with linear constraints [67,68]. The present approach within the context of linear bifurcation buckling provides a similar solution in a small number of iterations. To perform an iterative contact solution for acceptable mode shapes, user input to RESTRAN specifies the maximum number of iterations together with a tolerance which is a normalized measure of overall contact above which the compatibility is acceptable. This measure is given by

$$1 - \frac{N_{IP}}{N_T} \geq Tol \tag{150}$$

where N_{IP} is the number of interpenetrating nodes, and N_T is the total number of nodes in the delamination set. If convergence is not obtained, the mode is assumed impossible and is excluded from consideration in the current analysis cycle.

For a physically acceptable local sublaminate buckling mode, the next procedure is to determine whether the sublaminate layer undergoing buckling is along the positive or negative normal to the delamination plane. As shown in Figure 21, the nodes defining the element face and contained in the delamination node set are used to form two local vectors, $\mathbf{V}_1$ and $\mathbf{V}_2$, which define the local positive normal to the delamination surface as

$$\mathbf{n} = \frac{\mathbf{V}_1 \times \mathbf{V}_2}{|\mathbf{V}_1 \times \mathbf{V}_2|} \tag{151}$$

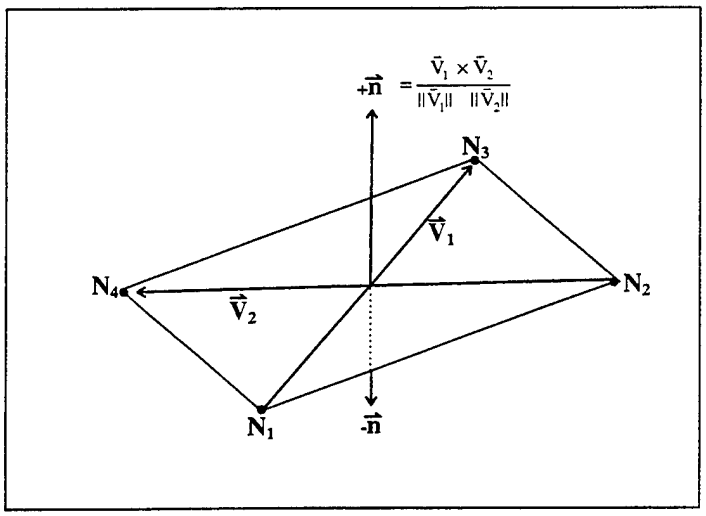

Figure 21. Definition of positive normal to delamination plane.

The buckling surface is determined by forming displacement vectors from nodes in the delamination plane to the upper and lower surfaces and computing vector norms. The surface which demonstrates the greatest magnitude of displacement then determines which sublaminate is undergoing buckling. Figure 22 shows a depiction of an opening delamination with local displacement vectors at node points.

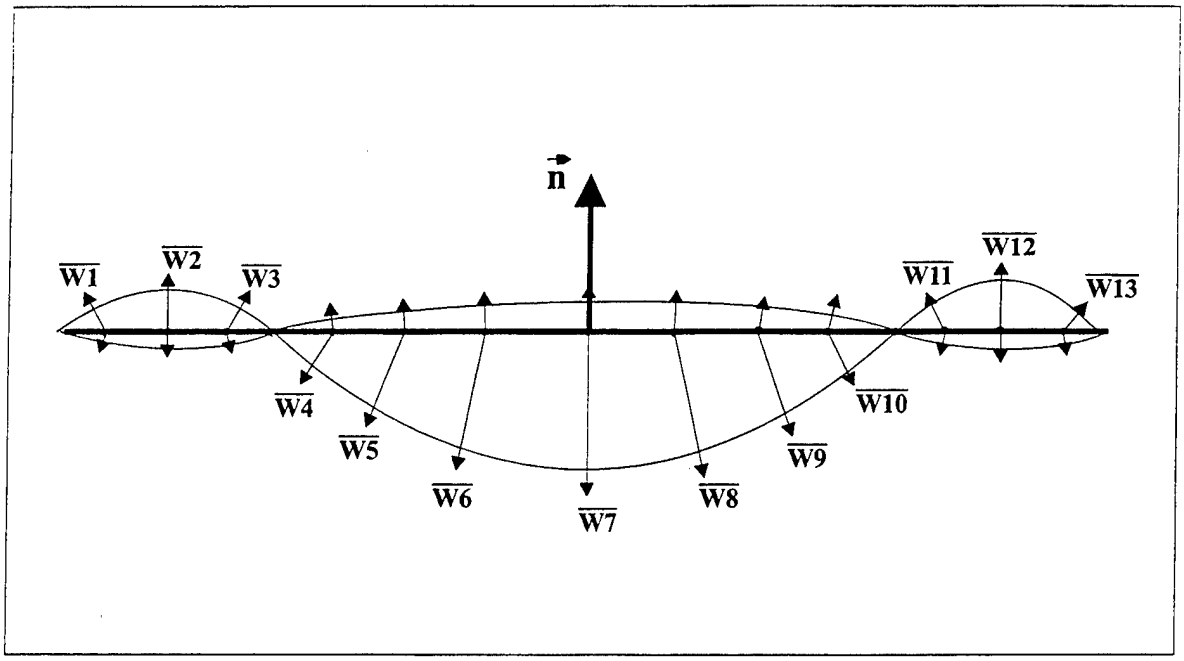

Figure 22. Opening mode in delamination buckling.

The direction of opening with respect to the delamination surface normal is determined by computing the angle between the nodal displacement vectors and the surface normal. The individual angles are summed, and an average opening angle $\bar{\alpha}$ is computed.

$$\bar{\alpha} = \frac{1}{N} \sum_{i=1}^{N} cos^{-1} \left[\frac{\mathbf{n} \cdot \mathbf{w}_i}{|\mathbf{n}||\mathbf{w}_i|} \right] \tag{152}$$

The direction d is thus determined as

$$d = \begin{cases} +\mathbf{n} & : \quad \bar{\alpha} < \pi/2 \\ -\mathbf{n} & : \quad \bar{\alpha} > \pi/2 \end{cases} \tag{153}$$

In the event of a centrally located delamination (Figure 23) wherein both surfaces are moving symmetrically apart, $\bar{\alpha}$ may be identically equal to $\pi/2$, and the positive normal direction is taken by default. This will cause the proper critical applied load to be accounted, but only one of the layers will be failed. The other layer will remain and be assessed during the next analysis cycle. Again, this suggests that sequencing failures through sublaminate buckling compared with attempting to account for simultaneous failures will alter the progression of failure while maintaining an accurate estimate for failure loads.

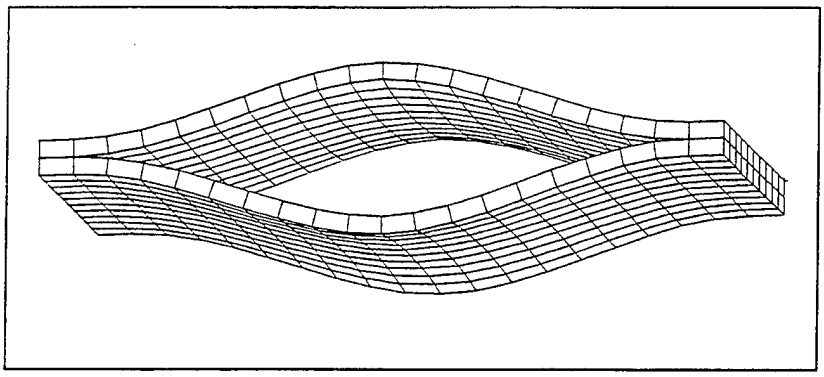

Figure 23. Buckling failure in a centrally located delamination.

As each delamination is processed, a continuous update is made keeping account of the delamination with the lowest predicted critical buckling load, associated mode shape, and direction of failure. If no other material failures are predicted at a lower load level, the selected critical delamination is then designated as the next failure event. Processing the failed delamination consists of performing a search through the sublaminate undergoing buckling and determining what elements are involved in the instability failure. Once determined, a selected damage law is applied to each of the elements. An additional search is performed to determine if any other delaminations are contained in the buckled sublaminate. This is depicted in Figure 24. All delaminations involved in the current buckling failure are then removed from the node set and removed from the model by eliminating the involved coincident nodes. An internal node renumbering is then performed.

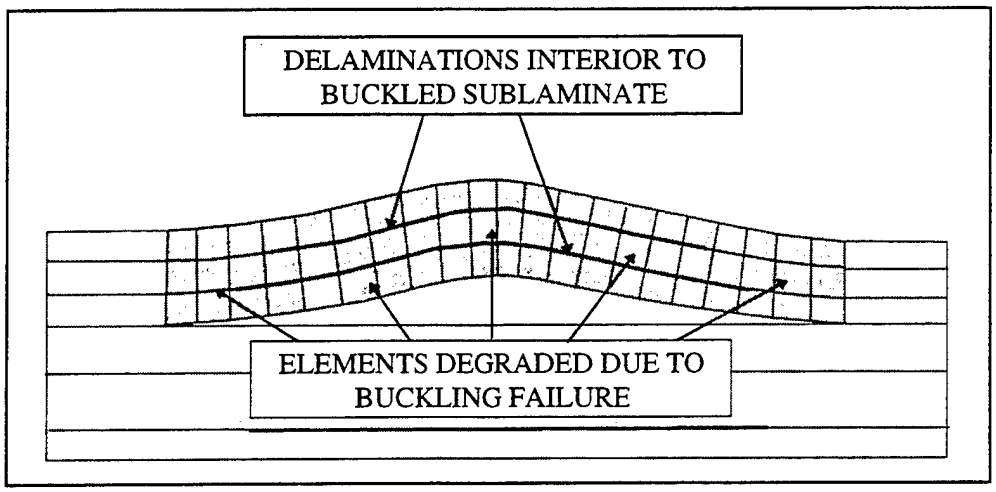

Figure 24. Failure assessment of buckled sublaminate.

5.3 Distributed Delaminations and Simultaneous Local Buckling

The algorithms incorporated into RESTRAN for automatically processing delamination buckling can be used to analyze more complicated delamination configurations. For example, a traversing-type delamination which progresses along several ply interfaces can be modeled. As shown in Figure 25, the user must initially create the model with connectivity removed between elements along the perpendicular segments where the delamination jumps between different ply interfaces. The remaining portions of the delamination can be defined by specifying a delamination node set. Additionally, as shown in Figure 26, delaminations do not have to be similarily oriented. Each independent delamination may be arbitrarily positioned in different areas of the structural model. The only restriction is that each separate delamination must form a planar surface for proper interpretation of buckling motion. To allow the capability of analyzing general, nonplanar delamination surfaces or the simultaneous buckling of multiple delaminations, RESTRAN provides user-defined subroutine options to interpret buckling in non-plate-type geometries. Delaminations are defined in RESTRAN by inputting node sets which are used to automatically generate coincident nodes to redefine element connectivity. Thus, any discontinuous inner surface may be simulated, and multiple delaminations may be considered simultaneously by including the participating nodes in the same delamination node set. A user-defined subroutine which is compiled and linked into the RESTRAN executable must then be provided to interpret the resulting mode shapes and assess associated element failures.

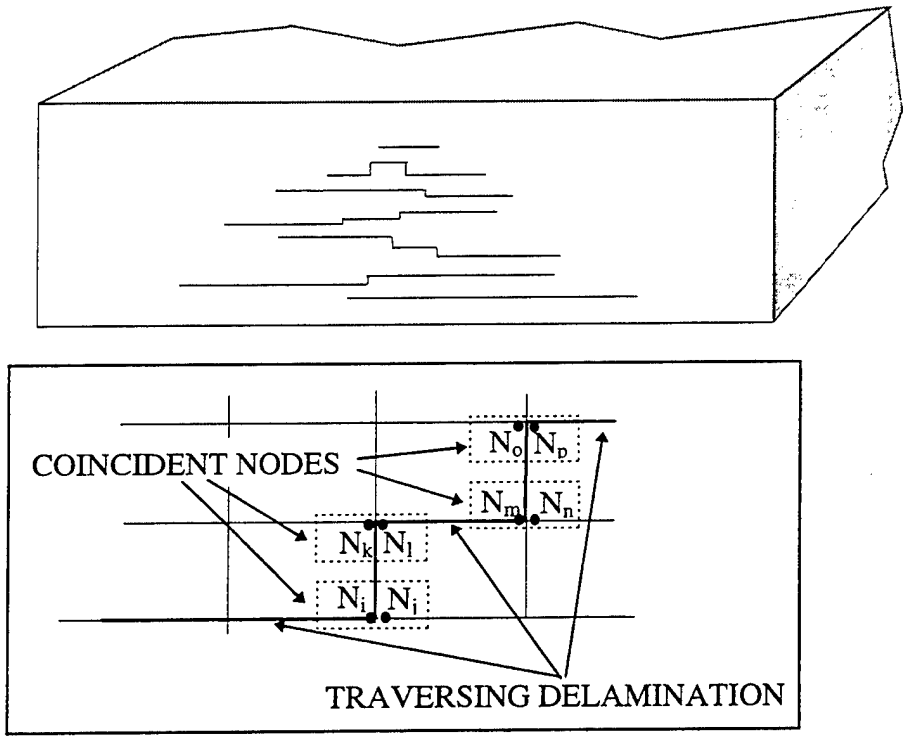

Figure 25. Modeling traversing delaminations.

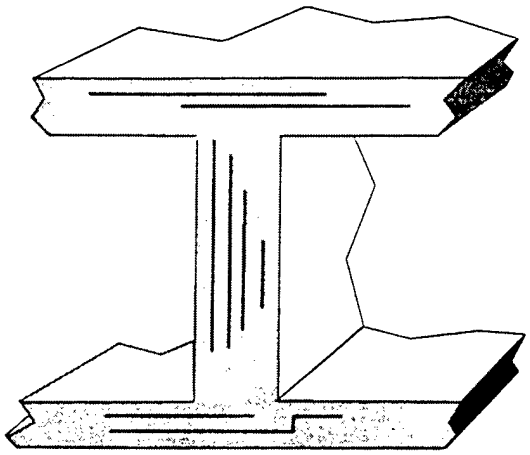

Figure 26. Arbitrarily oriented delaminations.

5.4 Post-Buckled Failure Modeling

The stability analysis incorporated into RESTRAN is linear. However, because local buckling is predicted during the progressive failure analysis, some approximation to post-buckled layer response must be applied while failure of the remaining laminate is being calculated. Towards this aim, after the prediction of local buckling is made, the coincident nodes defining the failed delamination are removed through condensation from the model, and assumptions are made regarding the remaining strength of the elements participating in the buckling mode. As depicted in Figure 27, different structures exhibit a range of post-buckled load-deflection response. As shown, a plate-type structure can exhibit significant further load carrying capability with possible transition to higher-order mode shapes with an effective reduction in material stiffness. To approximate post–buckled material behavior, RESTRAN permits an inelastic reduction in moduli to be applied. This implies a permanent reduction in properties; no elastic recovery of properties is assumed possible with unloading of the buckled layer. Several assumptions on post–buckled material behavior may be specified in RESTRAN. In the extreme case, moduli may be set to zero to remove any load carrying capability in the buckled layer and thus redistribute the applied loads to the remaining structure. An alternative assumption is that the buckled layer can further absorb load – and exhibit possible subsequent or additional material failure modes – but at a reduced modulus. Finally, the intermediate assumption of carrying the constant load in the post-buckled sublaminate corresponding to the critical load is approximated in RESTRAN through the option of a scaling procedure of element stiffness coefficients. This scaling for maintaining a constant load in a buckled sublaminate is accurate to the degree that the resulting layer deformations at subsequent loading remain similar to the pattern existing at the buckling failure load. This may be formulated by considering the initial element-level equilibrium expressed as

$$\{\mathbf{F}_o\} = [\mathbf{K}]\{\mathbf{U}_o\} \tag{154}$$

where $\{\mathbf{F}_o\}$ are internal forces due to the initial set of external applied loads. For a linear structure, the equilibrium relation at a critical multiple of the initial loads can be given by

$$\alpha_{cr}\{\mathbf{F}_o\} = [\mathbf{K}]\alpha_{cr}\{\mathbf{U}_o\} \tag{155}$$

If the displacement field remains similar such that at a higher load scale factor α_i yielding a set of displacement $\{\mathbf{U}_i\}$, it remains true that

$$\{\mathbf{U}_o\} \approx \frac{1}{\alpha_i}\{\mathbf{U}_i\} \tag{156}$$

Then, for any applied load, a scaling of the element stiffness matrices for those elements involved in the buckled sublaminate given by

$$\alpha_{cr}\{\mathbf{F}_o\} = \beta[\mathbf{K}]\{\mathbf{U}_i\} \tag{157}$$

will fix the equilibrium element forces at the level at which buckling was predicted with β given by

$$\beta = \frac{\alpha_{cr}}{\alpha_i} \tag{158}$$

Or, to allow increasing loads, β is implemented in RESTRAN as

$$\beta = \left(\frac{\alpha_{cr}}{\alpha_i} - 1\right) C_l + 1 \tag{159}$$

where C_l may be varied between 0 and 1. Thus, representing post-buckled behavior in a linear analysis is highly approximate, and the selection of a plausible post-buckled elastic response is important to guarantee a conservative estimate of the overall residual strength.

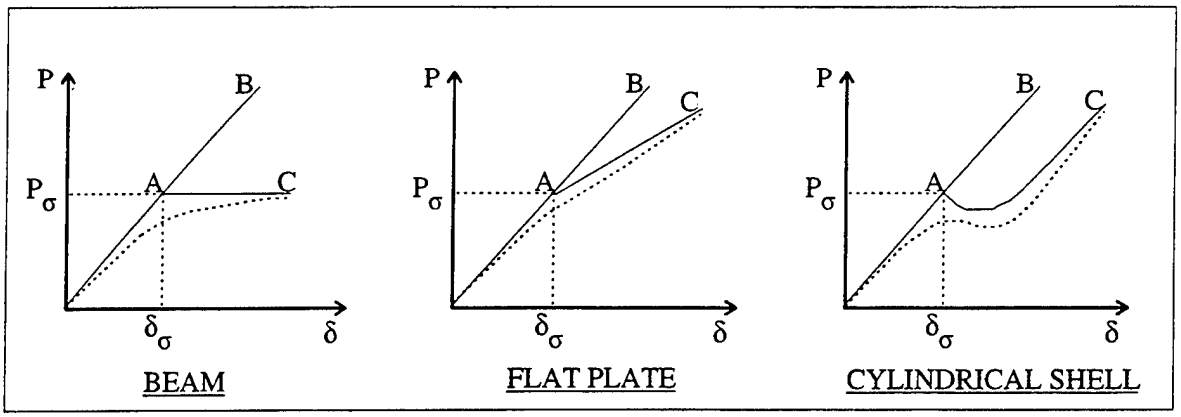

Figure 27. Post-buckling load carrying capability.

6 Solution Algorithms

Four different analysis procedures have been incorporated into RESTRAN. As depicted schematically in Figure 28, the available options are Prespass, Linear Static Analysis, Linear Buckling Analysis, and Residual Strength Analysis.

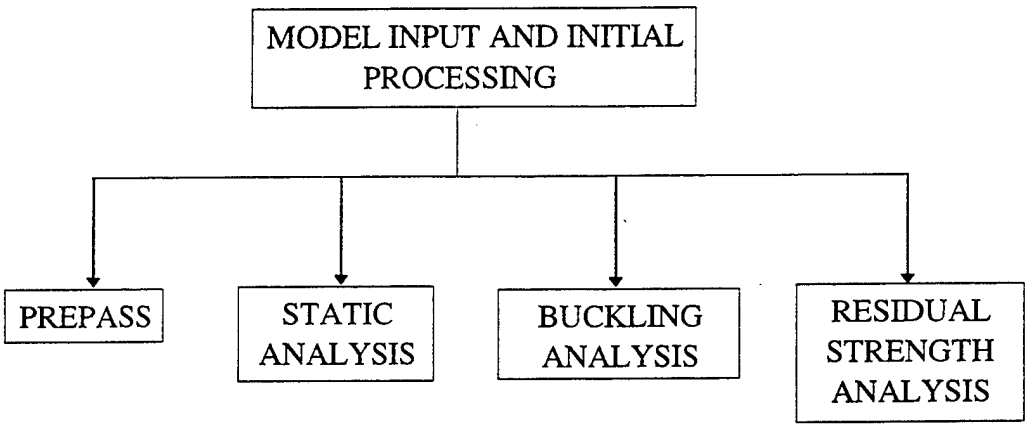

Figure 28. RESTRAN solution control options.

6.1 Prepass

Selecting prepass invokes assembling and checking the inputted model after which the program is terminated. This causes numerous tests on the finite element model to be performed which are written to the standard output file. The internal tests performed include checks on element connectivity and geometry, boundary conditions, applied point or pressure loads, and material property assignments. In addition, RESTRAN provides an optional feature which creates an output file containing graphics information to view the input model. RESTRAN supports output formats for MATHEMATICA [69] or TECPLOT [70] and has the option for a user-defined subroutine to format graphics data as required. This feature is used as an additional test to check for possible modeling errors prior to performing a detailed residual strength analysis. The graphical depiction is particularly useful in complex geometries which may have been created using general preprocessing codes such as PATRAN [71], or using the node and element generation option available in RESTRAN. The flowchart of execution in Prepass is depicted in Figure 29.

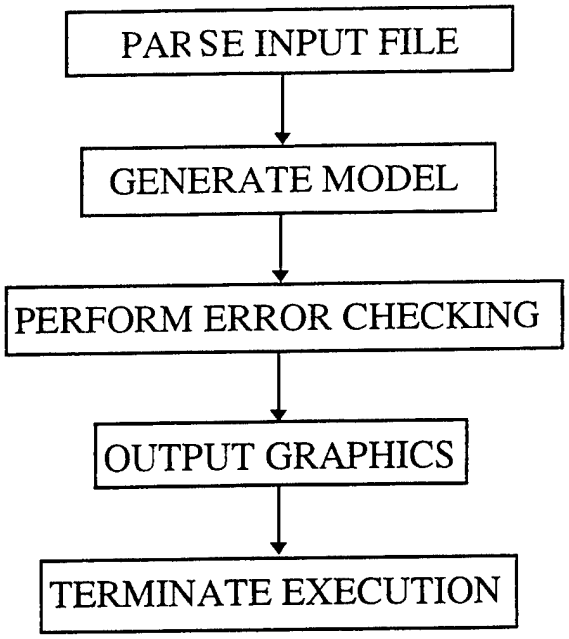

Figure 29. Prepass flow chart.

6.2 Static and Buckling Analysis

The single-pass displacement and buckling solutions are made available to obtain the linear elastic response of the model under applied loads. Schematic flow charts of these solution sequences are presented in Figures 30 and 31. The displacement solution yields the basic deformation pattern together with optional stress and strain output at ply layers or Gauss points. In addition, requesting a ply failure output will cause additional computations of failure indices within elements. This information is used to output the minimum predicted scale factor to the applied loads to cause the next material failure. Within the context of a linear static analysis, this scale factor may be considered as a residual strength measure based on an overall first-ply failure prediction. The buckling solution may be used as a preliminary check on single-layer buckling response or the simultaneous instability of multiple delaminations as a comparison to running a residual strength analysis in which multiple delaminations are automatically analyzed individually. In both displacement and buckling solutions, graphical output may be requested that is generated in the form of an external file which may be directly inputted into a selected graphics program such as MATHEMATICA or TECPLOT to view deformed geometry or buckling mode shape.

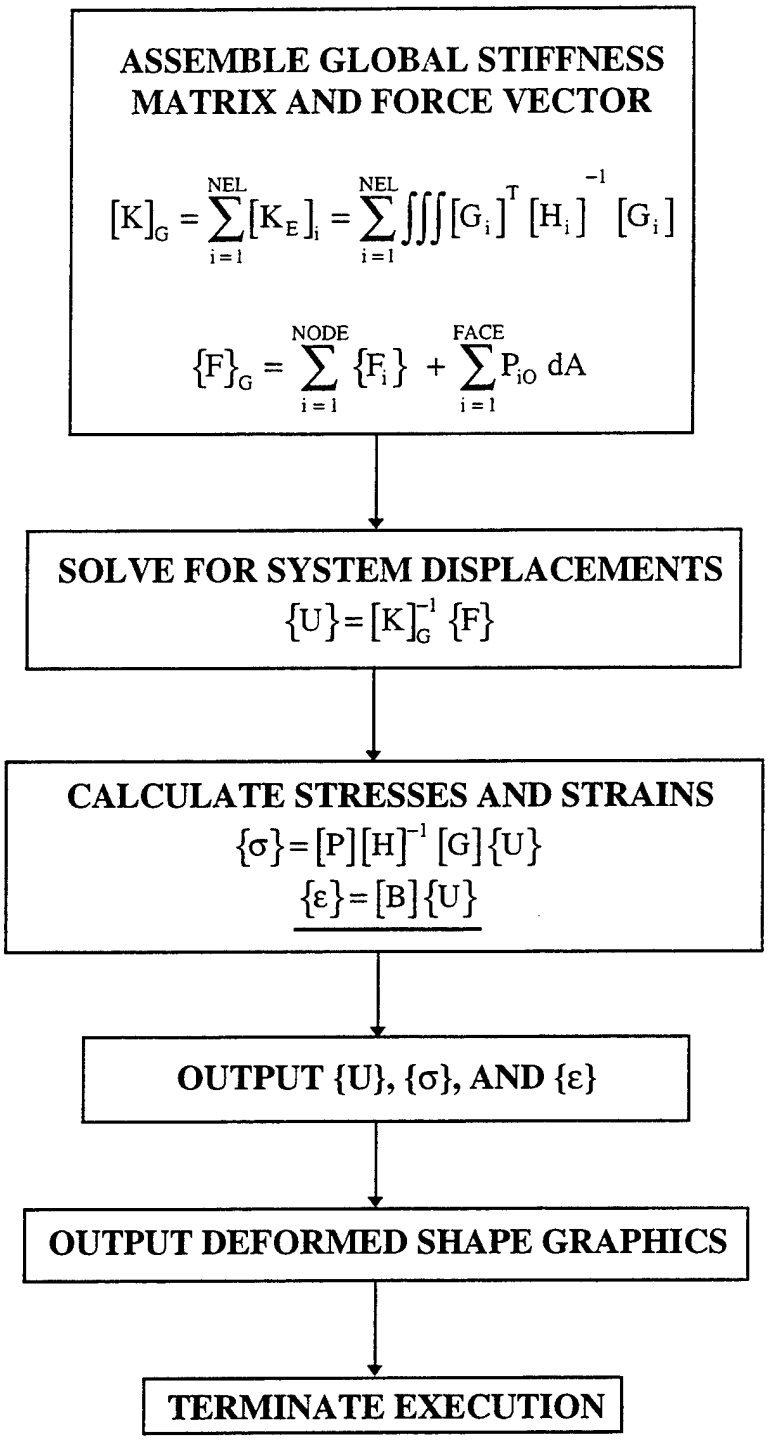

Figure 30. Flow chart of static analysis.

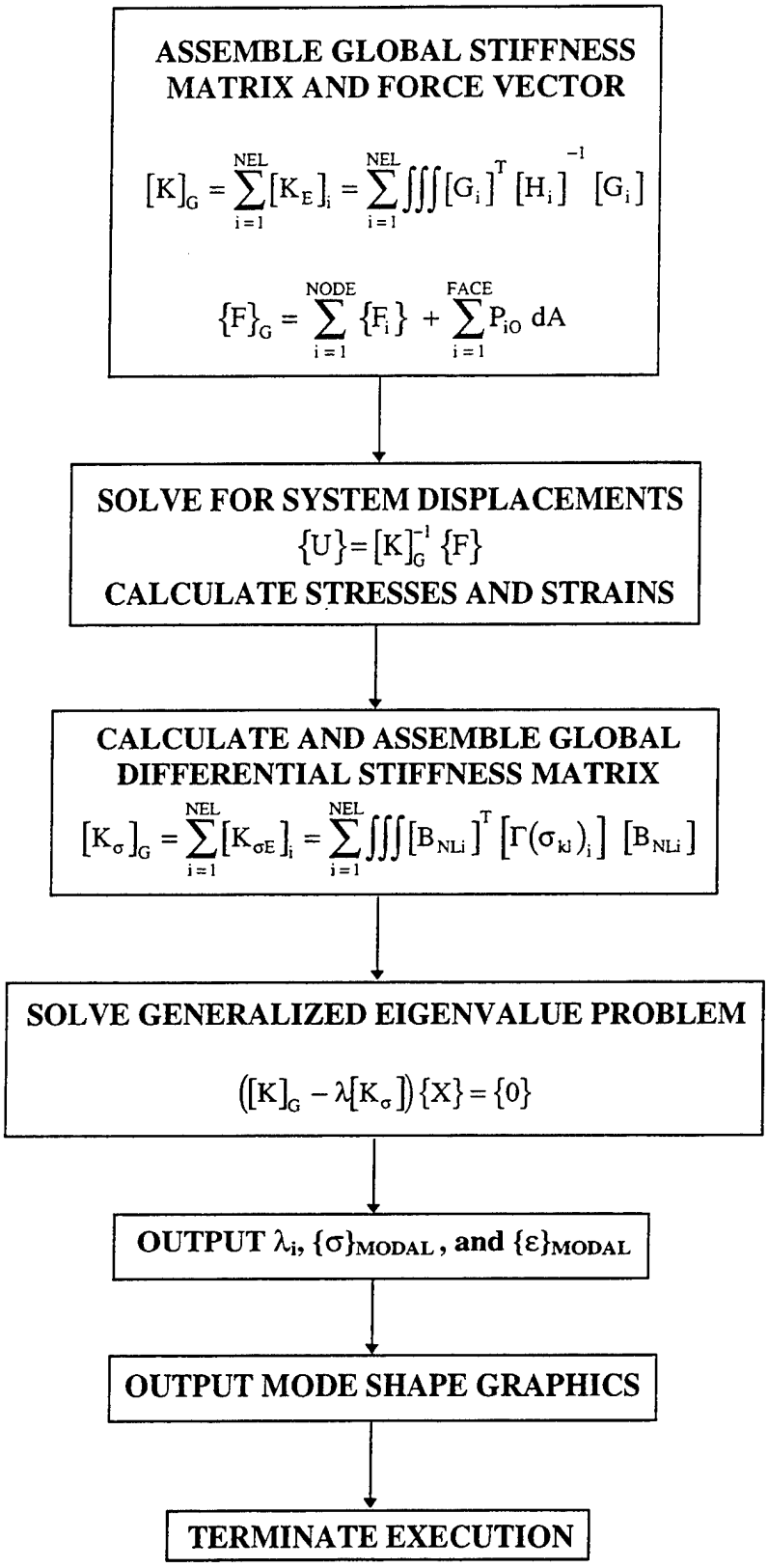

Figure 31. Flow chart of buckling analysis.

6.3 Residual Strength Analysis Algorithm

In representing realistic structural geometries and support and load conditions, a viable algorithmic treatment in simulating material behavior and failure modes under increasing load is critical to the success of the analysis. In real structures, the progression of local failure modes are not independent, but tend to be coupled and occur simultaneously. A sequential algorithm, however, to be tractable, requires that these effects be considered separately. The important structural behaviors simulated by RESTRAN are nonlinear material moduli, material ply–level failure differentiated into various modes, local instability of delaminated sublaminates and global buckling of the entire model, and approximate post–buckled material response. The primary variable is the scale factor applied to the vector of initial loads to determine a sequence of failure in a combined incremental and iterative fashion. The estimated scale factor for causing material failure is obtained from linear extrapolations for each ply using selected failure criteria. The scale factor for minimum buckling loads are obtained from eigenanalysis. The effects of material nonlinearity due to stress/strain relationship and post-buckled behavior of delaminated layers are considered separately from failure prediction. Thus, at the i^{th} failure cycle, iterations are first performed to converge both the incremental displacements and the minimum positive buckling eigenvalue. At convergence, the load multipliers are compared, and the minimum dictates whether the next failure event is predicted to be a material mode or a buckling mode. For buckling failure, the element set involved is computed, selected post-buckled failure assumptions imposed, and the failed delamination is condensed out of the model. For material failure, iterations are performed at fixed load to update element properties due to applied damage laws, stress redistribution is calculated, and additional element failures are processed. Convergence is established when no additional element failures are predicted at the current load. A flowchart of the residual strength prediction algorithm is contained in Figure 32. The residual strength solution analysis combines a number of available options. These options modify the solution algorithm to assess assumed modes of failure or to tailor the analysis for specialized failure/damage laws or complicated geometries. Table 3 shows the analysis options.

Table 3. RESTRAN solution options.

• Predict progressive material failures only.
• Predict sequential buckling failures only.
• Predict combined material and instability failures.
• Apply standard material failure criteria.
• Apply user-defined material failure criteria.
• Apply standard material damage laws.
• Apply user-defined material damage laws.
• Access user-defined subroutine to interpret complex buckling modes such as simultaneous multiple delamination buckling.
• Process nonlinear elastic material behavior.
• Apply specific post-buckled material behavior.

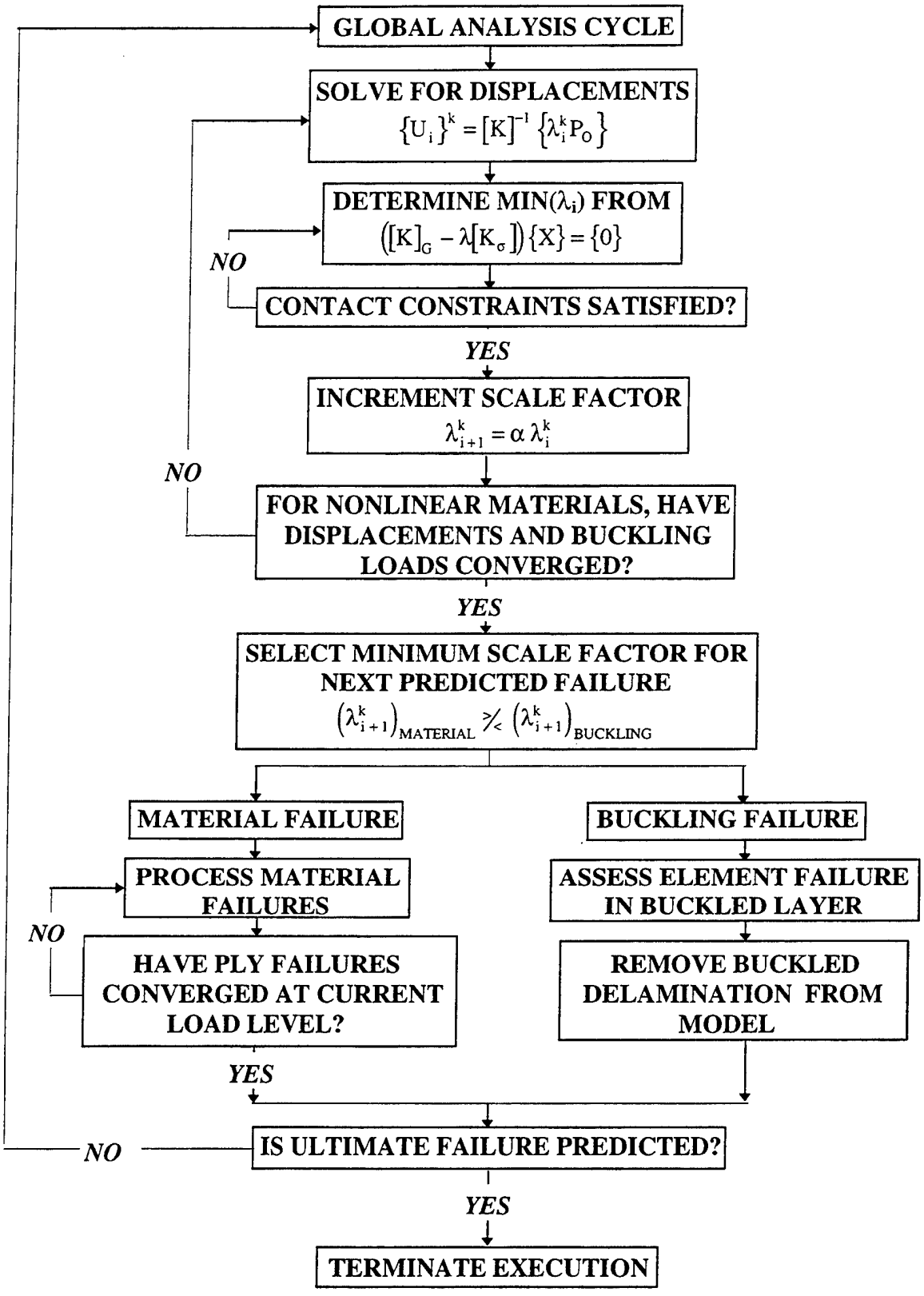

Figure 32. Flow chart of residual strength solution algorithm.

7 Ultimate Failure Prediction

The residual strength of a damaged laminated composite is obtained when catastrophic or ultimate failure is predicted. During execution of the solution sequence in which incremental failures are assessed, a running account of the maximum scale factor to the applied loads is maintained. A typical failure sequence may initially demonstrate low loads to cause local failures such as near-surface delamination buckling or material failure in an area of high stress concentration. Subsequent failures may involve simultaneous buckling of thick sublaminate ply groups or large regions of material damage. Final failure may be precipitated through global buckling of remaining layers or through a catastrophic cascade of element material failures as loads are redistributed at each iteration. Specific checks performed in RESTRAN are listed in Table 4.

Table 4. Tests for catastrophic failure.

• Existence of 'soft' deformation or rigid body displacement modes.
• Prediction of global or mixed-mode buckling.
• Stiffness loss exceeding 90% due to material and structural failure.
• Failure at nodes at which external loads have been applied.

If the lowest load multiplier in a particular analysis cycle predicts global buckling, no further load–carrying capability in the post–buckled regime is assumed, and ultimate failure is predicted. As element material properties are degraded due to material or local buckling failure, possible fragmentation is assessed by testing for positive indefiniteness by performing an L^TDL decomposition. Related to this, if the percentage of individual degrees of freedom with no associated stiffness exceeds 90%, ultimate failure is assumed, regardless if the remaining model is unfragmented. Finally, if failure has occurred at nodal degrees of freedom to which external loads are applied, total failure is assumed because subsequent scalar load multipliers lose definition as the initial vector of applied loads has been changed. An input parameter is available to preclude elements associated with applied loads from exhibiting failure.

8 Computer Implementation of RESTRAN

RESTRAN is written in FORTRAN 77. In the development of the various algorithms, no special features dependent on specific computer platforms have been exploited to speed execution in order to guarantee portability of the code. The finite element basis of RESTRAN naturally leads to the generation of large, sparse, banded matrices in representing the global elastic and differential stiffness properties of the complete model. Internal algorithms have been created to process matrix storage modes in various formats. These include full matrix storage for small problems, half-bandwidth storage format (default), and out-of-core storage for large problems that exceed internal RAM memory capacity or user stacksize limits and require most data storage to be placed in external files. These features were incorporated as-

suming that not all platforms on which RESTRAN would be installed would support internal virtual memory swap operations. Setting the internal memory parameters and selecting the algorithmic path are discussed in the RESTRAN User's Manual [31]. The choice of internal operation is entirely dependent on execution speed, which is determined by the amount of data that can be held in high-speed in-core memory. Thus, the out-of-core solution mode is slowest due to the high I/O overhead of transfering data between core and external files. Although different algorithmic approaches are sometimes used for the different memory storage modes to perform various operations, excluding I/O operations, they are computationally competitive in terms of operation counts.

After parsing the input file, element connectivity information is used in a modified Sloan's bandwidth minimization procedure [72] to obtain internal equation numbers. The bandwidth is determined as the maximum of the bandwidth resulting from considering only the initial input connectivity and from that determined by considering the coincident nodes due to all input delamination planes. These operations are performed in a preface section of the RESTRAN code which liberally allocates memory to various arrays used in input file processing. After basic model characteristics are determined, such as the number of degrees of freedom, nodes, elements, and connectivity as represented by the bandwidth, the internal memory is reconfigured such that array dimensions are streamlined to the required job size.

The global elastic and differential stiffness matrices are formed using a direct assembly approach. For in-core operation, the entire global stiffness matrix is accumulated before being written out to disk. In an out-of-core operational mode, blocks of eight rows of the global stiffness matrix are read in and element contributions are added based on the internal equation numbering of element degrees of freedom (DOF). This block is then written to an external file and the process repeated until all stiffnesses have been assembled.

During execution, degrees of freedom are removed from the active analysis set through applied zero displacement boundary conditions, failed DOF's at which material failure has reduced the stiffness to zero, and eliminated DOF's associated with coincident nodes removed when failed delaminations are removed from the model. The condensation procedure utilizes a direct row/column elimination on the global matrices. Disk space utilization requires that in addition to the elastic and differential stiffness terms stored externally, decompositon and reduction of these data blocks are written to separate files. This leads to the requirement that four global matrices need to be stored externally in scratch files; thus, care must be given to configuring an adequate size of the disk partition in which RESTRAN is to be executed. Internally, as soon as a matrix is no longer needed, the external file in which it is resident is closed to free up disk space.

The solution for displacements is obtained using different equation solvers depending on storage mode. For full matrix storage a Gaussian elimation scheme with full pivoting is employed. For band storage, the sparse symmetric banded solver routines DPBCO and DPBSL, available from the LINPACK [73] linear algebra library, are used. The solution is based on a Cholesky decomposition followed by a back substitution using the triangular Cholesky factor. A variation of this algorithm is used for out-of-core solution and is implemented

in RESTRAN based on the program SESOL presented by Wilson et al. [74]. This solver calculates the maximum equation block size that can be held in core. Upon completing the decomposition of each block, the solution vector is formed by sequentially accessing each block contained on direct storage. The minimum memory requirements of this routine is for at least two equations being held in memory per equation block. The number of blocks is dictated by the amount of high-speed RAM memory available.

Eigenanalysis using full and band storage modes can be performed using a subspace iteration method detailed in section 2.4. The current implementation uses the implicitly restarted Arnoldi iteration method for band and out-of-core storage modes. A robust implementation of this method is contained in the routines DSAUPD and DSEUPD available in the ARPACK distribution [75]. In turn, these routines are dependent on basic operations and algorithms provided by the BLAS and LAPACK libraries [76,77]. As implemented in RESTRAN, minimum memory requirements are approximately $12 \times N_I$, where N_I is the order of the eigenproblem. In forming iteration vectors, ϕ, it is required to repeatedly solve a linear system of the form

$$\{\phi\} = [\mathbf{K} - \lambda[\mathbf{K}_\alpha]]^{-1}\{\mathbf{K}\overline{\mathbf{V}}\} \tag{160}$$

where $\overline{\mathbf{V}}$ is an iteration vector. This is accomplished using an appropriate solver discussed above and constitutes the major computational expense in performing the eigenanalysis.

A single large working array is used in RESTRAN to perform computations. Total memory requirements for in-core storage modes are essentially dictated by the size of this array. In a full matrix storage mode used for small problems, core memory is essentially $N_D \times N_D$ double precision words, where N_D is greater or equal to the number of input DOF. For band storage, in-core memory is on the order of $N_D \times M_B$, where M_B is the half bandwidth of the global matrix. Finally, using the out-of-core algorithm reduces the size of the working array such that the collective size of the numerous other small arrays used in RESTRAN become dominant in setting the program memory size. In the current program release, this requirement is approximately equal to $21 \times N_D$.

9 Numerical Studies

An initial set of benchmark problems were solved to assess the accuracy and convergence properties of the hexahedral element incorporated into RESTRAN, and to suggest a degree of discretization required to adequately simulate local laminate behavior. Of particular interest is in quantifying the effect of the incompatible modes incorporated into the Pian-Tong element in accurately supporting bending behavior within a three-dimensional continuum element formulation. The Pian-Tong element is well known to be insensitive to geometric distortion and has a superior accuracy over displacement–based elements in predicting stresses. These features yield an ideal element for modeling three-dimensional stress states for local failure prediction, and thereby yield accurate differential stiffnesses which are evidenced by the rapid convergence of buckling load predictions. A first illustration of the basic

element performance is the prediction of Euler column buckling loads. Three models shown in Figure 33 were selected using 3, 5, and 10 elements, repectively. The column dimensions are $10 \times 1 \times 1$, and material properties are given by E = 1.0E9 and $\nu = 0.3$. The results presented in Table 5 show a rapid convergence to the exact solution.

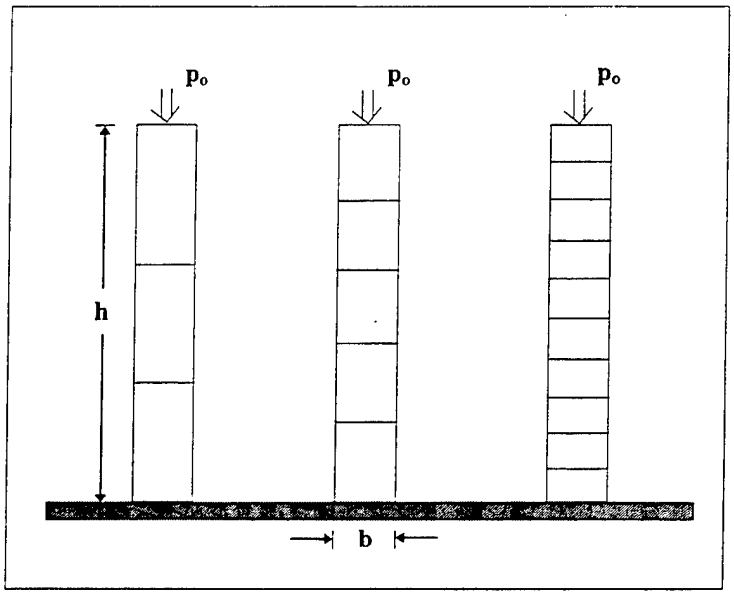

Figure 33. Models for Euler column buckling load determination.

Table 5. Convergence of column buckling loads.

Model	λ	% error
3-Element	2187.00	6.363
5-Element	2099.67	2.126
10-Element	2060.65	0.218
Exact	2056.17	

The modeling of plates using three-dimensional solid elements has been demonstrated to generate accurate results with large element aspect ratios while representing full three–dimensional elasticity [78-81]. To illustrate the capability of the current three-dimensional continuum element to predict plate-like behavior, a simply supported square plate was selected with dimensions $10 \times 10 \times 0.1$ and isotropic material properties given by

$$\begin{aligned} E &= 1.0000E9 \\ G &= 0.3846E9 \\ \nu &= 0.3 \end{aligned} \tag{161}$$

This plate was analyzed statically to determine maximum deflections due to a uniform applied surface pressure, and instability was analyzed by considering the plate subjected to end-loading in compression and determining the fundamental buckling load. The geometry and loading conditions are depicted in Figure 34. The convergence of the solution with increasing discretization is presented in Table 6.

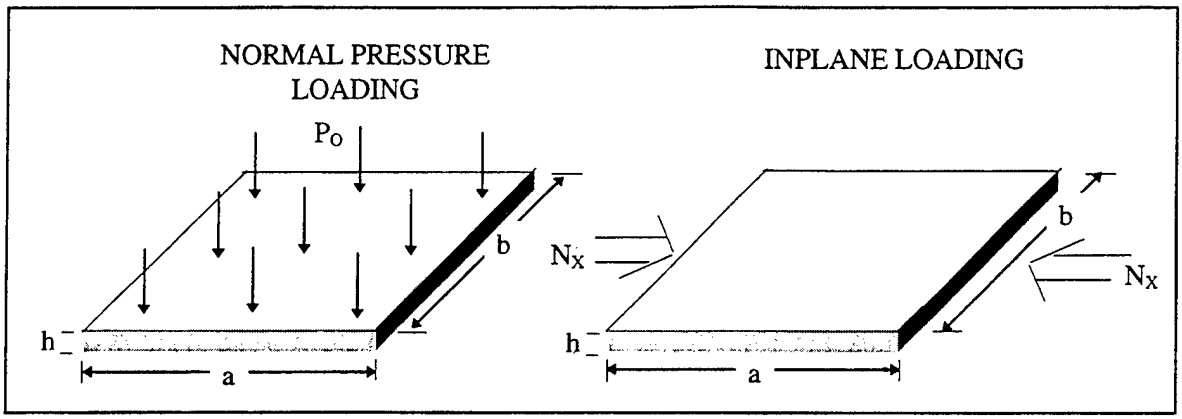

Figure 34. Geometry and loading of a flat plate.

Table 6. Convergence study for an isotropic plate model.

Model*	$Wmax_1$	λ
2 x 2f[a]	-.0003707	5.0569E4
4 x 4f[a]	-.0004391	3.8996E4
4 x 4s[b]	-.0004431	3.6791E4
8 x 8s[b]	-.0004441	3.6252E4
Exact	-.0004443	3.6152E4

[a] A full plate was used in generating results.
[b] A symmetric quarter plate was used in generating results.

To assess the effect of aspect ratio in the solution for plate deflections, the isotropic plate used above was analyzed with different thickness ratios. The solutions are presented in Table 7 and are compared with the exact solution for a thin plate in plane stress given by Timoshenko and Woinowsy-Krieger [82] by

$$w_{max} = 4.433 \times 10^{-4}\left(\frac{1}{h^3}\right)^{-1} \tag{162}$$

Table 7. Effect of element aspect ratio.

a/h	W_{Max}/W_{CPT}
10	1.1293
100	1.0017
1000	1.0000
10000	0.9194
100000	0.0035

In comparison with a classical plate solution (CPT), an element aspect ratio of 10 – which is considered in the regime of thick plates – shows an increased flexibility attributed to transverse normal and shear deformation effects. In the thin plate regime where a/h $\geq$ 100, the maximum deflections are shown to agree with the classical solution for several reduced orders of magnitude in plate thickness. Above a/h = 10^4, the solution deteriorates due to locking which is clearly evident at a/h = 10^5. Thus, with the present use of the Pian-Tong hexahedral, most expected layer aspect ratios can be accurately simulated.

In modeling composite laminates, as the number of plies being modeled in a single layer increases, the effects of membrane–bending and twisting coupling diminish [42]. As these coupling phenomena vanish, the behavior of the ply group tends towards the behavior of a single equivalent homogenous specially orthotropic layer. To demonstrate convergence, a highly orthotropic layer with properties listed below is analyzed.

$$\begin{array}{llllllll} E_1 & = & 40.0\text{E}6 & E_2 & = & 1.0\text{E}6 & E_3 & = & 1.\text{E}6 \\ G_{23} & = & 5.0\text{E}5 & G_{13} & = & 2.0\text{E}5 & G_{12} & = & 5.0\text{E}5 \\ \nu_{23} & = & 0.25 & \nu_{13} & = & 0.25 & \nu_{12} & = & 0.25 \end{array}$$

Plate dimensions were selected as $10 \times 10 \times 0.05$, and a uniform normal pressure was applied. Comparison to the exact solution yields a rapidly convergent solution, as shown in Table 8.

Table 8. Deflections of an equivalent homogeneous orthotropic plate.

Model	W_{Max}/W_{Exact}
2 x 2f	0.7911
8 x 8f	0.9968
10 x 10f	0.9981
16 x 16f	1.0002

To assess the behavior of the present element in the case of significant coupling between membrane and bending deformations, a cross ply [0/90] ply group is analyzed. The finite element model was composed of two layers to assign the different ply properties to each layer. Using the orthotropic material with a material aspect ratio of 40 and analyzing a

thin rectangular plate with a/b = 2 and h = 0.01 under a uniform load, Table 9 shows the convergence of the solution compared to a classical solution presented by Jones [42].

Table 9. Deflections of a cross-ply [0/90] laminate.

Model	W_{Max}/W_{Exact}
2 x 2f	0.8220
4 x 4f	0.9601
8 x 8f	0.9598
10 x 10f	0.9599
16 x 16f	0.9604

The results show that the three-dimensional formulation converges rapidly to a maximum deflection 4% less than the series solution derived utilizing two-dimensional plane stress assumptions for the maximum center deflections in a highly coupled, cross-ply [0/90] ply group. For multiple cross-ply or angle-ply groups modeled in a single effective layer, the combined ply properties exhibit diminishing coupling and behave increasingly as a homogeneous orthotropic layer.

The essential behavior of the solid continuum element incorporated into RESTRAN has been shown in a variety of plate configurations which have investigated solution accuracy as a function of element aspect ratio, material orthotropy, coupling effects, and the prediction of instability buckling. These results have been quantified through comparison with exact solutions.

The following illustration in modeling composite sublaminates is presented without comparison to any known exact solution. A rectangular laminated plate with a central elliptical delamination is selected to demonstrate convergence and contact constraints in a more complicated case of instability. All models were generated using the RESTRAN *MODEL GENERATION feature with the parameter NDIV used to determine the level of discretization. The laminate contains 96 plies of nominal thickness 0.0052 in with a near surface delamination between the eighth and ninth plies. The layup is given by $[\pm 45/0_6||(\pm 45)_5/90_{12}/(\pm 45)_5/0_6/ \pm 45/(\pm 45/0_6/(\pm 45)_5/90_6)_S]$, where || indicates the location of the delamination. The plate dimensions are 15 in × 15 in × 0.4992 in, and the elliptical delamination is centrally located with semimajor axis given by a = 10.0 in and semiminor axis by b = 7.5 in. Undamaged ply properties are given by

$$\begin{array}{llllll} E_1 = 181.0E9 & E_2 = 10.3E9 & E_3 = 10.3E9 \\ G_{23} = 7.17E9 & G_{13} = 1.0E9 & G_{12} = 1.0E9 \\ \nu_{23} = 0.28 & \nu_{13} = 0.28 & \nu_{12} = 0.28 \end{array}$$

Reduced, isotropic properties were assigned to the elements above the delamination to simulate impact damage. These properties are given by

$$E = 1.0\text{E}9 \qquad G = 3.846\text{E}8 \qquad \nu = 0.3$$

The entire plate model is shown in Figure 35.

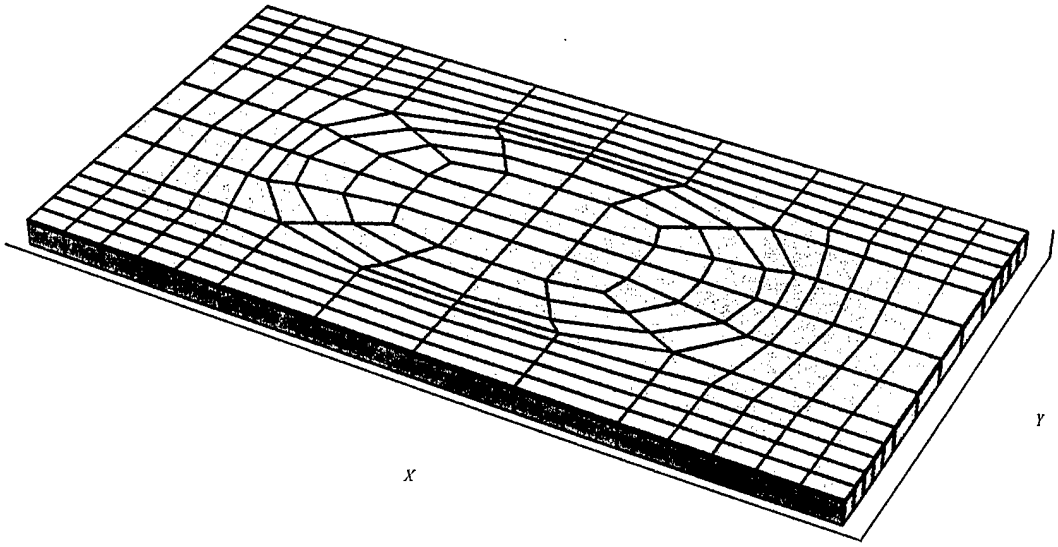

Figure 35. Laminated plate with elliptical delamination.

The full model is reduced to a half model by assuming that the buckling modes will have the x-axis as a plane of symmetry. The tolerance for assessing relative motion of the opposing delamination surfaces was set to zero. Figure 36 shows the convergence of the unconstrained and constrained buckling modes and the associated eigenvalues.

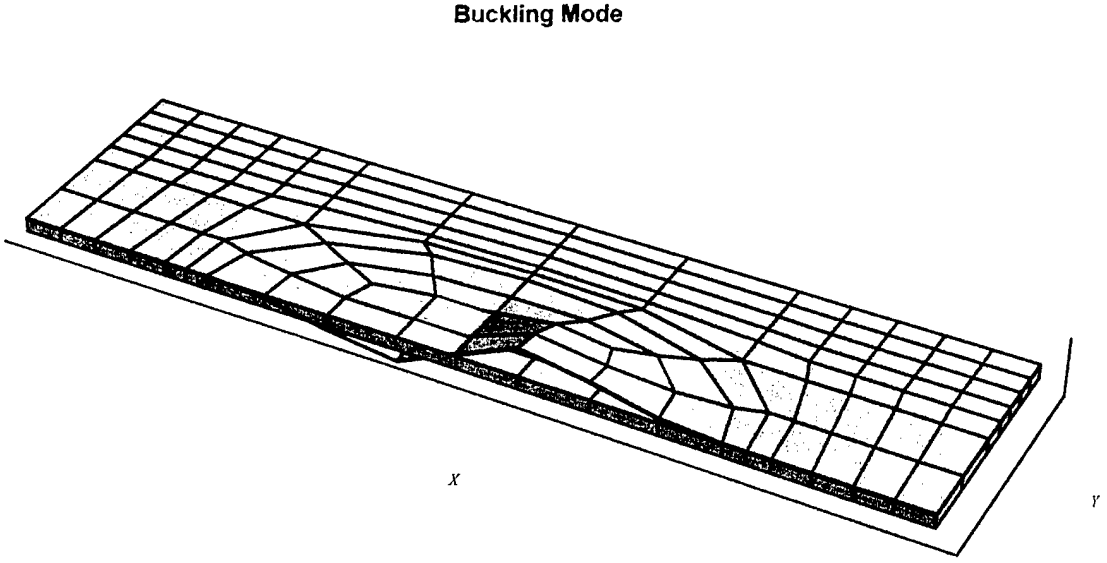

Figure 36(a). NDIV = 4. No constraints applied. $\lambda = 2.0525E5$.

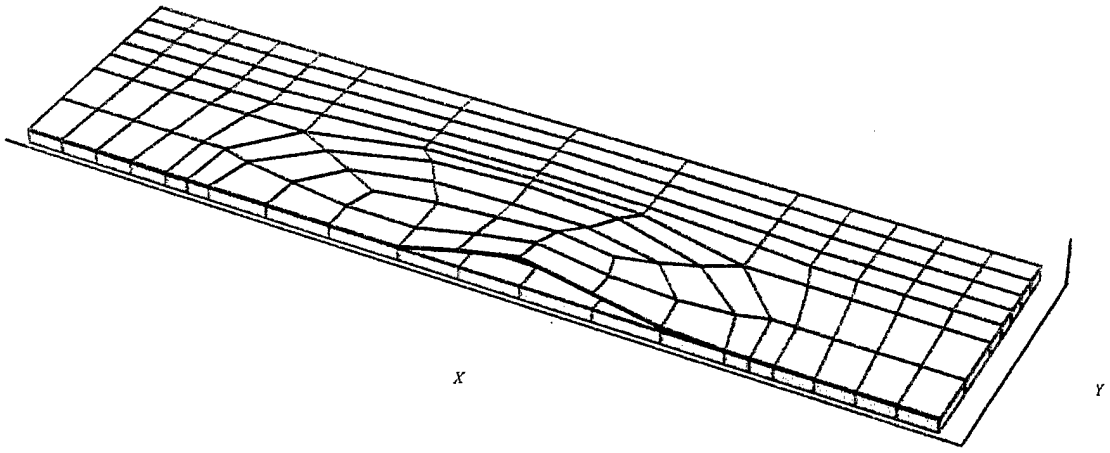

Figure 36(b). NDIV = 4. Compatibilty constraints enforced. $\lambda = 3.1637E5$.

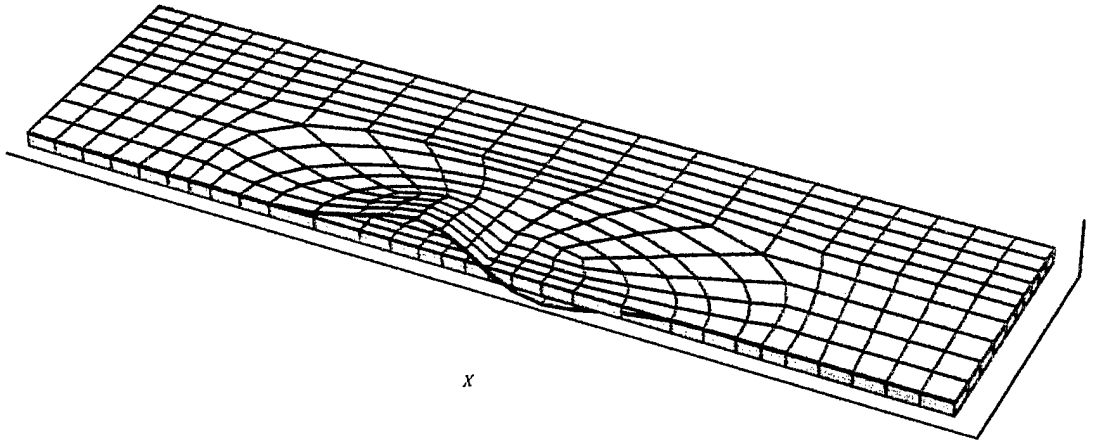

Figure 36(c). NDIV = 8. No constraints applied. $\lambda = 1.4667E5$.

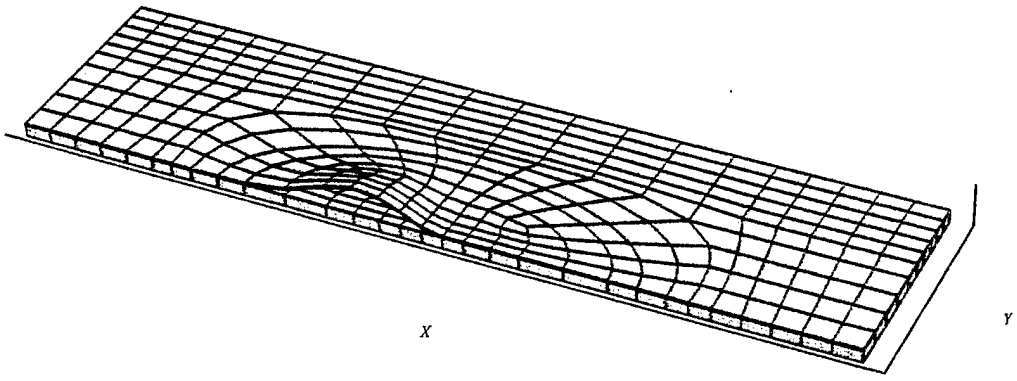

Figure 36(d). NDIV = 8. Compatibility constraints enforced. $\lambda = 2.1523E5$.

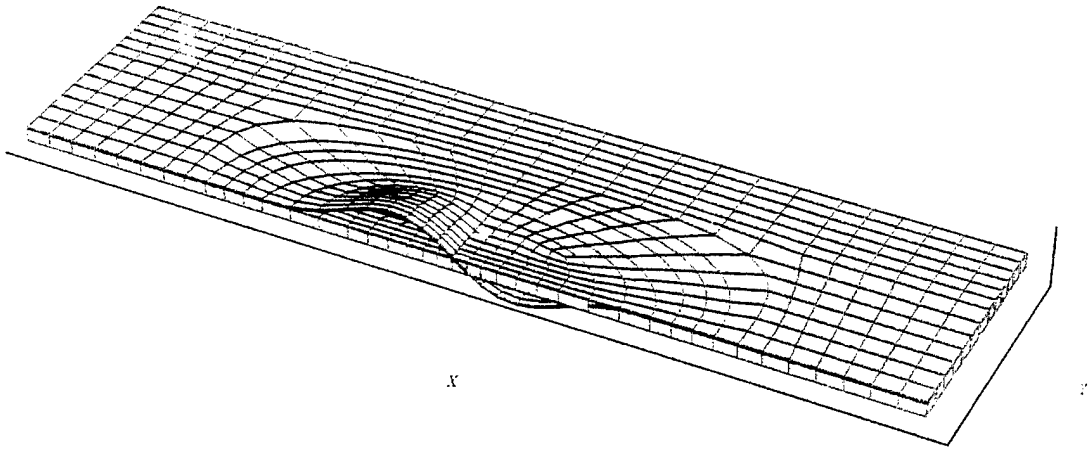

Figure 36(e). NDIV = 12. No constraints enforced. $\lambda = 1.3864E5$.

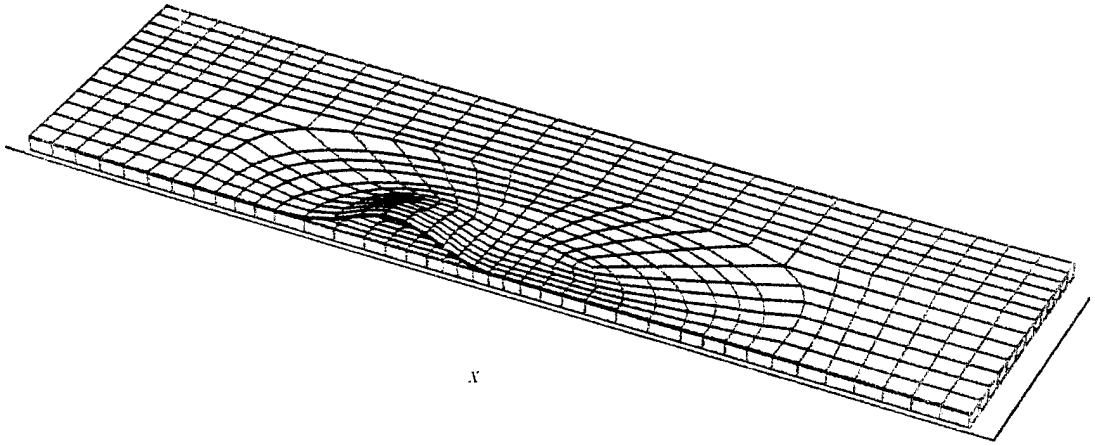

Figure 36(f). NDIV = 12. Compatiblity constraints enforced. $\lambda = 1.9803E5$.

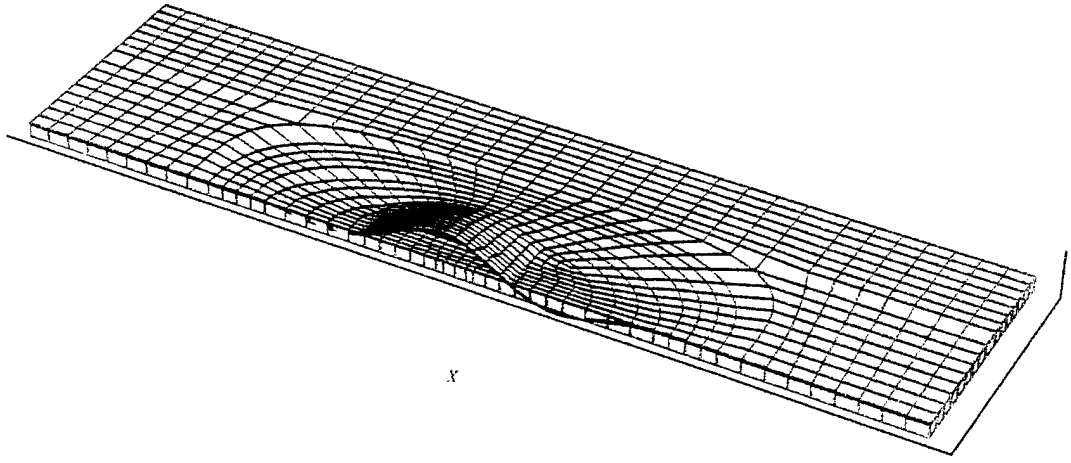

Figure 36(g). NDIV = 16. No constraints applied. $\lambda = 1.3956E5$.

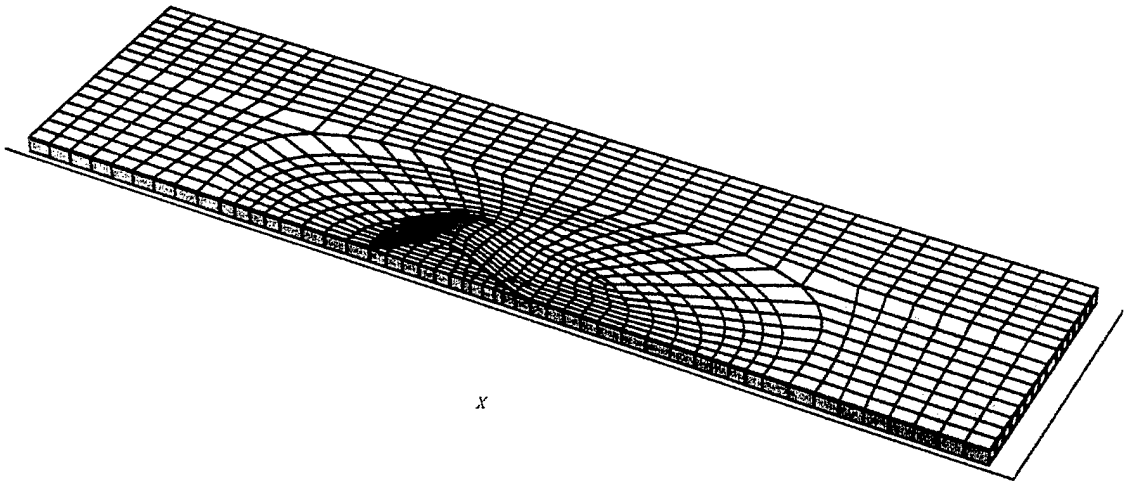

Figure 36(h). NDIV = 16. Compatibility constraints applied. $\lambda = 2.0527E5$.

The eigenvalues show a rapid convergence and are tabulated in Table 10. In a linear analysis, the mode shapes are of arbitrary sign and magnitude and can, thus, alternate between equivalent configurations. The minimum energy state corresponding to the fundamental buckling mode is a function of geometry, loading, and material properties. For plate geometries, the buckling mode can be described by the number of half waves lengths exhibited by the mode shape along each inplane coordinate, (n,m). Depending on the value of the independent plate variables, different modal buckling patterns can be elicited. In a finite element analysis the degree of discretization becomes a variable in resolving the mode shape, and in the example, for the first three levels of model refinement, the mode shapes demonstrate a (2,1) pattern. At the highest level of discretization however, a mode crossover is seen in Figure 36(g), where the mode shape changes from a (2,1) to a (3,1) pattern at essentially the same critical load as that determined in the model shown in Figure 36(e).

Table 10. Convergence of unconstrained and constrained critical buckling loads.

NDIV	Unconstrained	Constrained
4	2.0525E+5	3.1637E+5
8	1.4667E+5	2.1523E+5
12	1.3864E+5	1.9803E+5
16	1.3956E+5	2.0527E+5

The above set of standard deformation and buckling problems demonstrate an accurate simulation of plate-like bending and instability behavior using the incorporated hexahedral element while calculating three-dimensional stress states for material failure to be predicted using the same model.

10 Practical Analysis of Residual Strength

Because of the complex state of internal damage in impacted composites, the practical application of any residual strength predictive methodology requires a simplified definition of the type of damage and its spatial distribution. This definition is required to analyze existing structures exposed to impact and new design concepts with assumed internal damage states. The accuracy in predicting residual strength is entirely dependent on the accuracy in which internal damage can be resolved. For in-service structural components, a depot-level inspection must be capable of discerning interal damage accurately enough to safely assess repair/no-repair options for continued service applications. For design, specific characterizations of maximum sustained impact damage need to be developed to assess survivability and damage tolerance of structures to expected impact threats.

10.1 Damage Characterization

For a given impact event, the extent of impact damage can be determined from a simulation of the impact event based on first principles in elastodynamics, nonlinear material constitutive relations, and contact dynamics. A basic measure is the amount of energy absorbed due to impact. This may be expressed as

$$U = v_o \int_0^t F dt + g \int_0^t F t dt - \frac{1}{2M} \left(\int_0^t F dt \right)^2 \tag{163}$$

where v_o is the velocity of the impactor, M is the mass of the impactor, F is the impact force, g is the acceleration due to gravity, and t is the time duration of the impact event. In turn, this energy can be differentiated into components, U_E and U_D, where U_E is the energy converted into elastic deformation of the specimen, and U_D is the component of energy absorbed in irreversible daqmage causing mechanisms. Assuming basic damage modes in composite materials, the damage energy may be further decomposed as

$$U_D = U_M + U_F + U_C \tag{164}$$

where U_M is the energy absorbed in matrix cracking, U_F is the energy consumed in figer breakage, and U_C is the energy required to cause the creation of fracture surfaces in the form of interlaminar delaminations and transverse cracks. The apportioning of energy to each damage mode must be assumed, measured, or calculated to analytically predict the three-dimensional spatial distribution of damage [63].

The increasing development and application of health monitoring technologies such as embedded fiber optic sensors will permit an increasingly accurate characterization of internal damage states due to sustained impacts. Continued improvements in established nondestructive evaluation methods such as acoustics/ultrasonics [83-89], thermography [90,91], and computed tomography [92-95] are providing increasingly accurate resolutions of internal damage states and the ability to distinguish different damage modes.

The increasing ability to characterize internal damage states in existing composite structures exposed to impact will better define damage tolerant design objectives and provide more accurate initial damage conditions for input to analytical methodologies such as RESTRAN for predicting residual strength.

10.2 Demonstration Problem

To illustrate the execution of the RESTRAN analysis program, a model of an elastically supported laminated composite face plate is analyzed. Due to the lack of data of sufficient resolution regarding the spatial distribution of specific internal damage modes and subsequent experimental determination of residual strength, a specific state of internal damage is assumed for the following example. The geometry and applied loading is shown in Figure 37.

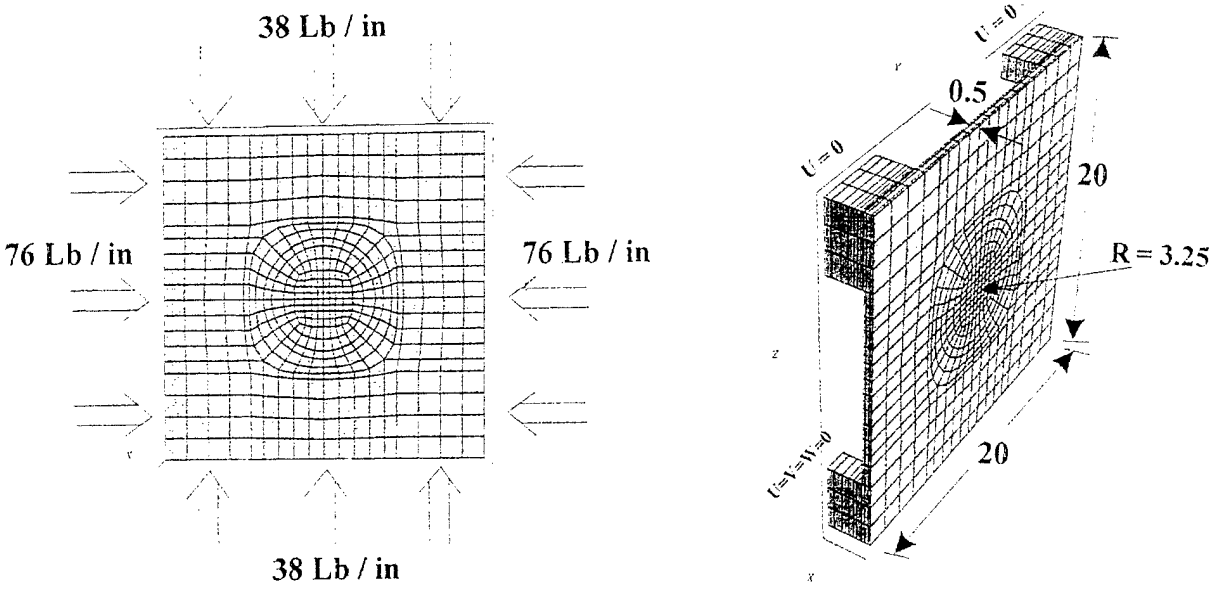

Figure 37. Geometry and loading of an elastically supported composite plate.

Material properties were selected as S2-Glass/3501 Epoxy tape with a nominal ply thickness of 0.0052 in. The material elastic properties are given by

E_1	=	7.150E6 Psi	E_2	=	2.13E6 Psi	E_3	=	2.13E6 Psi
G_{23}	=	0.71E6 Psi	G_{13}	=	0.98E6 Psi	G_{12}	=	0.98E6 Psi
ν_{23}	=	0.499	ν_{13}	=	0.306	ν_{12}	=	0.296

with strengths given by

X_{Ten}	=	2.43E5 Psi	X_{Comp}	=	1.77E5 Psi	Y_{Ten}	=	7.0E3 Psi
Y_{Comp}	=	3.06E4 Psi	Z_{Ten}	=	7.03E3 Psi	Z_{Comp}	=	3.5E4 Psi
R	=	1.7E4 Psi	S	=	1.57E4 Psi	T	=	1.57E4 Psi

The face plate is composed of 96 plies and is assumed to have been subjected to a normal impact leading to an inner circular region where two delaminations exist located eight plies or 0.0416 in from the outer and inner laminate surface. Furthermore, the material properties of these outer two layers are assumed to have experienced fiber damage such that the longitudinal modulus has been reduced to the matrix-dominated properties of the transverse moduli. The layup and location of these delaminations, indicated by '||' in the layup description, is given by $[\pm 45/0_6 \,||\, \pm 45_5/90_6 \pm 45_5/0_6 \pm 45_2/0_8/\mp 45_2/0_6 \mp 45_5/90_6/\mp 45_5 \,||\, 0_6/\mp 45]$. A residual strength analysis is performed, which is selected to evaluate both delamination instability and material failure. For this example, the maximum stress failure criteria is used with a nonspecific damage law that assigns zero modulus to plies experiencing failure without regard to failure mode. Abbreviated input and output files are shown in the following subsections, followed by a graphical presentation of the progression of failure.

10.2.1 Input Data File for a Residual Strength Problem

```
*HEADING
 MODEL OF AN ELASTICALLY SUPPORTED COMPOSITE PLATE
**
** [45/-45/0_6||(45/-45)_5/90_6/(45/-45)_5/0_6/(45/-45)_2/0_8/
** (-45/45)_2/0_6/(-45/45)_5/90_6/(-45/45)_5||0_6/-45/45]
**
**          LAYUP TAPE THICKNESS = 0.0052''
**
**     TWO INTERIOR DELAMINATIONS MODELLED AT
**     LAYER INTERFACES 2|3 AND 3|4
**
*SOLUTION, METH = CMB
 6,15,1.05
**ECHO
**PREPASS
**NODE PRINT
**  D,M
*PLY FAILURE PRINT
*parameter directory = current
*parameter lapfail
*parameter status
*MEMORY ALLOCATION
 BAND
*GRAPHICS, format = mathematica
 2, 2, 1.0
**
**   NODE DEFINITIONS
**
*NODE
```

```
** TOP FRONT COMPONENT
   1   5.0        -10.0        10.0
   2   5.8        -10.0        10.0
   3   6.3        -10.0        10.0
                     .
                     .
                     .
3511   9.3375      10.0        -5.9189
3512   9.4375      10.0        -5.9189
3513   9.5         10.0        -5.9189
**
** BOTTOM, FRONT COMPONENT
**
3601   5.0        -10.0       -10.0
3602   5.8        -10.0       -10.0
3603   6.3        -10.0       -10.0
                     .
                     .
                     .
4711   9.3375      -8.6396     -5.9189
4712   9.4375      -8.6396     -5.9189
4713   9.5         -8.6396     -5.9189
**
**       NODES, ELEMENTS, AND NODE SETS FOR DELAMINATED VERTICAL
**       COMPONENT OBTAINED FROM THE FOLLOWING *MODEL GENERATION
**       STATEMENT:
**
**                  *MODEL GENERATION
**                   8,4,10.0,10.0,4,4,4,4
**                   2.0,1,1,1,1,1
**                   0.0, 0.0, 1.0
**                   0.0, 1.0, 0.0
**                   1.0, 0.0, 0.0
**                   1.0,10.0
**                   1,5,250,5000,5000
**                   0.95,9.875
**                   2,6,255,7000,7000
**                   0.85,9.625
**                   3,7,265,11000,11000
**                   0.8,9.50
**                   4,8,270,13000,13000
**
*NODE
   5001   0.1000000E+02   0.0000000E+00   0.0000000E+00
   5002   0.1000000E+02   0.3750000E+00   0.0000000E+00
   5003   0.1000000E+02   0.3750000E+00   0.3750000E+00
                     .
```

```
  13519   0.9500000E+01   0.1000000E+02   0.7279306E+01
  13520   0.9500000E+01   0.1000000E+02   0.8639653E+01
  13521   0.9500000E+01   0.1000000E+02   0.1000000E+02
**
**   DEFINE GENERATOR ELEMENTS
**
*ELEMENT, LAYUP = 7, elset = 300
**
** top front elastic support
**
   1,   401,   402,  902,  901,    1,    2,  102,  101
 101,   501,   502,  802,  801,  401,  402,  902,  901
 201,   601,   602,  702,  701,  501,  502,  802,  801
 301,   901,   902, 1002, 1001,  101,  102,  202,  201
 401,  1001,  1002, 1102, 1101,  201,  202,  302,  301
**
** top back elastic support
**
 501,  1601,  1602, 1702, 1701, 1201, 1202, 1302, 1301
 601,  1701,  1702, 1802, 1801, 1301, 1302, 1402, 1401
 701,  1801,  1802, 1902, 1901, 1401, 1402, 1502, 1501
 801,  2001,  2002, 2102, 2101, 1801, 1802, 1902, 1901
 901,  2201,  2202, 2302, 2301, 2001, 2002, 2102, 2101
**
** bottom front elastic support
**
1001,  3601,  3602, 3702, 3701, 4001, 4002, 4102, 4101
1101,  4001,  4002, 4102, 4101, 4401, 4402, 4502, 4501
1201,  4401,  4402, 4502, 4501, 4601, 4602, 4702, 4701
1301,  3701,  3702, 3802, 3801, 4101, 4102, 4202, 4201
1401,  3801,  3802, 3902, 3901, 4201, 4202, 4302, 4301
**
** bottom back elastic support
**
1501,  2401,  2402, 2502, 2501, 2801, 2802, 2902, 2901
1601,  2501,  2502, 2602, 2601, 2901, 2902, 3002, 3001
1701,  2601,  2602, 2702, 2701, 3001, 3002, 3102, 3101
1801,  3001,  3002, 3102, 3101, 3201, 3202, 3302, 3301
1901,  3201,  3202, 3302, 3301, 3401, 3402, 3502, 3501
**
**   ELEMENT GENERATION FOR ELASTIC SUPPORTS
**
*ELGEN, ELID = 300
   1, 12,1,1,,,,,,
 101, 12,1,1,,,,,,
```

```
 201, 12,1,1,,,,,,
         .
         .
         .
1701, 12,1,1,,,,,,
1801, 12,1,1,,,,,,
1901, 12,1,1,,,,,,
**
** CREATE NODE SETS FOR EQUIVALENCING
**
*NSET, NSID =  10
   13,   113,   213,   313,   413,   913,  1013,  1113
  513,   813,   613,   713
*NSET, NSID = 20
13300, 13319, 13338, 13357, 13299, 13318, 13337, 13356
13298, 13317, 13297, 13316
*NSET, NSID = 30
 1213,  1313,  1413,  1513,  1613,  1713,  1813,  1913
 2013,  2113,  2213,  2313
*NSET, NSID = 40
13464, 13483, 13502, 13521, 13463, 13482, 13501, 13520
13500, 13519, 13499, 13518
*NSET, NSID = 50
 4613,  4713,  4413,  4513,  4013,  4113,  4213,  4313
 3613,  3713,  3813,  3913
*NSET, NSID = 60
13285, 13304, 13284, 13303, 13283, 13302, 13321, 13340
13282, 13301, 13320, 13339
*NSET, NSID = 70
 3413,  3513,  3213,  3313,  2813,  2913,  3013,  3113
 2413,  2513,  2613,  2713
*NSET, NSID = 80
13487, 13506, 13486, 13505, 13447, 13466, 13485, 13504
13446, 13465, 13484, 13503
**
** EQUIVALENCE NODE SETS
**
*EQUIVALENCE
 10, 20
 30, 40
 50, 60
 70, 80
**
** ELEMENTS IN VERTICAL COMPONENT FROM PRIOR *MODEL GENERATION RUN
**
*ELEMENT, LAYUP =          1 ORIENTATION =          1
   5001    7001    7004    7003    7002    5001    5004    5003    5002
```

```
   5002    7006    7005    7004    7001    5006    5005    5004    5001
   5003    7007    7006    7001    7008    5007    5006    5001    5008
                                    .
                                    .
                                    .
   5126    7111    7112    7144    7143    5111    5112    5144    5143
   5127    7112    7113    7145    7144    5112    5113    5145    5144
   5128    7113    7082    7114    7145    5113    5082    5114    5145
*ELEMENT, LAYUP =         4 ORIENTATION =          1
   5129    7114    7115    7147    7146    5114    5115    5147    5146
   5130    7115    7116    7148    7147    5115    5116    5148    5147
   5131    7116    7117    7149    7148    5116    5117    5149    5148
                                    .
                                    .
                                    .
   5482    7499    7500    7519    7518    5499    5500    5519    5518
   5483    7500    7501    7520    7519    5500    5501    5520    5519
   5484    7501    7502    7521    7520    5501    5502    5521    5520
*ELEMENT, LAYUP =         2 ORIENTATION =          1
   7001   11001   11004   11003   11002    7001    7004    7003    7002
   7002   11006   11005   11004   11001    7006    7005    7004    7001
   7003   11007   11006   11001   11008    7007    7006    7001    7008
                                    .
                                    .
                                    .
   7126   11111   11112   11144   11143    7111    7112    7144    7143
   7127   11112   11113   11145   11144    7112    7113    7145    7144
   7128   11113   11082   11114   11145    7113    7082    7114    7145
*ELEMENT, LAYUP =         5 ORIENTATION =          1
   7129   11114   11115   11147   11146    7114    7115    7147    7146
   7130   11115   11116   11148   11147    7115    7116    7148    7147
   7131   11116   11117   11149   11148    7116    7117    7149    7148
                                    .
                                    .
                                    .
   7482   11499   11500   11519   11518    7499    7500    7519    7518
   7483   11500   11501   11520   11519    7500    7501    7520    7519
   7484   11501   11502   11521   11520    7501    7502    7521    7520
*ELEMENT, LAYUP =         3 ORIENTATION =          1
  11001   13001   13004   13003   13002   11001   11004   11003   11002
  11002   13006   13005   13004   13001   11006   11005   11004   11001
  11003   13007   13006   13001   13008   11007   11006   11001   11008
                                    .
                                    .
                                    .
  11126   13111   13112   13144   13143   11111   11112   11144   11143
  11127   13112   13113   13145   13144   11112   11113   11145   11144
```

```
  11128   13113   13082   13114   13145   11113   11082   11114   11145
*ELEMENT, LAYUP =          6 ORIENTATION =          1
  11129   13114   13115   13147   13146   11114   11115   11147   11146
  11130   13115   13116   13148   13147   11115   11116   11148   11147
  11131   13116   13117   13149   13148   11116   11117   11149   11148
                                    .
                                    .
                                    .
  11482   13499   13500   13519   13518   11499   11500   11519   11518
  11483   13500   13501   13520   13519   11500   11501   11520   11519
  11484   13501   13502   13521   13520   11501   11502   11521   11520
**
** RELAX TOLERANCE OF DEFORMED GEOMETRY CHECKS
**
*DEFORMED GEOMETRY
20.0
**
** LAMINATE DESCRIPTION
**
*LAYER, LAYUP = 1
 3, 0.0052,  45.0
 3, 0.0052, -45.0
 3, 0.0312,   0.0
*LAYER, LAYUP = 2
 1, 0.0260,  45.0
 1, 0.0260, -45.0
 1, 0.0312,  90.0
 1, 0.0260,  45.0
 1, 0.0260, -45.0
 1, 0.0312,   0.0
 1, 0.0104, -45.0
 1, 0.0104,  45.0
 1, 0.0416,   0.0
 1, 0.0104, -45.0
 1, 0.0104,  45.0
 1, 0.0312,   0.0
 1, 0.0260, -45.0
 1, 0.0260,  45.0
 1, 0.0312,  90.0
 1, 0.0260, -45.0
 1, 0.0260,  45.0
*LAYER, LAYUP=3
 3, 0.0312,   0.0
 3, 0.0052, -45.0
 3, 0.0052,  45.0
*LAYER, LAYUP = 4
 1, 0.0052,  45.0
```

```
 1, 0.0052, -45.0
 1, 0.0312,   0.0
*LAYER, LAYUP = 5
 1, 0.0260,  45.0
 1, 0.0260, -45.0
 1, 0.0312,  90.0
 1, 0.0260,  45.0
 1, 0.0260, -45.0
 1, 0.0312,   0.0
 1, 0.0104, -45.0
 1, 0.0104,  45.0
 1, 0.0416,   0.0
 1, 0.0104, -45.0
 1, 0.0104,  45.0
 1, 0.0312,   0.0
 1, 0.0260, -45.0
 1, 0.0260,  45.0
 1, 0.0312,  90.0
 1, 0.0260, -45.0
 1, 0.0260,  45.0
*LAYER, LAYUP=6
 1, 0.0312,   0.0
 1, 0.0052, -45.0
 1, 0.0052,  45.0
*LAYER, LAYUP = 7
 2, 1.0, 0.0
**
**   MATERIAL DEFINITIONS
**
** COMPOSITE PLY PROPERTIES (S2-GLASS/3501 EPOXY)
**
*MATERIAL, MATID = 1
 7.150E6, 2.13E6, 2.13E6, 0.98E6, 0.71E6, 0.98E6
  0.306, 0.499, 0.296
*FAILURE CRITERIA, FCID = 1
 MAX-STRESS
 2.43E5, 1.77E5, 7.0E3, 3.06E4, 7.0E3, 3.5E4
 1.7E4, 1.57E4, 1.57E4
*DAMAGE LAW, DLID = 1
 NULL
**
** REDUCED PROPERTIES WITHIN INNER REGION
**
*MATERIAL, MATID = 3
 2.13E6, 2.13E6, 2.13E6, 8.15E5, 8.15E5, 8.15E5
  0.306, 0.306, 0.306
*FAILURE CRITERIA, FCID = 3
```

```
 MAX-STRESS
 2.43E5, 1.77E5, 7.0E3, 3.06E4, 7.0E3, 3.5E4
 1.7E4, 1.57E4, 1.57E4
*DAMAGE LAW, DLID = 3
 NULL
**
** METALLIC PROPERTIES
**
*MATERIAL, MATID = 2
 1.0E8, 1.0E8, 1.0E8, 0.3846E8, 0.3846E8, 0.3846E8
  0.3, 0.3, 0.3
*FAILURE CRITERIA, FCID = 2
 MAX-STRESS
 5.3E5, 2.2E6, 5.3E5, 2.2E6, 5.3E5, 2.2E6
 4.8E5, 4.8E5, 4.8E5
*DAMAGE LAW, DLID = 2
 NULL
**
**  ESTABLISH LOCAL COORDINATE SYSTEM
**
*ORIENTATION
 1,  0.0, 1.0, 0.0,  0.0, 0.0, 1.0
**
** NODE SET DEFINITION FOR BOUNDARY CONSTRAINT INPUT
**
*NSET, NSID = 100
    1,  101,  201,  301,  401,  501,  601,  701,  801
  901, 1001, 1101
*NSET, NSID = 110
 1201, 1301, 1401, 1501, 1601, 1701, 1801, 1901, 2001
 2101, 2201, 2301
*NSET, NSID = 120
 2401, 2501, 2601, 2701, 2801, 2901, 3001, 3101, 3201
 3301, 3401, 3501
*NSET, NSID = 130
 3601, 3701, 3801, 3901, 4001, 4101, 4201, 4301, 4401
 4501, 4601, 4701
*BOUNDARY2
  100, 1, 1
  110, 1, 2
  120, 1, 3
  130, 1, 3
**
** INPUT NODE SETS USED TO DEFINE DELAMINATION PLANES
**
*NSET, NSID =     955
   7001    7002    7003    ...    7143    7144   7145
```

```
*NSET, NSID =      960
  11001   11002   11003   ...  11143   11144  11145
**
**  INPUT DELAMINATIONS AS SPECIFIED NODE SETS
**
*DELAMINATION
 955 960
**
** EXCLUDE ELEMENTS COMPRISING ELASTIC SUPPORTS
** FROM FAILURE PREDICTION
**
*EXCLUDE ELEMENT
 300
**
** biaxial y-z plane loading
**
*CLOAD
**
** normal z-direction loads
**
    5300, 3, -.1000000E+02
    5319, 3, -.1000000E+02
    5338, 3, -.1000000E+02
                .
                .
                .
  13465, 3,  0.1000000E+02
  13484, 3,  0.1000000E+02
  13503, 3,  0.1000000E+02
**
** transverse y-direction loads
**
    5282, 2,  0.2000000E+02
    5283, 2,  0.2000000E+02
    5284, 2,  0.2000000E+02
                .
                .
                .
  13519, 2,  -.2000000E+02
  13520, 2,  -.2000000E+02
  13521, 2,  -.2000000E+02
*ENDDATA
```

10.2.2 Output Data File for a Residual Strength Problem

```
@@@@@@@@@@@@@@@@@@@@@@@@@@@@@@@@@@@@@@@@@@@@@@
@@                                          @@
@@       U.S. ARMY RESEARCH LABORATORY      @@
@@                                          @@
@@               R E S T R A N              @@
@@                                          @@
@@   RESIDUAL STRENGTH ANALYSIS OF IMPACT   @@
@@       DAMAGED COMPOSITE LAMINATES        @@
@@                                          @@
@@               VERSION 1.0                @@
@@                                          @@
@@@@@@@@@@@@@@@@@@@@@@@@@@@@@@@@@@@@@@@@@@@@@@

*** MESSAGE: ELEMENT NODE ORDER IS BEING CONVERTED TO RESTRAN FORMAT

*** WARNING: MATERIAL ID      1 HAS A MIXED MODE FAILURE CRITERIA
             ASSOCIATED WITH A SINGLE MODE DAMAGE LAW (NULL).
             NULL ACCEPTED

*** WARNING: MATERIAL ID      3 HAS A MIXED MODE FAILURE CRITERIA
             ASSOCIATED WITH A SINGLE MODE DAMAGE LAW (NULL).
             NULL ACCEPTED

*** WARNING: MATERIAL ID      2 HAS A MIXED MODE FAILURE CRITERIA
             ASSOCIATED WITH A SINGLE MODE DAMAGE LAW (NULL).
             NULL ACCEPTED


                ######################################
                ###                                ###
                ### M O D E L   D E F I N I T I O N ###
                ###                                ###
                ######################################
                                .
                                .
                                .
                FORCE/MOMENT RESULTANTS AT ORIGIN:

                |R| = 0.400E+02     |M| = 0.456E+03

          Rx = 0.000E+00  Ry = 0.000E+00  Rz = -.400E+02

          Mx = 0.237E+03  My = -.390E+03  Mz = 0.000E+00
```

```
   Xo = 0.975E+01  Yo = 0.592E+01  Zo = 0.000E+00


  *** E N D  O F  M O D E L  D E F I N I T I O N ***

        M O D E L  S I Z E  P A R A M E T E R S

           NUMBER OF ELEMENTS =       1692
           NUMBER OF NODES    =       2950
           DEGREES OF FREEDOM =       8850
           SYSTEM BANDWIDTH   =       2892

    ################################################
    ##                                            ##
    ## B E G I N  F A I L U R E  A N A L Y S I S ##
    ##                                            ##
    ################################################


  @@@@@@@@@@@@@@@@@@@@@@@@@@@@@@@@@@@@@@@@@@@@@@@@@@@@@@@@@@@@@@@@@@@@@@@@
  @@                                                                      @@
  @@     PRIMARY ANALYSIS CYCLE. PASS NUMBER    1                         @@
  @@                                                                      @@
  @@@@@@@@@@@@@@@@@@@@@@@@@@@@@@@@@@@@@@@@@@@@@@@@@@@@@@@@@@@@@@@@@@@@@@@@

    <<< ANALYZING DELAMINATION SET:     1  >>>
    <<< CONTACT ITERATION NUMBER:       1  >>>

              CONVERGED EIGENVALUES:

               NUMBER     LAMBDA

                  1   0.1825575E+02
                  2   0.1482253E+02
                  3   0.1040733E+02
                  4   0.6461659E+01

DELAMINATION    1 AT ITERATION    1 IS EXHIBITING
A CONTACT COMPATIBILITY OF  100.00 PERCENT

    <<< ANALYZING DELAMINATION SET:     2  >>>
    <<< CONTACT ITERATION NUMBER:       1  >>>

              CONVERGED EIGENVALUES:

               NUMBER     LAMBDA
```

```
                    1   0.1826281E+02
                    2   0.1488730E+02
                    3   0.1037982E+02
                    4   0.6463456E+01

 DELAMINATION    2 AT ITERATION    1 IS EXHIBITING
 A CONTACT COMPATIBILITY OF  100.00 PERCENT

      ************************************************
      **                                            **
      ** ALGORITHMIC PATH FOR MINIMUM LOAD INCREMENT **
      ** TO NEXT FAILURE: DELAMINATION INSTABILITY   **
      **                                            **
      **          MATERIAL          BUCKLING        **
      **         ----------        ----------       **
      ** SCALE:   0.540E+02         0.646E+01       **
      **                                            **
      ************************************************

         ******************************************
         **                                      **
         ** SUBLAMINATE BUCKLING FAILURE ANALYSIS **
         **                                      **
         ******************************************

  * DELAMINATION DEFINED BY NODE SET   955
    IS PREDICTED TO BUCKLE AT AN APPLIED
    LOAD FACTOR OF 0.646E+01

  * FAILURE IS PREDICTED TO INCLUDE ALL ELEMENTS ALONG
    POSITIVE NORMAL TO THE DELAMINATION PLANE.

  * THE FOLLOWING ELEMENTS HAVE BEEN DEGRADED
    OR FAILED VIA LOCAL SUBLAMINATE BUCKLING:

 5001    5002    5003    5004    ...  5157    5158    5159    5160

  * LOCAL SUBLAMINATE BUCKLING IS PREDICTED.

          ELEMENT PLY FAILURE STATUS AT CYCLE NO    1

       ELEMENT          PLY FAILURE MODES:
         ID      %FIBER   %MATRIX   %BUCKLING   %TOTAL
       5001          0         0         100       100
       5002          0         0         100       100
       5003          0         0         100       100
```

```
                    .
                    .
     5158           0        0        49        49
     5159           0        0        49        49
     5160           0        0        49        49

 * THE FOLLOWING DELAMINATION NODE SET(S) WILL
   BE REMOVED DUE TO BUCKLING FAILURE:

 955

    @@@@@@@@@@@@@@@@@@@@@@@@@@@@@@@@@@@@@@@@@@@@@@@@@@@@@@@@@@@@@@@@@@@@@@@@
    @@                                                                    @@
    @@      PRIMARY ANALYSIS CYCLE. PASS NUMBER    2                      @@
    @@                                                                    @@
    @@@@@@@@@@@@@@@@@@@@@@@@@@@@@@@@@@@@@@@@@@@@@@@@@@@@@@@@@@@@@@@@@@@@@@@@

   339 DEGREES OF FREEDOM ARE CURRENTLY ASSOCIATED WITH
       ZERO STIFFNESS AND HAVE BEEN REMOVED

      <<< ANALYZING DELAMINATION SET:      1  >>>
      <<< CONTACT ITERATION NUMBER:        1  >>>

                 CONVERGED EIGENVALUES:

                  NUMBER      LAMBDA

                     1    0.2931583E+01
                     2    0.2453289E+01
                     3    0.1653048E+01
                     4    0.1043609E+01

 DELAMINATION    1 AT ITERATION    1 IS EXHIBITING
 A CONTACT COMPATIBILITY OF  100.00 PERCENT

       ************************************************
       **                                            **
       ** ALGORITHMIC PATH FOR MINIMUM LOAD INCREMENT **
       ** TO NEXT FAILURE: DELAMINATION INSTABILITY   **
       **                                            **
       **          MATERIAL          BUCKLING        **
       **         ----------        ----------       **
       ** SCALE:   0.536E+02         0.674E+01       **
       **                                            **
       ************************************************
```

```
          ******************************************
          **                                      **
          ** SUBLAMINATE BUCKLING FAILURE ANALYSIS **
          **                                      **
          ******************************************

  * DELAMINATION DEFINED BY NODE SET   960
    IS PREDICTED TO BUCKLE AT AN APPLIED
    LOAD FACTOR OF 0.674E+01

  * FAILURE IS PREDICTED TO INCLUDE ALL ELEMENTS ALONG
    NEGATIVE NORMAL TO THE DELAMINATION PLANE.

  * THE FOLLOWING ELEMENTS HAVE BEEN DEGRADED
    OR FAILED VIA LOCAL SUBLAMINATE BUCKLING:

11001   11002   11003   11004   ... 11157   11158   11159  11160

  * LOCAL SUBLAMINATE BUCKLING IS PREDICTED.

        ELEMENT PLY FAILURE STATUS AT CYCLE NO    2

      ELEMENT          PLY FAILURE MODES:
        ID     %FIBER   %MATRIX   %BUCKLING   %TOTAL

      5001          0         0         100       100
      5002          0         0         100       100
      5003          0         0         100       100
                                .
                                .
                                .
     11158          0         0          49        49
     11159          0         0          49        49
     11160          0         0          49        49

  * THE FOLLOWING DELAMINATION NODE SET(S) WILL
    BE REMOVED DUE TO BUCKLING FAILURE:

  960

    @@@@@@@@@@@@@@@@@@@@@@@@@@@@@@@@@@@@@@@@@@@@@@@@@@@@@@@@@@@@@@@@@@@@
    @@                                                              @@
    @@     PRIMARY ANALYSIS CYCLE. PASS NUMBER    3                 @@
    @@                                                              @@
    @@@@@@@@@@@@@@@@@@@@@@@@@@@@@@@@@@@@@@@@@@@@@@@@@@@@@@@@@@@@@@@@@@@@
```

```
<<< ANALYZING DELAMINATION SET:      1  >>>
<<< CONTACT ITERATION NUMBER:        1  >>>

            CONVERGED EIGENVALUES:

             NUMBER      LAMBDA

                1    0.2200270E+02
                2    0.1958573E+02
                3    0.1437475E+02
                4    0.8520247E+01

 ************************************************
 **                                            **
 ** ALGORITHMIC PATH FOR MINIMUM LOAD INCREMENT **
 ** TO NEXT FAILURE: MATERIAL DEGRADATION       **
 **                                            **
 **          MATERIAL         BUCKLING         **
 **         ----------       ----------        **
 ** SCALE:   0.535E+02        0.575E+02        **
 **                                            **
 ************************************************

        **********************************
        *                                *
        *   MATERIAL FAILURE ANALYSIS    *
        *                                *
        *  ITERATION NO.  SCALE FACTOR   *
        *  -------------  ------------   *
        *       1           0.535E+02    *
        *                                *
        **********************************

* NUMBER OF ELEMENTS DEGRADED =        0

        **********************************
        *                                *
        *   MATERIAL FAILURE ANALYSIS    *
        *                                *
        *  ITERATION NO.  SCALE FACTOR   *
        *  -------------  ------------   *
        *       2           0.535E+02    *
        *                                *
        **********************************

* NUMBER OF ELEMENTS DEGRADED =        8
```

```
**********************************
*                                *
*   MATERIAL FAILURE ANALYSIS    *
*                                *
*  ITERATION NO.  SCALE FACTOR   *
*  -------------  ------------   *
*       3           0.535E+02    *
*                                *
**********************************
```

* NUMBER OF ELEMENTS DEGRADED = 30

```
**********************************
*                                *
*   MATERIAL FAILURE ANALYSIS    *
*                                *
*  ITERATION NO.  SCALE FACTOR   *
*  -------------  ------------   *
*       4           0.535E+02    *
*                                *
**********************************
```

* NUMBER OF ELEMENTS DEGRADED = 111

```
**********************************
*                                *
*   MATERIAL FAILURE ANALYSIS    *
*                                *
*  ITERATION NO.  SCALE FACTOR   *
*  -------------  ------------   *
*       5           0.535E+02    *
*                                *
**********************************
```

* NUMBER OF ELEMENTS DEGRADED = 211

* ELEMENT FAILURE HAS ALTERED MODEL STABILITY SUCH
  THAT RIGID BODY MODES HAVE BEEN DETECTED.

TOTAL FAILURE IS ASSUMED.

ELEMENT PLY FAILURE STATUS AT CYCLE NO 3

ELEMENT	PLY FAILURE MODES:			
ID	%FIBER	%MATRIX	%BUCKLING	%TOTAL

5001	0	0	100	100
5002	0	0	100	100
5003	0	0	100	100
		.		
		.		
		.		
11462	0	0	0	33
11463	0	0	0	100
11464	0	0	0	100

```
##################################################
##                                              ##
## ANALYSIS PREDICTS CATASTROPHIC FAILURE OF ##
## THE MODEL AT AN ULTIMATE LOAD GIVEN BY:    ##
##                                              ##
##    P(ULT) = (0.53468E+02) * P(INITIAL)       ##
##                                              ##
##################################################
```

```
@@@@@@@@@@@@@@@@@@@@@@@@@@@@@@@@@@@@@@@@@@@@@@@@@@@@@@@@@@@@
@@                                                        @@
@@ F A I L U R E   A N A L Y S I S   C O M P L E T E D @@
@@                                                        @@
@@@@@@@@@@@@@@@@@@@@@@@@@@@@@@@@@@@@@@@@@@@@@@@@@@@@@@@@@@@@
```

10.2.3 Graphical Output Using MATHEMATICA

Preface graphic pages are generated to show the color codes used to display various element failure modes. In the specific demonstration problem analyzed, complete element failure is indicated by a wireframe depiction, and because no specific failure modes were predicted using the maximum stress criterion, material failure is shown as using the general material failure color coding scheme.

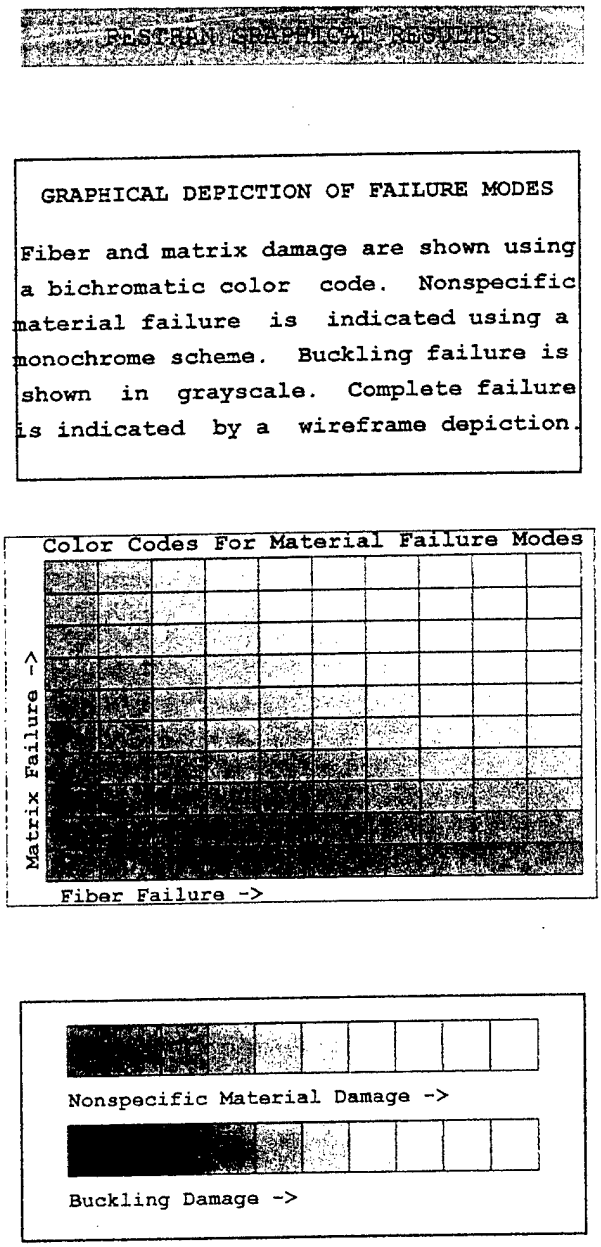

Both delaminations are analyzed separately for critical buckling load. These are compared to the load required to cause first ply failure, and it is determined that the outer surface delamination is the first failure to occur. Material properties for the elements involved in the sublaminate buckling are set to zero such that they appear in a wireframe depiction in the failure state graphic. This is followed by a magnified view of the buckling mode shown in the following illustration.

ANALYSIS CYCLE 1

Buckling Failure at Scale = 0.646E+01

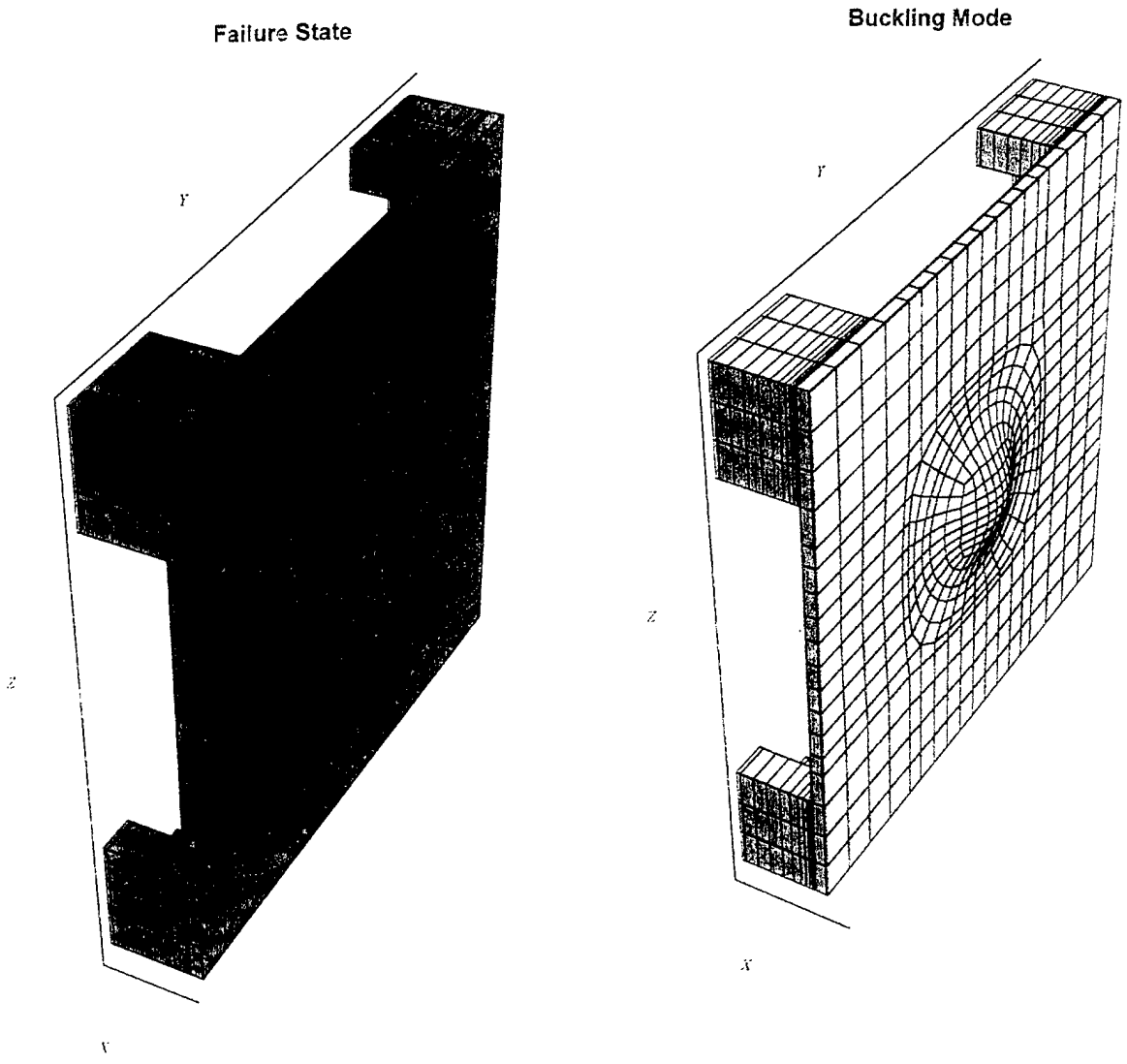

The next predicted failure is buckling of the layer on the inner plate surface, as shown next.

ANALYSIS CYCLE 2

Buckling Failure at Scale = 0.674E+01

Failure State

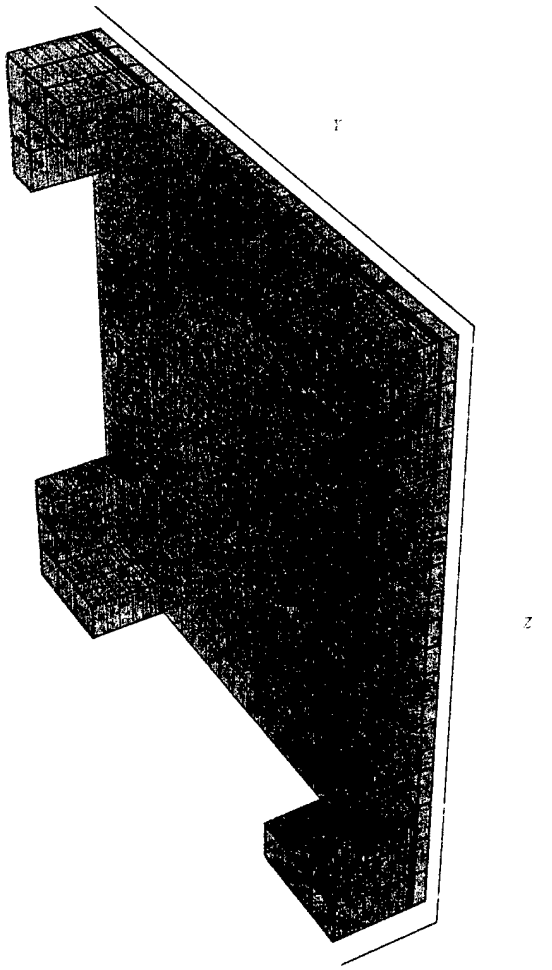

Buckling Mode

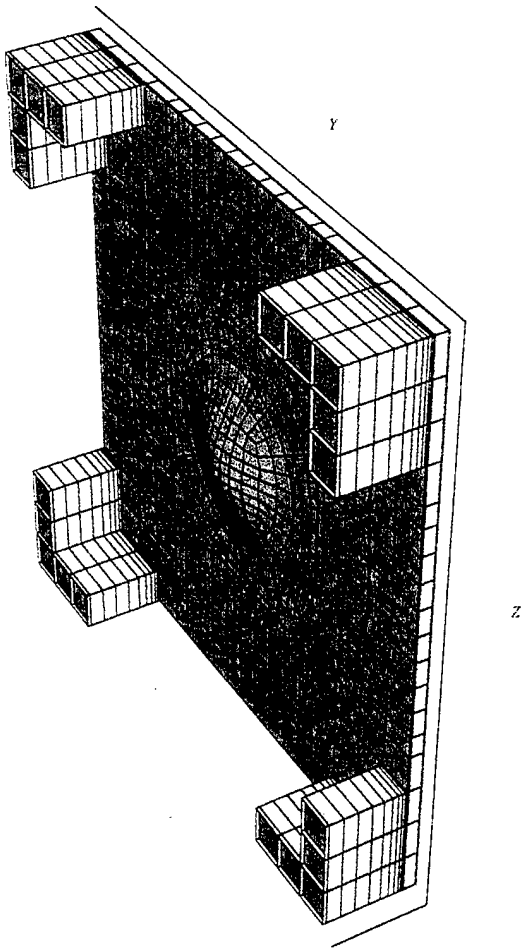

The final sequence of failure events as fully described in the output file involve a cascade of material ply failures. These occured during the third global analysis cycle which, after five iterations, had reduced the overall stiffness such that rigid body modes were detected and the analysis terminated. The final failure state is shown next, in which total element failures essentially created an opening through the inner region of the face plate. Mediating element failures are shown to have progressed to the outer plate boundary. Failure in the line of elements comprising the outer boundary have been precluded using the LAPFAIL parameter which prevents elements to which applied external loads have been applied from exhibiting failure.

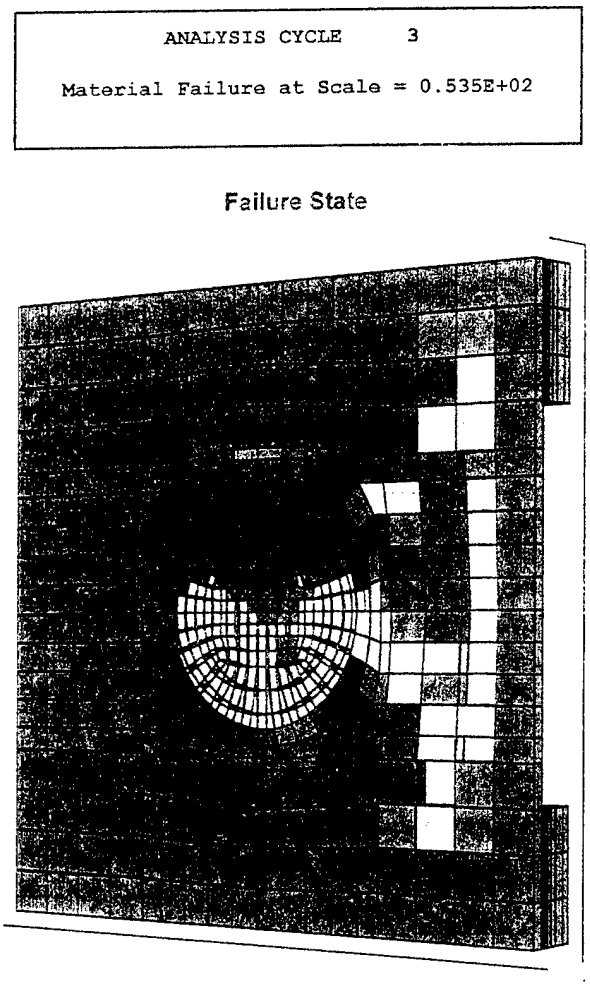

The final residual strength prediction yields the ultimate load carrying capability of the face plate containing the assumed damage as a factor of the initial biaxial loads equal to 53.47.

11 Conclusion

A general predictive methodology for determining residual strength in impact damaged composite laminates has been developed and incorporated into a computer code designated RESTRAN (*RE*sidual *STR*ength *AN*alysis). RESTRAN can be used to analyze composite structures with arbitrary three-dimensional geometry, loading and support conditions, material properties, and initial material and delamination damage. Material failure modes are predicted using a robust suite of failure criteria and damage laws. Structural failure due to sequential sublaminate buckling of delaminated layers is also accounted. A progressive failure analysis is performed until ultimate structural failure is predicted yielding an estimate of the residual strength.

References

[1] Gottesman, T., S. Grishovich, E. Drukker, N. Sela, and J. Loy. "Residual Strenght of Impacted Composites: Analysis and Tests" *Journal of Composites Technology and Research*, JCTRER, vol. 16, pp. 244–255, 1994.

[2] Madaras, E. I., C. C. Poe, and J. S. Heyman. "Combining Fracture Mechanics and Ultrasonic NDE to Predict the Strength Remaining in Thick Composites Subjected to Low-Level Impact" *1986 Ultrasonics Symposium*, pp. 1051–1059.

[3] Cairns, D. S., and P. A. Lagace. "Residual Tensile Strength of Graphite/Epoxy and Kevlar/Epoxy Laminates with Impact Damage" *Composite Materials: Testing and Design (Ninth Volume)*, ASTM STP 1059, American Society for Testing and Materials, pp. 48–63, 1990.

[4] Caprino, G. "Residual Strength Predictions of Impacted CFRP Laminates" *J. Comp. Mats.*, vol. 18, pp. 508–518, 1984.

[5] Lal, K. M. "Prediction of Residual Tensile Strength of Transversely Impacted Composite Laminates" *Research in Structural and Solid Mechanics - 1982*, NASA Conference Publication 2245, pp. 97–112, 1982.

[6] Shu, D., and Y. W. Mai. "Buckling of Delaminated Composites Re-examined" *Comp. Sci. Tech.*, vol. 47, pp. 35–41, 1993.

[7] Chai, H., C. D. Babcock, and W. G. Knauss. "One Dimensional Modeling of Failure in Laminated Plates by Delamination Buckling" *Int. J. Solids Struct.*, vol. 17, no. 11, pp.1069–1083, 1981.

[8] Lui, D. "Delamination Resistance in Stitched and Unstitched Composite Plates Subjected to Impact Loading" *J. Reinf. Plastics Compos.*, vol. 9, pp. 59–69, 1990.

[9] Simitses, G. J., S. Sallam, and W. L. Yin. "Effect of Delamination of Axially Loaded Homogeneous Laminated Plates" *AIAA*, vol. 23, no. 9, pp. 1437–1444, 1985.

[10] Shivakumar, K. N., and J. D. Whitcomb. "Buckling of a Sublaminate in a Quasi-Isotropic Composite Laminate" *J. Comp. Mats.*, vol. 19, pp. 2–18, 1985.

[11] Wang, S. S., N. M. Zahlan, and H. Suemasu. "Compressive Stability of Delaminated Random Short-Fiber Composites, Part I - Modeling and Methods of Analysis" *J. Comp. Mats.*, vol. 19, pp. 296–316, 1985.

[12] Wang, S. S., N. M. Zahlan, and H. Suemasu. "Compressive Stability of Delaminated Random Short-Fiber Composites, Part II - Experimental and Analytical Results" *J. Comp. Mats.*, vol. 19, pp. 317–333, 1985.

[13] Madenci, E., and R. A. Westmann. "Local Delamination Growth in Layered Systems Under Compressive Load" *J. Appl. Mech. ASME*, vol. 60, pp. 895–902, 1993.

[14] Madenci, E., and R. A. Westmann. "Local Delamination Buckling in Layered Systems" *J. Appl. Mech. ASME*, vol. 58, pp. 157–166, 1991.

[15] Chang, F. K., and K. Y. Chang. "Post-Failure Analysis of Bolted Composite Joints in Tension or Shear-Out Mode Failure" *J. Comp. Mats.*, vol. 21, pp. 809–833, 1987.

[16] Chang, F. K., R. A. Scott, and G. S. Springer. "Failure Strength of Nonlinearly Elastic Composite Laminates Containing a Pin Loaded Hole" *J. Comp. Mats.*, vol. 18, pp. 464–477, 1984.

[17] Zienkiewicz, O. C., and R. L. Taylor. *The Finite Element Method, vol. I, Basic Introduction and Linear Problem* 4th edition. McGraw-Hill 1989.

[18] Chang, F. K., and K. Y. Chang. "A Progressive Damage Model for Laminated Composites Containing Stress Concentrations" *J. Comp. Mats.*, vol. 21, pp. 834–855, 1987.

[19] Tian, Z., and S. R. Swanson. "Residual Tensile Strength Prediction on a Ply-by-Ply Basis for Laminates Containing Impact Damage" *J. Comp. Mats.*, vol. 26, pp. 1193–1206, 1992.

[20] Reddy, Y. S., and J. N. Reddy. "Three-Dimensional Finite Element Progressive Failure Analysis of Composite Laminates Under Axial Extension" *J. of Composites Technology & Research*, vol. 15, no. 2, pp. 73–87, 1993.

[21] Reddy, J. N. "On Refined Computational Models of Composite Materials" *Int. J. Num. Meth. Engrg.*, vol. 27, pp. 361–382, 1989.

[22] Tan, S. C. "A Progressive Failure Model of Composite Laminates Containing Openings" *J. Comp. Mats.*, vol. 25, pp. 556–577, 1991.

[23] Ochoa, O. O., and J. J. Engblom. "Analysis of Progressive Failure in Composites" *Comp. Sci. Tech.*, vol. 28, pp. 87–102, 1987.

[24] Lee, J. D. "Three Dimensional Finite Element Analysis of Damage Accumulation in Composite Laminate" *Comp. Struct.*, vol. 15, pp. 335–350, 1982.

[25] Sun, C. T. "Failure Analysis of Laminated Composites by Using Iterative Three Dimensional Finite Element Method" *Comp. Struct.*, vol. 33, pp. 41–47, 1989.

[26] Pian, T. H. H., and P. Tong. "Relations Between Incompatible Displacement Model and Hybrid Stress Model" *Int. J. Num. Meth. Engrg.*, vol. 22, pp. 173–181, 1986.

[27] Pian, T. H. H., and P. Tong. "Basis of Finite Element Methods for Solid Continua" *Int. J. Num. Meth. Engrg.*, vol. 1, pp. 3–28, 1969.

[28] Pian, T. H. H., and D. P. Chen. "Alternative Ways for Formulation of Hybrid Stress Elements" *Int. J. Num. Meth. Engrg.*, vol. 18, pp. 1679–1684, 1982.

[29] Pian, T. H. H., and D. P. Chen. "On the Suppression of Zero Energy Deformation Modes" *Int. J. Num. Meth. Engrg.*, vol. 19, pp. 1741–1752, 1983.

[30] Pian, T. H. H., and K. Sumihara. "Rational Approach for Assumed Stress Finite Element" *Int. J. Num. Meth. Engrg.*, vol. 20, pp. 1685–1695, 1984.

[31] Saether, E. "**RESTRAN: RE**sidual **STR**ength **AN**anlysis of Impact Damaged Composite Laminates. volume II: User's Manual" ARL-TR- , U.S. Army Research Laboratory, Aberdeen Proving Ground, MD, 1999.

[32] Dym, C.L., and I. H. Shames. *Solid Mechanics–A Variational Approach,* New York, McGraw Hill, 1973.

[33] Bathe, K.J. *Finite Element Procedures in Engineering Analysis,* Prentice-Hall, 1982.

[34] Sorensen, D.C. "Implicit Application of Polynomial Filters in a k-Step Arnoldi Method" *SIAM J. Matr. Anal. Apps.*, vol. 13, pp 357–385, 1992.

[35] Lehoucq, R.B. "Analysis and Implementation of an Implicitly Restarted Arnoldi Iteration" Rice University Technical Report TR95-13, Department of Computational and Applied Mathematics, Houston, TX.

[36] Parlett, B.N. "*The Symmetric Eigenvalue Problem*" New York, Prentice-Hall, 1980.

[37] Parlett, B. N., and B. Nour-Omid. "Towards a Black Box Lanczos Program", *Computer Physics Communications*, vol. 53, pp 169–179, 1989.

[38] Nour-Omid, B., B. N. Parlett, T. Ericson, and P. S. Jensen. "How to Implement the Spectral Transformation" *Math. Comp.*, vol. 48, pp 663–673, 1987.

[39] Grimes, R. G., J. G. Lewis, and H. D. Simon. "A Shifted Block Lanczos Algorithm for Solving Sparse Symmetric Generalized Eigenproblems" *SIAM J. Matr. Anal. Apps.*, January 1993.

[40] Reichel, L., and W. B. Gragg. "Algorithm 686: FORTRAN Subroutines for Updating the QR Decomposition" *ACM TOMS*, vol. 16, no. 4, pp 369–377, December 1990.

[41] Tsai, S. W., and H. T. Hahn. *Introduction to Composite Materials,* Lancaster PA: Technomic Publishing Company, 1980.

[42] Jones, R. M. *Mechanics of Composite Materials*, New York, McGraw-Hill, 1975.

[43] Chou, P. C., J. Carleone, and C. M. Hsu. "Elastic Constants of Layered Media" *J. Comp. Mats.*, vol. 6, pp. 80–93, 1972.

[44] Sun, C. T., and S. Li. "Three-Dimensional Effective Elastic Constants for Thick Laminates" *J. Comp. Mats.*, vol. 22, pp. 629–639, 1988.

[45] Sun, C. T., and N. C. Liao. "Analysis of Thick Section Composite Laminates using Effective Moduli" *J. Comp. Mats.*, vol. 24, pp. 977–993, 1990.

[46] Nahas, M. N. "Survey of Failure and Post-Failure Theories of Laminated Fiber-Reinforced Composites" *J. of Comp. Tech. and Research*, vol. 8, pp. 138–153, 1986.

[47] Feng, W. W. "A Failure Criterion for Composite Materials" *J. Comp. Mats.*, vol. 25, pp. 88–100, 1991.

[48] Christensen, R. M. "Tensor Transformations and Failure Criteria for the Analysis of Fiber Composite Materials" *J. Comp. Mats.*, vol. 22, pp. 874–897, 1988.

[49] Hashin, Z. "Failure Criteria for Unidirectional Fiber Composites" *J. Appl. Mech.*, vol. 47, pp. 329–334, 1980.

[50] Hill, R. "A Theory of Yielding and Plastic Flow of Anisotropic Metals" *Proceedings of the Royal Society, Series A*, vol. 193, p. 281, 1948.

[51] Tsai, S. W. "Strength Characterization of Composite Materials" NASA CR-224, 1965.

[52] Hoffman, O. "The Brittle Strength of Orthotropic Materials" *J. Comp. Mats.*, vol. 1, p. 200, 1967.

[53] Tsai, S. W., and E. M. Wu. "A General Theory of Strength for Anisotropic Materials" *J. Comp. Mats.*, vol. 5, p. 58, 1971.

[54] Sandhu, R. S. "A Survey of Failure Theories of Isotropic and Anisotropic Materials" Technical Report, AFFDL-TR-72-71.

[55] Tsai, S. W. "A Survey of Macroscopic Failure Criteria for Composite Materials" Technical Report, AFWAL-TR-84-4025.

[56] Reddy, N. J., and A. K. Pandey. "A First-Ply Failure Analysis of Composite Laminates" *Comp. Struct.*, vol. 25, pp. 371–393, 1987.

[57] Narayanaswami, R. "Evaluation of the Tensor Polynomial and Hoffman Strength Theories for Composite Materials" *J. Comp. Mats.*, vol. 11, pp. 366–377, 1977.

[58] Wu, R. Y., and Z. Stachursky. "Evaluation of the Normal Stress Interaction Parameter in the Tensor Polynomial Strength Theory for Anisotropic Materials" *J. Comp. Mats.*, vol. 18, pp. 456–463, 1984.

[59] Bogetti, T. A., C. P. R. Hoppel, and W. H. Drysdale. "Three-dimensional Effective Properties and Strength Prediction of Thick Laminated Composite Media" ARL-TR-911, U.S. Army Research Laboratory, Aberdeen Proving Ground, MD, 1995.

[60] Larsson, P. L. "On Multiple Delamination Buckling and Growth in Composite Plates" *Int. J. Solids Structures*, vol. 27, pp. 1623–1637, 1991.

[61] Choi, H. Y., H. T. Wu, and F. Chang. "A New Approach Toward Understanding Damage Mechanisms and Mechanics of Laminated Composites Due to Low Velocity impact: Part I - Experiments" *J. Comp. Mats.*, vol. 25, pp. 992–1011, 1991.

[62] Choi, H. Y., H. T. Wu, and F. Chang. "A New Approach Toward Understanding Damage Mechanisms and Mechanics of Laminated Composites Due to Low Velocity impact: Part II - Analysis" *J. Comp. Mats.*, vol. 25, pp. 1012–1038, 1991.

[63] Doucet, A. B., and J. Qin. "Microstructural Analysis of Impact Damage in Two Glass/Epoxy Composite Laminates" *Composite Engineering*, vol. 3, pp. 55–68, 1993.

[64] Wu, H. T., and G. S. Springer. "Measurement of Matrix Cracking and Delamination Caused by Impact on Composite Plates" *J. Comp. Mats.*, vol. 22, pp. 518–531, 1988.

[65] Wu, H. T., and G. S. Springer. "Impact Induced Stresses, Strains, and Delaminations in Composite Plates" *J. Comp. Mats.*, vol. 22, pp. 533–559, 1988.

[66] Clark, G. "Modelling of Impact Damage in Composite Laminates" *Composites*, vol. 20, no. 2, pp. 209–214, 1989.

[67] Jeusette, J. P., and V. Sonzogni. "A Projected Conjugate Gradient Method for Structural Stability Analysis with Linear Constraints" *Comp. Struct.*, vol. 33, no. 1, pp. 31–39, 1989.

[68] Whitcomb, J. D. "Analysis of a Laminate with a Postbuckled Embedded Delamination, Including Contact Effects" *J. Comp. Mats.*, vol. 26, pp. 1523–1535, 1992.

[69] Wolfram, S. *MATHEMATICA*, Second Edition, New York, Addison-Wesley Publishing Company, 1991.

[70] Amtec Engineering, Inc., *TECPLOT, Version 7*, Bellevue, Washington, 1996.

[71] PDA Engineering, PATRAN Division, *PATRAN Plus User Manual, Release 2.5*, Costa Mesa, CA, 1990.

[72] Sloan, S.W. "A FORTRAN Program for Profile and Wavefront Reduction" *Int. J. Num. Meth. Engng.*, vol. 28 pp. 2651–2679, 1989.

[73] Dongarra, J.J., C.B. Moler, J.R. Bunch, and G.W. Stewart. *LINPACK Users' Guide* ICTP Library, 1979.

[74] Wilson, E. L., K. J. Bathe, and W. P. Doherty. "Direct Solution of Large Systems of Linear Equations" *Comp. Struct.*, vol. 4, pp. 363–372, 1974.

[75] Lehoucq, R., D. C. Sorensen, and P. A. Vu. "ARPACK: Fortran Subroutines for Solving Large Scale Eigenvalue Problems" Release 2.1, available from **netlib@ornl.gov**, in the **scalapack** directory, 1994.

[76] Dongarra, J. J., J. Du Croz, and S. Hammarling. "Algorithm 679: A Set of Level 3 Basic Linear Algebra Subroutines" *ACM Trans. Math. Soft.*, vol. 16, pp. 18–28, 1990.

[77] Anderson, E., and J. J. Dongarra. "Implementation Guide for LAPACK" ,Technical Report CS-90-101, University of Texas, TX, 1990.

[78] Ozakca, M, *et al.* "Comparion of Three-Dimensional Solid Elements in the Analysis of Plates" *Comp. Struct.*, vol. 42, no. 6, pp. 953–968, 1994.

[79] Asch, M., and M. A. Bercovier. "A Mixed 3D finite Element for Modelling Thick Plates" *Comp. Mech.*, vol. 30, no. 5, pp. 332–342, 1994.

[80] Dorfmann, A., and R. B. Nelson. "Three-Dimensional Finite Element for Analyzing Plate/Shell Structures" *Int. J. Num. Meth. Engrg.*, vol. 30, no. 20, pp. 3453–3482, 1995.

[81] Han, J., and S. V. Hoa. "A Three-Dimensional Multilayer Composite Finite Element for Stress Analysis of Composite Laminates" *Int. J. Num. Meth. Engrg.*, vol. 36, no. 22, pp. 3903–3914, 1993.

[82] Timoshenko, S., and S. Woinowsky-Krieger. *Theory of Plates and Shells*, Second Edition, New York, McGraw-Hill, 1959.

[83] Berthelot, J. M., and J. Rhazi. "Acoustic Emission in Carbon Fibre Composites" *Comp. Sci. Tech.*, vol. 37, pp. 411–428, 1990.

[84] Daniel, I. M., and S. C. Wooh. "Ultrasonic Characterization of Defects and Damage in Thick Composites" *Review of Progress in Quantitative Nondestructive Evaluation.*, vol. 9, pp. 1489–1496, 1990.

[85] Hamstad, M. A. "A Review: Acoustic Emission, a Tool for Composite Material Studies" *Exp. Mech.*, pp. 7–13, 1986.

[86] Michaels, T. E., and B. D. Davidson. "Ultrasonic Inspection Detects Hidden Damage in Composites" *Advanced Materials & Processes.*, vol. 143, no. 3, pp. 34–38, 1993.

[87] Hsu, D. K., and F. J. Margetan. "Analysis of Acousto-Ultrasonic Signal in Unidirectional Thick Composites Using the Slowness Surfaces" *J. Comp. Mats.*, vol. 26, no. 4, pp. 1050–1061, 1992.

[88] Schechter, R. S., H. H. Chaskelis, R. B. Mignogna, and P. P. Delsanto. "Real-Time Parallel Computation and Visualization of Ultrasonic Pulses in Solids" *Science*, vol. 265, pp. 1188–1192, 1994.

[89] Bakuckas, J. G., W. H. Prosser, and W. S. Johnson. "Monitoring Damage Growth in Titanium Matrix Composites Using Acoustic Emission" *J. Comp. Mats.*, vol. 28, pp. 305–316, 1994.

[90] Hobbs, C., and A. Temple. "The Inspection of Aerospace Structures Using Transient Thermography" *British Journal of NDT.*, vol. 35, no. 4, pp. 183–189, 1993.

[91] Jones, T., and H. Berger. "Thermographic Detection of Impact Damage in Graphite-Epoxy Composites" *Mater. Eval.*, vol. 50, no. 12, pp. 1446–1453, 1992.

[92] Henry, D. L., C. D. McCall, and B. P. Burns. "Nondestructive Evaluation of Composite Materials by Computed Tomography (CT)" ARL-MR-32, U.S. Army Research Laboratory, Aberdeen Proving Ground, 1993.

[93] Lambrineas, P., J. R. Davis, B. Suendermann, P. Wells, K. R. Thomson, R. L. Woodward, G. T. Egglestone, and K. Challis. "X-Ray Computed Tomography Examination of Inshore Mine-Hunter Hull Composite Material" *NDT & E International*, pp. 207–213, 1991.

[94] Doering, E. R., J. P. Basart, and J. N. Bray. "Three-Dimensional Flaw Reconstruction and Dimensional Analysis Using a Real-Time X-Ray Imaging System" *NDT & E International*, vol. 26, no. 1, pp. 7–17, 1993.

[95] Weight, K. "An Overview on NDE Methods for Thick Composites and a Proposal for Analysis of Computed Tomography Data" ARL-TR-516, U.S. Army Research Laboratory, Aberdeen Proving Ground, 1994.

INTENTIONALLY LEFT BLANK.

NO. OF COPIES	ORGANIZATION
2	DEFENSE TECHNICAL INFORMATION CENTER DTIC OCA 8725 JOHN J KINGMAN RD STE 0944 FT BELVOIR VA 22060-6218
1	HQDA DAMO FDT 400 ARMY PENTAGON WASHINGTON DC 20310-0460
1	OSD OUSD(A&T)/ODDR&E(R) DR R J TREW 3800 DEFENSE PENTAGON WASHINGTON DC 20301-3800
1	COMMANDING GENERAL US ARMY MATERIEL CMD AMCRDA TF 5001 EISENHOWER AVE ALEXANDRIA VA 22333-0001
1	INST FOR ADVNCD TCHNLGY THE UNIV OF TEXAS AT AUSTIN 3925 W BRAKER LN STE 400 AUSTIN TX 78759-5316
1	DARPA SPECIAL PROJECTS OFFICE J CARLINI 3701 N FAIRFAX DR ARLINGTON VA 22203-1714
1	US MILITARY ACADEMY MATH SCI CTR EXCELLENCE MADN MATH MAJ HUBER THAYER HALL WEST POINT NY 10996-1786
1	DIRECTOR US ARMY RESEARCH LAB AMSRL D DR D SMITH 2800 POWDER MILL RD ADELPHI MD 20783-1197

NO. OF COPIES	ORGANIZATION
1	DIRECTOR US ARMY RESEARCH LAB AMSRL CI AI R 2800 POWDER MILL RD ADELPHI MD 20783-1197
3	DIRECTOR US ARMY RESEARCH LAB AMSRL CI LL 2800 POWDER MILL RD ADELPHI MD 20783-1197
3	DIRECTOR US ARMY RESEARCH LAB AMSRL CI IS T 2800 POWDER MILL RD ADELPHI MD 20783-1197
	ABERDEEN PROVING GROUND
2	DIR USARL AMSRL CI LP (BLDG 305)

NO. OF COPIES	ORGANIZATION
1	DIRECTOR US ARMY RESEARCH LAB AMSRL CP CA D SNIDER 2800 POWDER MILL RD ADELPHI MD 20783-1145
1	DIRECTOR US ARMY RESEARCH LAB AMSRL OP SD TA 2800 POWDER MILL RD ADELPHI MD 20783-1145
3	DIRECTOR US ARMY RESEARCH LAB AMSRL OP SD TL 2800 POWDER MILL RD ADELPHI MD 20783-1145
1	DIRECTOR US ARMY RESEARCH LAB AMSRL CI IS T 2800 POWDER MILL RD ADELPHI MD 20783-1145
1	DIRECTOR DA OASARDA SARD SO 103 ARMY PENTAGON WASHINGTON DC 20310-0103
1	DPTY ASST SECY FOR R&T SARD TT THE PENTAGON RM 3EA79 WASHINGTON DC 20301-7100
1	COMMANDER US ARMY MATERIEL CMD AMXMI INT 5001 EISENHOWER AVE ALEXANDRIA VA 22333-0001
4	COMMANDER US ARMY ARDEC AMSTA AR CC G PAYNE J GEHBAUER C BAULIEU H OPAT PICATINNY ARSENAL NJ 07806-5000

NO. OF COPIES	ORGANIZATION
2	COMMANDER US ARMY ARDEC AMSTA AR AE WW E BAKER J PEARSON PICATINNY ARSENAL NJ 07806-5000
1	COMMANDER US ARMY ARDEC AMSTA AR TD C SPINELLI PICATINNY ARSENAL NJ 07806-5000
1	COMMANDER US ARMY ARDEC AMSTA AR FSE PICATINNY ARSENAL NJ 07806-5000
6	COMMANDER US ARMY ARDEC AMSTA AR CCH A W ANDREWS S MUSALLI R CARR M LUCIANO E LOGSDEN T LOUZEIRO PICATINNY ARSENAL NJ 07806-5000
1	COMMANDER US ARMY ARDEC AMSTA AR CCH P J LUTZ PICATINNY ARSENAL NJ 07806-5000
1	COMMANDER US ARMY ARDEC AMSTA AR FSF T C LIVECCHIA PICATINNY ARSENAL NJ 07806-5000
1	COMMANDER US ARMY ARDEC AMSTA ASF PICATINNY ARSENAL NJ 07806-5000

NO. OF COPIES	ORGANIZATION
1	COMMANDER US ARMY ARDEC AMSTA AR QAC T C C PATEL PICATINNY ARSENAL NJ 07806-5000
1	COMMANDER US ARMY ARDEC AMSTA AR M D DEMELLA PICATINNY ARSENAL NJ 07806-5000
3	COMMANDER US ARMY ARDEC AMSTA AR FSA A WARNASH B MACHAK M CHIEFA PICATINNY ARSENAL NJ 07806-5000
2	COMMANDER US ARMY ARDEC AMSTA AR FSP G M SCHIKSNIS D CARLUCCI PICATINNY ARSENAL NJ 07806-5000
1	COMMANDER US ARMY ARDEC AMSTA AR FSP A P KISATSKY PICATINNY ARSENAL NJ 07806-5000
2	COMMANDER US ARMY ARDEC AMSTA AR CCH C H CHANIN S CHICO PICATINNY ARSENAL NJ 07806-5000
1	COMMANDER US ARMY ARDEC AMSTA AR QAC T D RIGOGLIOSO PICATINNY ARSENAL NJ 07806-5000

NO. OF COPIES	ORGANIZATION
1	COMMANDER US ARMY ARDEC AMSTA AR WET T SACHAR BLDG 172 PICATINNY ARSENAL NJ 07806-5000
9	COMMANDER US ARMY ARDEC AMSTA AR CCH B P DONADIA F DONLON P VALENTI C KNUTSON G EUSTICE S PATEL G WAGNECZ R SAYER F CHANG PICATINNY ARSENAL NJ 07806-5000
6	COMMANDER US ARMY ARDEC AMSTA AR CCL F PUZYCKI R MCHUGH D CONWAY E JAROSZEWSKI R SCHLENNER M CLUNE PICATINNY ARSENAL NJ 07806-5000
5	PM SADARM SFAE GCSS SD COL B ELLIS M DEVINE W DEMASSI J PRITCHARD S HROWNAK PICATINNY ARSENAL NJ 07806-5000
1	US ARMY ARDEC INTELLIGENCE SPECIALIST AMSTA AR WEL F M GUERRIERE PICATINNY ARSENAL NJ 07806-5000

NO. OF COPIES	ORGANIZATION
2	PEO FIELD ARTILLERY SYS SFAE FAS PM H GOLDMAN T MCWILLIAMS PICATINNY ARSENAL NJ 07806-5000
12	PM TMAS SFAE GSSC TMA R MORRIS C KIMKER D GUZIEWICZ E KOPACZ R ROESER R DARCY R KOWALSKI R MCDANOLDS L D ULISSE C ROLLER J MCGREEN B PATTER PICATINNY ARSENAL NJ 07806-5000
1	COMMANDER US ARMY ARDEC AMSTA AR WEA J BRESCIA PICATINNY ARSENAL NJ 07806-5000
1	COMMANDER US ARMY ARDEC PRODUCTION BASE MODERN ACTY AMSMC PBM K PICATINNY ARSENAL NJ 07806-5000
1	COMMANDER US ARMY TACOM PM ABRAMS SFAE ASM AB 6501 ELEVEN MILE RD WARREN MI 48397-5000
1	COMMANDER US ARMY TACOM AMSTA SF WARREN MI 48397-5000
3	COMMANDER US ARMY TACOM PM TACTICAL VEHICLES SFAE TVL SFAE TVM SFAE TVH 6501 ELEVEN MILE RD WARREN MI 48397-5000
1	COMMANDER US ARMY TACOM PM BFVS SFAE ASM BV 6501 ELEVEN MILE RD WARREN MI 48397-5000
1	COMMANDER US ARMY TACOM PM AFAS SFAE ASM AF 6501 ELEVEN MILE RD WARREN MI 48397-5000
1	COMMANDER US ARMY TACOM PM RDT&E SFAE GCSS W AB J GODELL 6501 ELEVEN MILE RD WARREN MI 48397-5000
2	COMMANDER US ARMY TACOM PM SURV SYS SFAE ASM SS T DEAN SFAE GCSS W GSI M D COCHRAN 6501 ELEVEN MILE RD WARREN MI 48397-5000
1	US ARMY CERL R LAMPO 2902 NEWMARK DR CHAMPAIGN IL 61822

NO. OF COPIES	ORGANIZATION
1	COMMANDER US ARMY TACOM PM SURVIVABLE SYSTEMS SFAE GCSS W GSI H M RYZYI 6501 ELEVEN MILE RD WARREN MI 48397-5000
1	COMMANDER US ARMY TACOM PM BFV SFAE GCSS W BV S DAVIS 6501 ELEVEN MILE RD WARREN MI 48397-5000
1	COMMANDER US ARMY TACOM CHIEF ABRAMS TESTING SFAE GCSS W AB QT T KRASKIEWICZ 6501 ELEVEN MILE RD WARREN MI 48397-5000
1	COMMANDER WATERVLIET ARSENAL SMCWV QAE Q B VANINA BLDG 44 WATERVLIET NY 12189-4050
2	TSM ABRAMS ATZK TS S JABURG W MEINSHAUSEN FT KNOX KY 40121
3	ARMOR SCHOOL ATZK TD R BAUEN J BERG A POMEY FT KNOX KY 40121
14	COMMANDER US ARMY TACOM AMSTA TR R R MCCLELLAND D THOMAS J BENNETT D HANSEN AMSTA JSK S GOODMAN J FLORENCE K IYER D TEMPLETON A SCHUMACHER AMSTA TR D D OSTBERG L HINOJOSA B RAJU AMSTA CS SF H HUTCHINSON F SCHWARZ WARREN MI 48397-5000
14	BENET LABORATORIES AMSTA AR CCB R FISCELLA M SOJA E KATHE M SCAVULO G SPENCER P WHEELER S KRUPSKI J VASILAKIS G FRIAR R HASENBEIN AMSTA CCB R S SOPOK E HYLAND D CRAYON R DILLON WATERVLIET NY 12189-4050
2	HQ IOC TANK AMMUNITION TEAM AMSIO SMT R CRAWFORD W HARRIS ROCK ISLAND IL 61299-6000

NO. OF COPIES	ORGANIZATION
2	COMMANDER US ARMY AMCOM AVIATION APPLIED TECH DIR J SCHUCK FT EUSTIS VA 23604-5577
1	DIRECTOR US ARMY AMCOM SFAE AV RAM TV D CALDWELL BLDG 5300 REDSTONE ARSENAL AL 35898
2	US ARMY CORPS OF ENGINEERS CERD C T LIU CEW ET T TAN 20 MASS AVE NW WASHINGTON DC 20314
1	US ARMY COLD REGIONS RSCH & ENGRNG LAB P DUTTA 72 LYME RD HANOVER NH 03755
1	SYSTEM MANAGER ABRAMS ATZK TS LTC J H NUNN BLDG 1002 RM 110 FT KNOX KY 40121
1	USA SBCCOM PM SOLDIER SPT AMSSB PM RSS A J CONNORS KANSAS ST NATICK MA 01760-5057
2	USA SBCCOM MATERIAL SCIENCE TEAM AMSSB RSS J HERBERT M SENNETT KANSAS ST NATICK MA 01760-5057

NO. OF COPIES	ORGANIZATION
2	OFC OF NAVAL RESEARCH D SIEGEL CODE 351 J KELLY 800 N QUINCY ST ARLINGTON VA 22217-5660
1	NAVAL SURFACE WARFARE CTR DAHLGREN DIV CODE G06 DAHLGREN VA 22448
1	NAVAL SURFACE WARFARE CTR TECH LIBRARY CODE 323 17320 DAHLGREN RD DAHLGREN VA 22448
1	NAVAL SURFACE WARFARE CTR CRANE DIVISION M JOHNSON CODE 20H4 LOUISVILLE KY 40214-5245
8	DIRECTOR US ARMY NATIONAL GROUND INTELLIGENCE CTR D LEITER M HOLTUS M WOLFE S MINGLEDORF J GASTON W GSTATTENBAUER R WARNER J CRIDER 220 SEVENTH ST NE CHARLOTTESVILLE VA 22091
2	NAVAL SURFACE WARFARE CTR U SORATHIA C WILLIAMS CD 6551 9500 MACARTHUR BLVD WEST BETHESDA MD 20817
2	COMMANDER NAVAL SURFACE WARFARE CTR CARDEROCK DIVISION R PETERSON CODE 2020 M CRITCHFIELD CODE 1730 BETHESDA MD 20084

NO. OF COPIES	ORGANIZATION
8	US ARMY SBCCOM SOLDIER SYSTEMS CENTER BALLISTICS TEAM J WARD W ZUKAS P CUNNIFF J SONG MARINE CORPS TEAM J MACKIEWICZ BUS AREA ADVOCACY TEAM W HASKELL AMSSB RCP SS W NYKVIST S BEAUDOIN KANSAS ST NATICK MA 01760-5019
9	US ARMY RESEARCH OFC A CROWSON J CHANDRA H EVERETT J PRATER R SINGLETON G ANDERSON D STEPP D KISEROW J CHANG PO BOX 12211 RESEARCH TRIANGLE PARK NC 27709-2211
8	NAVAL SURFACE WARFARE CTR J FRANCIS CODE G30 D WILSON CODE G32 R D COOPER CODE G32 J FRAYSSE CODE G33 E ROWE CODE G33 T DURAN CODE G33 L DE SIMONE CODE G33 R HUBBARD CODE G33 DAHLGREN VA 22448
1	NAVAL SEA SYSTEMS CMD D LIESE 2531 JEFFERSON DAVIS HWY ARLINGTON VA 22242-5160
1	NAVAL SURFACE WARFARE CTR M LACY CODE B02 17320 DAHLGREN RD DAHLGREN VA 22448

NO. OF COPIES	ORGANIZATION
2	NAVAL SURFACE WARFARE CTR CARDEROCK DIVISION R CRANE CODE 2802 C WILLIAMS CODE 6553 3A LEGGETT CIR BETHESDA MD 20054-5000
1	EXPEDITIONARY WARFARE DIV N85 F SHOUP 2000 NAVY PENTAGON WASHINGTON DC 20350-2000
1	AFRL MLBC 2941 P ST RM 136 WRIGHT PATTERSON AFB OH 45433-7750
1	AFRL MLSS R THOMSON 2179 12TH ST RM 122 WRIGHT PATTERSON AFB OH 45433-7718
2	AFRL F ABRAMS J BROWN BLDG 653 2977 P ST STE 6 WRIGHT PATTERSON AFB OH 45433-7739
1	WATERWAYS EXPERIMENT D SCOTT 3909 HALLS FERRY RD SC C VICKSBURG MS 39180
5	DIRECTOR LLNL R CHRISTENSEN S DETERESA F MAGNESS M FINGER MS 313 M MURPHY L 282 PO BOX 808 LIVERMORE CA 94550
1	AFRL MLS OL L COULTER 7278 4TH ST BLDG 100 BAY D HILL AFB UT 84056-5205

NO. OF COPIES	ORGANIZATION
1	OSD JOINT CCD TEST FORCE OSD JCCD R WILLIAMS 3909 HALLS FERRY RD VICKSBURG MS 29180-6199
1	DEFENSE NUCLEAR AGENCY INNOVATIVE CONCEPTS DIV 6801 TELEGRAPH RD ALEXANDRIA VA 22310-3398
3	DARPA M VANFOSSEN S WAX L CHRISTODOULOU 3701 N FAIRFAX DR ARLINGTON VA 22203-1714
2	SERDP PROGRAM OFC PM P2 C PELLERIN B SMITH 901 N STUART ST STE 303 ARLINGTON VA 22203
1	FAA MIL HDBK 17 CHAIR L ILCEWICZ 1601 LIND AVE SW ANM 115N RESTON VA 98055
1	US DEPT OF ENERGY OFC OF ENVIRONMENTAL MANAGEMENT P RITZCOVAN 19901 GERMANTOWN RD GERMANTOWN MD 20874-1928
1	DIRECTOR LLNL F ADDESSIO MS B216 PO BOX 1633 LOS ALAMOS NM 87545
1	OAK RIDGE NATIONAL LABORATORY R M DAVIS PO BOX 2008 OAK RIDGE TN 37831-6195

NO. OF COPIES	ORGANIZATION
3	DIRECTOR SANDIA NATIONAL LABS APPLIED MECHANICS DEPT MS 9042 J HANDROCK Y R KAN J LAUFFER PO BOX 969 LIVERMORE CA 94551-0969
1	OAK RIDGE NATIONAL LABORATORY C EBERLE MS 8048 PO BOX 2008 OAK RIDGE TN 37831
1	OAK RIDGE NATIONAL LABORATORY C D WARREN MS 8039 PO BOX 2008 OAK RIDGE TN 37831
5	NIST J DUNKERS M VANLANDINGHAM MS 8621 J CHIN MS 8621 J MARTIN MS 8621 D DUTHINH MS 8611 100 BUREAU DR GAITHERSBURG MD 20899
1	HYDROGEOLOGIC INC SERDP ESTCP SPT OFC S WALSH 1155 HERNDON PKWY STE 900 HERNDON VA 20170
3	NASA LANGLEY RSCH CTR AMSRL VS W ELBER MS 266 F BARTLETT JR MS 266 G FARLEY MS 266 HAMPTON VA 23681-0001
1	NASA LANGLEY RSCH CTR T GATES MS 188E HAMPTON VA 23661-3400
1	FHWA E MUNLEY 6300 GEORGETOWN PIKE MCLEAN VA 22101

NO. OF COPIES	ORGANIZATION
3	CYTEC FIBERITE R DUNNE D KOHLI R MAYHEW 1300 REVOLUTION ST HAVRE DE GRACE MD 21078
1	USDOT FEDERAL RAILRD M FATEH RDV 31 WASHINGTON DC 20590
1	MARINE CORPS INTLLGNC ACTVTY D KOSITZKE 3300 RUSSELL RD STE 250 QUANTICO VA 22134-5011
1	DIRECTOR NATIONAL GRND INTLLGNC CTR IANG TMT 220 SEVENTH ST NE CHARLOTTESVILLE VA 22902-5396
1	SIOUX MFG B KRIEL PO BOX 400 FT TOTTEN ND 58335
2	3TEX CORPORATION A BOGDANOVICH J SINGLETARY 109 MACKENAN DR CARY NC 27511
1	3M CORPORATION J SKILDUM 3M CENTER BLDG 60 IN 01 ST PAUL MN 55144-1000
1	DIRECTOR DEFENSE INTLLGNC AGNCY TA 5 K CRELLING WASHINGTON DC 20310
1	ADVANCED GLASS FIBER YARNS T COLLINS 281 SPRING RUN LANE STE A DOWNINGTON PA 19335

NO. OF COPIES	ORGANIZATION
1	COMPOSITE MATERIALS INC D SHORTT 19105 63 AVE NE PO BOX 25 ARLINGTON WA 98223
1	JPS GLASS L CARTER PO BOX 260 SLATER RD SLATER SC 29683
1	COMPOSITE MATERIALS INC R HOLLAND 11 JEWEL CT ORINDA CA 94563
1	COMPOSITE MATERIALS INC C RILEY 14530 S ANSON AVE SANTA FE SPRINGS CA 90670
2	SIMULA J COLTMAN R HUYETT 10016 S 51ST ST PHOENIX AZ 85044
2	PROTECTION MATERIALS INC M MILLER F CRILLEY 14000 NW 58 CT MIAMI LAKES FL 33014
2	FOSTER MILLER M ROYLANCE W ZUKAS 195 BEAR HILL RD WALTHAM MA 02354-1196
1	ROM DEVELOPMENT CORP R O MEARA 136 SWINEBURNE ROW BRICK MARKET PLACE NEWPORT RI 02840

NO. OF COPIES	ORGANIZATION
2	TEXTRON SYSTEMS T FOLTZ M TREASURE 1449 MIDDLESEX ST LOWELL MA 01851
1	O GARA HESS & EISENHARDT M GILLESPIE 9113 LESAINT DR FAIRFIELD OH 45014
2	MILLIKEN RSCH CORP H KUHN M MACLEOD PO BOX 1926 SPARTANBURG SC 29303
1	CONNEAUGHT INDUSTRIES INC J SANTOS PO BOX 1425 COVENTRY RI 02816
1	BATTELLE NATICK OPNS B HALPIN 209 W CENTRAL ST STE 302 NATICK MA 01760
1	ARMTEC DEFENSE PRODUCTS S DYER 85 901 AVE 53 PO BOX 848 COACHELLA CA 92236
1	NATIONAL COMPOSITE CENTER T CORDELL 2000 COMPOSITE DR KETTERING OH 45420
3	PACIFIC NORTHWEST LAB M SMITH G VAN ARSDALE R SHIPPELL PO BOX 999 RICHLAND WA 99352
2	AMOCO PERFORMANCE PRODUCTS M MICHNO JR J BANISAUKAS 4500 MCGINNIS FERRY RD ALPHARETTA GA 30202-3944
8	ALLIANT TECHSYSTEMS INC C CANDLAND MN11 2830 C AAKHUS MN11 2830 B SEE MN11 2439 N VLAHAKUS MN11 2145 R DOHRN MN11 2830 S HAGLUND MN11 2439 M HISSONG MN11 2830 D KAMDAR MN11 2830 600 SECOND ST NE HOPKINS MN 55343-8367
1	SAIC M PALMER 1410 SPRING HILL RD STE 400 MS SH4 5 MCLEAN VA 22102
1	SAIC G CHRYSSOMALLIS 3800 W 80TH ST STE 1090 BLOOMINGTON MN 55431
1	AAI CORPORATION T G STASTNY PO BOX 126 HUNT VALLEY MD 21030-0126
1	APPLIED COMPOSITES W GRISCH 333 NORTH SIXTH ST ST CHARLES IL 60174
1	CUSTOM ANALYTICAL ENG SYS INC A ALEXANDER 13000 TENSOR LANE NE FLINTSTONE MD 21530
3	ALLIANT TECHSYSTEMS INC J CONDON E LYNAM J GERHARD WV01 16 STATE RT 956 PO BOX 210 ROCKET CENTER WV 26726-0210
1	OFC DEPUTY UNDER SEC DEFNS J THOMPSON 1745 JEFFERSON DAVIS HWY CRYSTAL SQ 4 STE 501 ARLINGTON VA 22202

NO. OF COPIES	ORGANIZATION
1	PROJECTILE TECHNOLOGY INC 515 GILES ST HAVRE DE GRACE MD 21078
5	AEROJET GEN CORP D PILLASCH T COULTER C FLYNN D RUBAREZUL M GREINER 1100 WEST HOLLYVALE ST AZUSA CA 91702-0296
3	HEXCEL INC R BOE PO BOX 18748 SALT LAKE CITY UT 84118
1	HERCULES INC HERCULES PLAZA WILMINGTON DE 19894
1	BRIGS COMPANY J BACKOFEN 2668 PETERBOROUGH ST HERNDON VA 22071-2443
1	ZERNOW TECHNICAL SERVICES L ZERNOW 425 W BONITA AVE STE 208 SAN DIMAS CA 91773
1	GENERAL DYNAMICS OTS L WHITMORE 10101 NINTH ST NORTH ST PETERSBURG FL 33702
3	GENERAL DYNAMICS OTS FLINCHBAUGH DIV E STEINER B STEWART T LYNCH PO BOX 127 RED LION PA 17356
1	GKN AEROSPACE D OLDS 15 STERLING DR WALLINGFORD CT 06492
5	SIKORSKY AIRCRAFT G JACARUSO T CARSTENSAN B KAY S GARBO MS S330A J ADELMANN 6900 MAIN ST PO BOX 9729 STRATFORD CT 06497-9729
1	PRATT & WHITNEY C WATSON 400 MAIN ST MS 114 37 EAST HARTFORD CT 06108
1	AEROSPACE CORP G HAWKINS M4 945 2350 E EL SEGUNDO BLVD EL SEGUNDO CA 90245
2	CYTEC FIBERITE M LIN W WEB 1440 N KRAEMER BLVD ANAHEIM CA 92806
1	UDLP G THOMAS PO BOX 58123 SANTA CLARA CA 95052
2	UDLP R BARRETT MAIL DROP M53 V HORVATICH MAIL DROP M53 328 W BROKAW RD SANTA CLARA CA 95052-0359
3	UDLP GROUND SYSTEMS DIVISION M PEDRAZZI MAIL DROP N09 A LEE MAIL DROP N11 M MACLEAN MAIL DROP N06 1205 COLEMAN AVE SANTA CLARA CA 95052
4	UDLP R BRYNSVOLD P JANKE MS 170 4800 EAST RIVER RD MINNEAPOLIS MN 55421-1498

NO. OF COPIES	ORGANIZATION
1	UDLP D MARTIN PO BOX 359 SANTA CLARA CA 95052
2	BOEING DFNSE & SPACE GP W HAMMOND S 4X55 J RUSSELL S 4X55 PO BOX 3707 SEATTLE WA 98124-2207
2	BOEING ROTORCRAFT P MINGURT P HANDEL 800 B PUTNAM BLVD WALLINGFORD PA 19086
1	BOEING DOUGLAS PRODUCTS DIV L J HART SMITH 3855 LAKEWOOD BLVD D800 0019 LONG BEACH CA 90846-0001
1	LOCKHEED MARTIN SKUNK WORKS D FORTNEY 1011 LOCKHEED WAY PALMDALE CA 93599-2502
1	LOCKHEED MARTIN R FIELDS 1195 IRWIN CT WINTER SPRINGS FL 32708
1	MATERIALS SCIENCES CORP G FLANAGAN 500 OFC CENTER DR STE 250 FT WASHINGTON PA 19034
1	NORTHRUP GRUMMAN CORP ELECTRONIC SENSORS & SYSTEMS DIV E SCHOCH MS V 16 1745A W NURSERY RD LINTHICUM MD 21090
1	GDLS DIVISION D BARTLE PO BOX 1901 WARREN MI 48090
2	GDLS D REES M PASIK PO BOX 2074 WARREN MI 48090-2074
1	GDLS MUSKEGON OPERATIONS W SOMMERS JR 76 GETTY ST MUSKEGON MI 49442
1	GENERAL DYNAMICS AMPHIBIOUS SYS SURVIVABILITY LEAD G WALKER 991 ANNAPOLIS WAY WOODBRIDGE VA 22191
6	INST FOR ADVANCED TECH H FAIR I MCNAB P SULLIVAN S BLESS W REINECKE C PERSAD 3925 W BRAKER LN STE 400 AUSTIN TX 78759-5316
2	CIVIL ENGR RSCH FOUNDATION PRESIDENT H BERNSTEIN R BELLE 1015 15TH ST NW STE 600 WASHINGTON DC 20005
1	ARROW TECH ASSO 1233 SHELBURNE RD STE D8 SOUTH BURLINGTON VT 05403-7700
1	R EICHELBERGER CONSULTANT 409 W CATHERINE ST BEL AIR MD 21014-3613

NO. OF COPIES	ORGANIZATION
1	UCLA MANE DEPT ENGR IV H T HAHN LOS ANGELES CA 90024-1597
2	UNIV OF DAYTON RESEARCH INST R Y KIM A K ROY 300 COLLEGE PARK AVE DAYTON OH 45469-0168
1	UMASS LOWELL PLASTICS DEPT N SCHOTT 1 UNIVERSITY AVE LOWELL MA 01854
1	IIT RESEARCH CENTER D ROSE 201 MILL ST ROME NY 13440-6916
1	GA TECH RSCH INST GA INST OF TCHNLGY P FRIEDERICH ATLANTA GA 30392
1	MICHIGAN ST UNIV MSM DEPT R AVERILL 3515 EB EAST LANSING MI 48824-1226
1	UNIV OF WYOMING D ADAMS PO BOX 3295 LARAMIE WY 82071
2	PENN STATE UNIV R MCNITT C BAKIS 212 EARTH ENGR SCIENCES BLDG UNIVERSITY PARK PA 16802
1	PENN STATE UNIV R S ENGEL 245 HAMMOND BLDG UNIVERSITY PARK PA 16801
1	PURDUE UNIV SCHOOL OF AERO & ASTRO C T SUN W LAFAYETTE IN 47907-1282
1	STANFORD UNIV DEPT OF AERONAUTICS & AEROBALLISTICS S TSAI DURANT BLDG STANFORD CA 94305
1	UNIV OF MAIN ADV STR & COMP LAB R LOPEZ ANIDO 5793 AEWC BLDG ORONO ME 04469-5793
1	JOHNS HOPKINS UNIV APPLIED PHYSICS LAB P WIENHOLD 11100 JOHNS HOPKINS RD LAUREL MD 20723-6099
1	UNIV OF DAYTON J M WHITNEY COLLEGE PARK AVE DAYTON OH 45469-0240
5	UNIV OF DELAWARE CTR FOR COMPOSITE MTRLS J GILLESPIE M SANTARE S YARLAGADDA S ADVANI D HEIDER 201 SPENCER LABORATORY NEWARK DE 19716
1	DEPT OF MATERIALS SCIENCE & ENGINEERING UNIVERSITY OF ILLINOIS AT URBANA CHAMPAIGN J ECONOMY 1304 WEST GREEN ST 115B URBANA IL 61801

NO. OF COPIES	ORGANIZATION
1	NORTH CAROLINA STATE UNIV CIVIL ENGINEERING DEPT W RASDORF PO BOX 7908 RALEIGH NC 27696-7908
1	UNIV OF MARYLAND DEPT OF AEROSPACE ENGNRNG A J VIZZINI COLLEGE PARK MD 20742
3	UNIV OF TEXAS AT AUSTIN CTR FOR ELECTROMECHANICS J PRICE A WALLS J KITZMILLER 10100 BURNET RD AUSTIN TX 78758-4497
3	VA POLYTECHNICAL INST & STATE UNIV DEPT OF ESM M W HYER K REIFSNIDER R JONES BLACKSBURG VA 24061-0219
1	DREXEL UNIV A S D WANG 32ND & CHESTNUT ST PHILADELPHIA PA 19104
1	SOUTHWEST RSCH INST ENGR & MATL SCIENCES DIV J RIEGEL 6220 CULEBRA RD PO DRAWER 28510 SAN ANTONIO TX 78228-0510
	ABERDEEN PROVING GROUND
1	US ARMY MATERIEL SYSTEMS ANALYSIS ACTIVITY P DIETZ 392 HOPKINS RD AMXSY TD APG MD 21005-5071
1	DIRECTOR US ARMY RESEARCH LAB AMSRL OP AP L APG MD 21005-5066

NO. OF COPIES	ORGANIZATION
	ABERDEEN PROVING GROUND (CONT)
91	DIR USARL AMSRL CI AMSRL CI H W STUREK AMSRL CI S A MARK AMSRL CS IO FI M ADAMSON AMSRL SL BA AMSRL SL BL D BELY R HENRY AMSRL SL BG AMSRL SL I AMSRL WM J SMITH AMSRL WM B A HORST AMSRL WM BA D LYON AMSRL WM BC P PLOSTINS J NEWILL S WILKERSON A ZIELINSKI AMSRL WM BD B FORCH R FIFER R PESCE RODRIGUEZ B RICE AMSRL WM BE C LEVERITT AMSRL WM BF J LACETERA AMSRL WM BR C SHOEMAKER J BORNSTEIN AMSRL WM M D VIECHNICKI G HAGNAUER J MCCAULEY AMSRL WM MA L GHIORSE S MCKNIGHT AMSRL WM MB B FINK J BENDER T BOGETTI R BOSSOLI L BURTON

NO. OF COPIES ORGANIZATION

ABERDEEN PROVING GROUND (CONT)

K BOYD
S CORNELISON
P DEHMER
R DOOLEY
W DRYSDALE
G GAZONAS
S GHIORSE
D GRANVILLE
D HOPKINS
C HOPPEL
D HENRY
R KASTE
M KLUSEWITZ
M LEADORE
R LIEB
E RIGAS
J SANDS
D SPAGNUOLO
W SPURGEON
J TZENG
E WETZEL
A FRYDMAN
AMRSL WM MC
J BEATTY
E CHIN
J MONTGOMERY
A WERECZCAK
J LASALVIA
J WELLS
AMSRL WM MD
W ROY
S WALSH
AMSRL WM T
B BURNS
M ZOLTOSKI
AMSRL WM TA
W GILLICH
T HAVEL
J RUNYEON
M BURKINS
E HORWATH
B GOOCH
W BRUCHEY
M NORMANDIA

NO. OF COPIES ORGANIZATION

ABERDEEN PROVING GROUND (CONT)

AMRSL WM TB
D KOOKER
P BAKER
AMSRL WM TC
R COATES
AMSRL WM TD
A DAS GUPTA
T HADUCH
T MOYNIHAN
F GREGORY
M RAFTENBERG
M BOTELER
T WEERASOORIYA
D DANDEKAR
A DIETRICH
AMSRL WM TE
A NIILER
J POWELL
AMSRL SS SD
H WALLACE
AMSRL SS SE DS
R REYZER
R ATKINSON

NO. OF COPIES	ORGANIZATION
1	LTD R MARTIN MERL TAMWORTH RD HERTFORD SG13 7DG UK
1	SMC SCOTLAND P W LAY DERA ROSYTH ROSYTH ROYAL DOCKYARD DUNFERMLINE FIFE KY 11 2XR UK
1	CIVIL AVIATION ADMINSTRATION T GOTTESMAN PO BOX 8 BEN GURION INTERNL AIRPORT LOD 70150 ISRAEL
1	AEROSPATIALE S ANDRE A BTE CC RTE MD132 316 ROUTE DE BAYONNE TOULOUSE 31060 FRANCE
1	DRA FORT HALSTEAD P N JONES SEVEN OAKS KENT TN 147BP UK
1	DEFENSE RESEARCH ESTAB VALCARTIER F LESAGE COURCELETTE QUEBEC COA IRO CANADA
1	SWISS FEDERAL ARMAMENTS WKS W LANZ ALLMENDSTRASSE 86 3602 THUN SWITZERLAND
1	DYNAMEC RESEARCH AB AKE PERSSON BOX 201 SE 151 23 SODERTALJE SWEDEN

NO. OF COPIES	ORGANIZATION
1	ISRAEL INST OF TECHNOLOGY S BODNER FACULTY OF MECHANICAL ENGR HAIFA 3200 ISRAEL
1	DSTO MATERIALS RESEARCH LAB NAVAL PLATFORM VULNERABILITY SHIP STRUCTURES & MTRLS DIV N BURMAN PO BOX 50 ASCOT VALE VICTORIA AUSTRALIA 3032
1	ECOLE ROYAL MILITAIRE E CELENS AVE DE LA RENAISSANCE 30 1040 BRUXELLE BELGIQUE
1	DEF RES ESTABLISHMENT VALCARTIER A DUPUIS 2459 BOULEVARD PIE XI NORTH VALCARTIER QUEBEC CANADA PO BOX 8800 COURCELETTE GOA IRO QUEBEC CANADA
1	INSTITUT FRANCO ALLEMAND DE RECHERCHES DE SAINT LOUIS DE M GIRAUD 5 RUE DU GENERAL CASSAGNOU BOITE POSTALE 34 F 68301 SAINT LOUIS CEDEX FRANCE
1	ECOLE POLYTECH J MANSON DMX LTC CH 1015 LAUSANNE SWITZERLAND

NO. OF COPIES	ORGANIZATION
1	TNO PRINS MAURITS LABORATORY R IJSSELSTEIN LANGE KLEIWEG 137 PO BOX 45 2280 AA RIJSWIJK THE NETHERLANDS
2	FOA NATL DEFENSE RESEARCH ESTAB DIR DEPT OF WEAPONS & PROTECTION B JANZON R HOLMLIN S 172 90 STOCKHOLM SWEDEN
2	DEFENSE TECH & PROC AGENCY GROUND I CREWTHER GENERAL HERZOG HAUS 3602 THUN SWITZERLAND
1	MINISTRY OF DEFENCE RAFAEL ARMAMENT DEVELOPMENT AUTH M MAYSELESS PO BOX 2250 HAIFA 31021 ISRAEL
1	TNO DEFENSE RESEARCH I H PASMAN POSTBUS 6006 2600 JA DELFT THE NETHERLANDS
1	B HIRSCH TACHKEMONY ST 6 NETAMUA 42611 ISRAEL
1	DEUTSCHE AEROSPACE AG DYNAMICS SYSTEMS M HELD PO BOX 1340 D 86523 SCHROBENHAUSEN GERMANY

NO. OF COPIES	ORGANIZATION
10	E SAETHER 104 MICHAEL PLACE YORKTOWN VA 23692

REPORT DOCUMENTATION PAGE

Form Approved
OMB No. 0704-0188

1. AGENCY USE ONLY *(Leave blank)*	2. REPORT DATE	3. REPORT TYPE AND DATES COVERED
	July 2001	Final, November 1995 - November 1997

4. TITLE AND SUBTITLE
RESTRAN: Residual Strength Analysis of Impact Damaged Composite Laminates
Volume I: Theoretical Manual

5. FUNDING NUMBERS
622105AH84

6. AUTHOR(S)
Erik Saether

7. PERFORMING ORGANIZATION NAME(S) AND ADDRESS(ES)
U.S. Army Research Laboratory
ATTN: AMSRL-WM-MB
Aberdeen Proving Ground, MD 21005-5069

8. PERFORMING ORGANIZATION REPORT NUMBER
ARL-TR-2549

9. SPONSORING/MONITORING AGENCY NAMES(S) AND ADDRESS(ES)

10.SPONSORING/MONITORING AGENCY REPORT NUMBER

11. SUPPLEMENTARY NOTES

12a. DISTRIBUTION/AVAILABILITY STATEMENT
Approved for public release; distribution is unlimited.

12b. DISTRIBUTION CODE

13. ABSTRACT *(Maximum 200 words)*

The use of composite material systems in structural design has yielded significant improvements in material efficiency by minimizing weight while meeting static and dynamic strength requirements. The complexity of composite materials, however, has presented a spectrum of additional design considerations in the areas of fabrication, strength tailoring, failure mechanisms, and damage tolerance. Laminated composites exhibit a variety of damage and failure modes which include matrix cracking, fiber breakage, delamination propagation, and instability. Of prime concern is the predication of residual strength in composite structures subjected to damage-causing impact threats in the intended service environment. The present effort aims to account for many of the salient damage mechanisms utilizing a numerical, finite element-based approach. Such an approach permits a broad range of failure modes to be accounted for while allowing the modeling of complex geometries, support conditions, and applied loading. This report details the theoretical and algorithmic basis of a developed computer program denoted RESTRAN (REsidual STRength ANalysis), incorporating both material and structural failure modes in the prediction of residual strength in composite structures containing internal damage.

14. SUBJECT TERMS
residual strength, multiple delaminations, material failure, impact damage

15. NUMBER OF PAGES
122

16. PRICE CODE

17. SECURITY CLASSIFICATION OF REPORT	18. SECURITY CLASSIFICATION OF THIS PAGE	19. SECURITY CLASSIFICATION OF ABSTRACT	20. LIMITATION OF ABSTRACT
UNCLASSIFIED	UNCLASSIFIED	UNCLASSIFIED	UL

INTENTIONALLY LEFT BLANK.

USER EVALUATION SHEET/CHANGE OF ADDRESS

This Laboratory undertakes a continuing effort to improve the quality of the reports it publishes. Your comments/answers to the items/questions below will aid us in our efforts.

1. ARL Report Number/Author ARL-TR-2549 (POC: Fink) Date of Report July 2001

2. Date Report Received _____

3. Does this report satisfy a need? (Comment on purpose, related project, or other area of interest for which the report will be used.) _____

4. Specifically, how is the report being used? (Information source, design data, procedure, source of ideas, etc.) _____

5. Has the information in this report led to any quantitative savings as far as man-hours or dollars saved, operating costs avoided, or efficiencies achieved, etc? If so, please elaborate. _____

6. General Comments. What do you think should be changed to improve future reports? (Indicate changes to organization, technical content, format, etc.) _____

CURRENT ADDRESS

_____
Organization

_____
Name E-mail Name

_____
Street or P.O. Box No.

_____
City, State, Zip Code

7. If indicating a Change of Address or Address Correction, please provide the Current or Correct address above and the Old or Incorrect address below.

OLD ADDRESS

_____
Organization

_____
Name

_____
Street or P.O. Box No.

_____
City, State, Zip Code

(Remove this sheet, fold as indicated, tape closed, and mail.)
(DO NOT STAPLE)